ELECTRONIC SUPPORTING INFORMATION (ESI) FOR

Sumanene–carbazole conjugate with push–pull structure and its chemoreceptor application

Dominika Ufnal[a,†], Jakub S. Cyniak[a,†], Maurycy Krzyzanowski[a], Krzysztof Durka[a], Hidehiro Sakurai[b,c], Artur Kasprzak[a]*

[a] Faculty of Chemistry, Warsaw University of Technology, Noakowskiego Str. 3, 00-664 Warsaw, Poland

* Corresponding author e-mail: artur.kasprzak@pw.edu.pl (A.K.)

[b] Division of Applied Chemistry, Graduate School of Engineering, Osaka University, 2-1 Yamadaoka, Suita, 565-0871 Osaka, Japan

[c] Innovative Catalysis Science Division, Institute for Open and Transdisciplinary Research Initiatives (ICSOTRI), Osaka University, Suita 565-0871 Osaka, Japan

† These authors contributed equally to this work.

Table on contents:

List of figures

S1. Experimental section

S1.1. Materials and methods.

Chemical reagents and solvents for the synthesis were commercially purchased and purified according to the standard methods, if necessary. Sumanene (**1**)[1], 1,3,5-tri(9*H*-carbazol-9-yl)benzene(**11**)[2], and 2-iodosumanene (**8**)[3] were synthesized following the literature procedures. Thin layer chromatography (TLC) and preparative thin layer chromatography (PTLC) were performed using Merck Silica gel 60 F254 plates.

The NMR experiments were carried out using a JEOL 600 MHz spectrometer (^{1}H and ^{19}F NMR at 600 MHz, {^{1}H}^{13}C NMR at 150 MHz) equipped with a multinuclear z-gradient inverse probe head or Varian VNMRS 500 MHz spectrometer (^{1}H NMR at 500 MHz, ^{13}C{^{1}H} NMR at 125 MHz) equipped with a multinuclear z-gradient inverse probe head. The spectra were recorded at 25 °C and standard 5 mm NMR tubes were used. ^{1}H and ^{13}C chemical shifts (δ) were reported in parts per million (ppm) relative to the solvent signal, *i.e.*, THF-d_8: δ_H (residual THF) 3.58 ppm, δ_C (residual THF) 67.6 ppm; $CDCl_3$: δ_H (residual $CHCl_3$) 7.26 ppm, δ_C (residual $CHCl_3$) 77.16 ppm. ^{1}H DOSY (Diffusion Ordered SpectroscopY) and ^{19}F DOSY NMR experiments (500 MHz) were performed using a stimulated echo sequence incorporating bipolar gradient pulses[4] and with convection compensation.[5] The gradient strength was logarithmically incremented in 15 steps from 25% up to 95% of the maximum gradient strength. NMR spectra were analyzed with the MestReNova v12.0 software (Mestrelab Research S.L).

ESI-HRMS (TOF) measurements were performed with a Q-Exactive ThermoScientific spectrometer.

Elemental analyzes were performed using CHNS Elementar Vario EL III apparatus. Each elemental composition was reported as an average of two analyses.

UV-vis measurements were performed with a WVR UV-1600PC spectrometer, with the spectral resolution of 2 cm^{-1}. For the UV-Vis measurements, the wavelengths for the absorption maxima λ_{max} were reported in nm.

Emission spectra were recorded with a HITACHI F-7100 FL spectrometer; parameters for the spectra of liquid samples: scan speed: 1200 nm/min, delay: 0.0 s, EX slit: 5.0 nm, EM slit: 5.0 nm, PMT voltage: 400 V; parameters for the spectra of solid samples: scan speed: 1200 nm/min, delay: 0.0 s, EX slit: 5.0 nm, EM slit: 5.0 nm, PMT voltage: 700 V. The wavelengths for the emission maxima (λ_{em}) were reported in nm.

S1.2. Synthesis of compounds 4-5.

General method for the synthesis of compounds 4-5.

Sumanene (**1**; 15.0 mg, 0.057 mmol, 1 equiv.) was placed in a reaction test tube. Tetrabutylammonium bromide (TBAB; 9.2 mg, 0.0285 mmol, 0.5 equiv.) was added, followed by the addition of THF (0.2 mL) and $NaOH_{aq}$ (30%, 2 mL). The reaction mixture was stirred for 5 min at room temperature. Solid aldehyde (**6-7**; 6 equiv.) was added in one portion, and the reaction mixture was stirred for 48 hours at room temperature. Distilled water (6 mL) was added, and the crude product was extracted with CH_2Cl_2 (3x20 mL). Organic layers were combined, washed with saturated NH_4Cl, water, and brine. After drying with $MgSO_4$ followed by filtration, volatiles were distilled off on a rotary evaporator. Finally, the product was purified using a column chromatography to provide the target compound **4-5**.

Compound 4. Red-orange solid. Yield 40% (23.2 mg). ^{1}H NMR (THF-d_8, 500 MHz, ppm) δ_H 8.28-8.17 (m, 12H), 7.79-7.67 (m, 10H), 7.59-7.52 (m, 9H), 7.44-7.35 (m, 8H), 7.28-7.26 (m, 6H). {^{1}H}^{13}C NMR (THF-d_8; 125 MHz, ppm) δ_C 149.3, 149.0, 148.6, 148.4, 148.3, 148.2, 147.4, 147.1, 146.5, 146.4, 146.3, 146.2, 144.3, 144.1, 142.5, 142.2, 141.8x2, 141.6x3, 139.3, 139.2, 136.4, 136.3, 136.2, 132.3, 132.2x2, 128.9, 128.7, 128.6, 138.3, 127.8x3, 126.9x2, 124.8x2, 124.7x2, 124.5, 124.4, 124.1, 122.3, 122.2, 122.1, 121.9, 121.1x2, 110.7x2. ESI-HRMS (TOF) *m/z* $[M]^+$ calcd. for $C_{78}H_{45}N_3$ 1024.3686, found 1024.3801. Elemental analysis: Anal. Calcd for $C_{78}H_{45}N_3$: C, 91.47; H, 4.43; N, 4.10. Found: C, 91.01; H, 4.45; N, 4.09. R_f (50% $CHCl_3$/hexane) = 0.56.

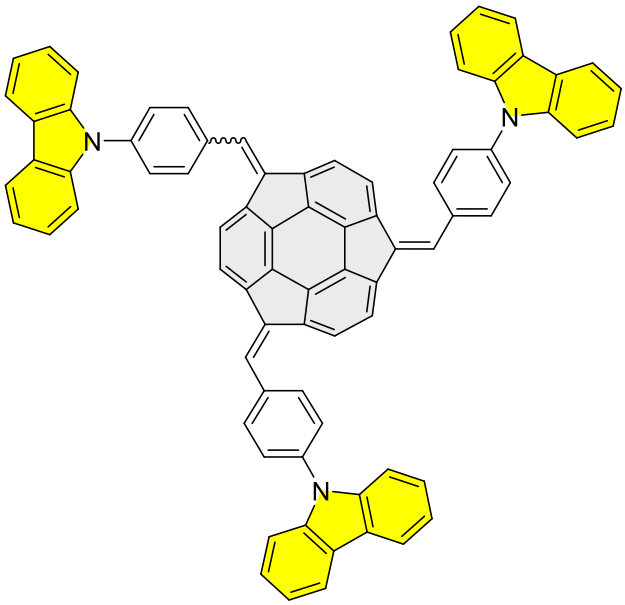

4

Compound 5. Red solid. Yield 53% (25.9 mg). ^{1}H NMR (THF-d_8, 500 MHz, ppm) δ_H 8.70-8.56 (m, 3H), 8.18-8.13 (m, 6H), 7.75-7.66 (m, 6H), 7.54-7.42 (m, 11H), 7.29-7.21 (m, 4H), 4.52-4.39 (m, 6H), 1.48-1.36 (m, 9H). {^{1}H}^{13}C NMR (THF-d_8; 125 MHz, ppm) δ_C 149.3, 148.9, 148.3, 148.2, 148.0x2, 147.2, 146.8, 146.1x2, 145.8x2, 144.4, 144.1, 142.4, 142.1, 141.6x2, 141.5x2, 141.4x2, 141.3x2, 139.1x2, 139.0x2, 130.8, 130.5, 130.4, 130.2, 128.7x2, 128.4x2, 128.3, 128.2, 12.,0, 126.9, 126.8, 124.4x2, 124.3x2, 124.1x2, 124.0x2, 123.9, 123.8, 123.6, 123.4, 123.3, 123.2, 123.0, 121.5, 121.4, 121.3x3, 121.2, 121.1, 120.2x2, 109.8, 109.7x2, 109.6x3. ESI-HRMS (TOF) *m/z* $[M]^+$ calcd. for $C_{66}H_{45}N_3$ 879.3608, found 879.3603. Elemental analysis: Anal. Calcd for $C_{66}H_{45}N_3$: C, 90.07; H, 5.15; N. 4.77. Found: C, 89.63; H, 5.18; N, 4.75. R_f (50% $CHCl_3$/hexane) = 0.51.

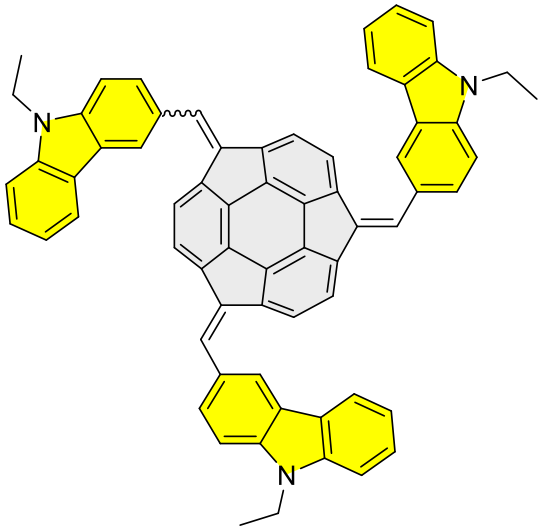

5

S1.3. Synthesis of compound 10.

A solution of 2-iodoosumanene (**8**; 37.0 mg, 0.095 mmol, 1 equiv.), copper(I) iodide (CuI; 1.0 mg, 0.00475 mmol, 0.05 equiv.) and bis(triphenylphosphine)palladium(II) dichloride ($Pd(PPh_3)_2Cl_2$; 6.7 mg, 0,0095 mmol, 0.1 equiv.) in triethylamine (TEA; 6 mL) was stirred under argon atmosphere at 45°C for 15 minutes. A solution of 1-ethynyl-4-(trifluoromethyl)benzene (**17**; 23.5 µL, 24.3 mg, 0,143 mmol, 1.5 equiv.) in TEA (5 mL) was added, and the reaction mixture was stirred under argon atmosphere at 45°C for 48 hours. Distilled water (10 mL) was added, and the crude product was extracted with CH_2Cl_2 (3x20 mL). Organic layers were combined, washed with 1M HCl (3x20 mL), water, and. After drying with $MgSO_4$ followed by filtration, volatiles were distilled off on a rotary evaporator. Finally, the product was purified using a PTLC (SiO_2, 30% CH_2Cl_2/hexane *Note 1*) to provide the target compound **10** as a light-yellow solid (29.6 mg, 72%).

*Note 1: Compound **10** can also be purified with PTLC (SiO_2) using 100% cyclohexane as the eluent (R_f = 0.25).*

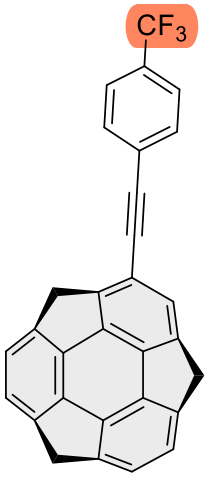

10

Compound 10. ^{1}H NMR ($CDCl_3$, 600 MHz, ppm) δ_H 7.64-7.61 (m, 4H), 7.27 (s, 1H), 7.15-7.1 (m, 4H), 4.78 (d, $^2J_{H-H}$ = 19.9 Hz, 1H), 4.73-4.72 (2xd, $^2J_{H-H}$ = 19.5 Hz, $^2J_{H-H}$ = 19.3 Hz, 2H), 3.62 (d, $^2J_{H-H}$ = 19.9 Hz, 1H), 3.64-3.42 (2xd, $^2J_{H-H}$ = 19.5 Hz, $^2J_{H-H}$ = 19.3 Hz, 2H). ^{19}F NMR ($CDCl_3$, 600 MHz, ppm) δ_F −62.60 ppm (s, 3F). {^{1}H}^{13}C NMR ($CDCl_3$; 150 MHz, ppm) 151.7, 149.3, 149.2x3, 149.1x2, 149.0x2, 148.8, 148.4, 148.3, 148.1, 131.9, 129.9 (q, $^2J_{C-F}$ = 32.7 Hz), 127.5, 126.9, 125.4 (q, $^3J_{C-F}$ = 3.7 Hz), 124.0x2, 124.1 (q, $^1J_{C-F}$ = 272.2 Hz), 123.5, 123.4, 117.2, 91.7, 89.5, 41.9x2, 41.8. ESI-HRMS (TOF) *m/z* $[M+H]^+$ calcd. for $C_{30}H_{16}F_3$ 433.1199, found 433.1120. R_f (50% $CHCl_3$/hexane) = 0.65.

S1.4. Synthesis of compound 3.

Compound **10** (16.0 mg, 0.039 mmol, 1 equiv.) was placed in a reaction test tube. Tetrabutylammonium bromide (TBAB; 10.0 mg, 0.020 mmol, 0.5 equiv.) was added, followed by the addition of dry THF (0.3 mL) and $NaOH_{aq}$ (30%, 2 mL). The reaction mixture was stirred under argon atmosphere for 5 min at room temperature. Solid 4-(9*H*-carbazol-9-yl)benzaldehyde (**6**; 85.0 mg, 0.312 mmol, 8 equiv.) was added in one portion, and the reaction mixture was stirred under argon atmosphere for 72 hours at room temperature. Distilled water (6 mL) was added, and the crude product was extracted with CH_2Cl_2 (3x20 mL). Organic layers were combined, washed with saturated NH_4Cl, water, and brine. After drying with $MgSO_4$ followed by filtration, volatiles were distilled off on a rotary evaporator. Finally, the product was purified using a PTLC (SiO_2, 50% CH_2Cl_2/hexane) to provide the target compound **3** as a red solid (22.3 mg, 48%).

Compound 3. ^{1}H NMR (THF-d_8, 600 MHz, ppm) δ_H 8.33-8.21 (m, 4H), 8.19-8.01 (m, 8H), 7.90-7.67 (m, 11H), 7.65-7.58 (m, 5H), 7.55-7.48 (m, 3H), 7.45-7.35 (m, 6H), 7.32-7.06 (m, 11H). ^{19}F NMR ($CDCl_3$, 600 MHz, ppm) δ_F −63.45 - −63.48 ppm (m, 3F). {^{1}H}^{13}C NMR (THF-d_8; 150 MHz, ppm) δ_C 149.3, 149.0, 148.5, 148.4, 148.3x2, 147.2, 147.0, 146.7, 146.4, 146.2, 145.4, 145.1, 144.6, 144.5x2, 144.4, 144.3, 141.9, 141.8x2, 141.7x3, 141.6x3, 139.7, 139.6x2, 139.5, 136.4, 136.3x2, 136.2x2, 134.1, 133.0x2, 132.6x4, 132.5x4, 132.4x4, 132.3x2, 132.2, 131.9, 131.1, 129.8, 129.6, 129.5, 129.4, 129.3x2, 129.1, 129.0x2, 128.1x3, 128.0x4, 127.9, 127.1, 127.0, 126.9x3, 126.8x2, 126.7, 126.6, 126.3, 125.9, 125.6, 125.4, 125.3, 125.2, 125.0x2, 124.9x3, 124.8, 124.7, 124.6, 124.5, 123.0, 122.9, 121.3x2, 121.2, 121.1x2, 121.0, 120.9, 110.8x3, 110.7x4, 110.6x2, 93.4, 93.2, 92.7, 92.4. ^{1}H DOSY NMR (500 MHz, THF-d_8), D 4.78·10^{-10} m^2/s. ^{19}F DOSY NMR (500 MHz, THF-d_8), D 4.76·10^{-10} m^2/s. ESI-HRMS (TOF) *m/z* $[M]^+$ calcd. for $C_{87}H_{48}F_3N_3$ 1191.3795, found 1191.3778. Elemental analysis: Anal. Calcd for $C_{87}H_{48}F_3N_3$: C, 87.64; H, 4.06; N, 3.52. Found: C, 87.20; H, 4.08; N, 3.50. R_f (50% CH_2Cl_2/hexane) = 0.40.

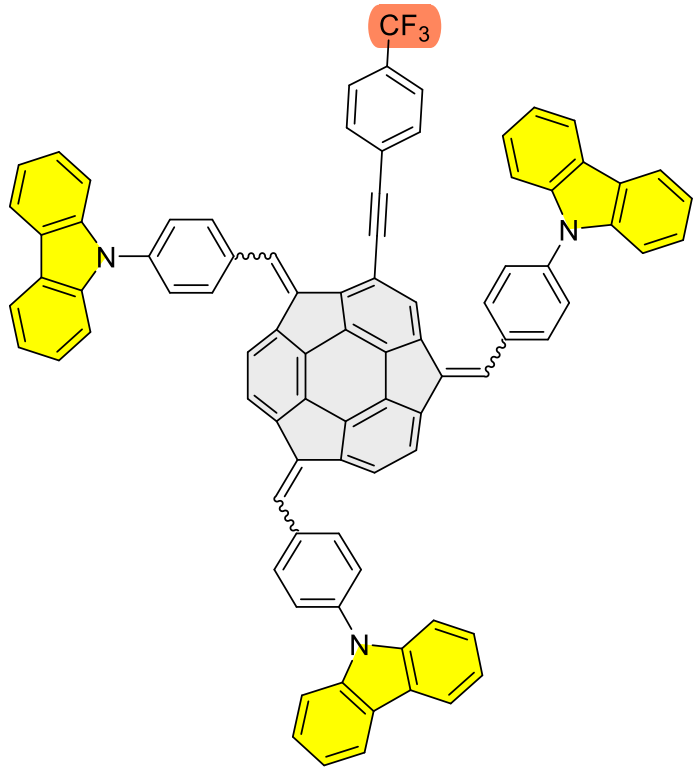

3

S1.5. Cation binding experiments.

The cation binding experiments between compounds **3-5** (optical chemoreceptors) and metal cations (analytes; Na^+, K^+, Li^+, Cs^+) were performed employing the emission spectra titration experiments. In the case of Na^+, K^+, Li^+ and Cs^+ hexafluorophosphate (PF_6^-) salts were used. The experiments were performed in the THF:H_2O 1:1 *v*/*v* solvent mixture as follows. Stock solutions of analyte ($1.5 \cdot 10^{-3}$ M or $6.0 \cdot 10^{-3}$ M in the case of compounds **4-5**, $1.5 \cdot 10^{-4}$ M or $6.0 \cdot 10^{-4}$ M in the case of compound **3**) in THF:H_2O 1:1 *v*/*v* were added to the solution of receptor ($2 \cdot 10^{-5}$ M in the case of compounds **4-5** and $2 \cdot 10^{-6}$ M in the case of compound **3**) in THF:H_2O 1:1 *v*/*v* (3 mL) to reach given receptor-to-cation molar ratio. The selectivity studies were performed as follows. Proper portions of stock solutions of $NaPF_6$, KPF_6, $LiPF_6$ and $CsPF_6$ ($6.0 \cdot 10^{-3}$ M in the case of compounds **4-5**, $6.0 \cdot 10^{-4}$ M in the case of compound **3**) in THF:H_2O 1:1 *v*/*v* were added in this order to the solution of the receptor ($2 \cdot 10^{-5}$ M in the case of compounds **4-5** and $2 \cdot 10^{-6}$ M in the case of compound **3**) in THF:H_2O 1:1 *v*/*v* (3 mL) to reach receptor-to-cation molar ratio of 1:5 in each case. The final solution contained the receptor, Na^+ (5 equiv.), K^+ (5 equiv.), Li^+ (5 equiv.) and Cs^+ (5 equiv.).

S1.6. Estimation of fluorescence quantum yield for 3-5

The measurements were performed at room temperature according to the published procedures.[6–8] Fluorescence quantum yields (Φ_F) were determined by comparison with known standard, namely Rhodamine 6G (R6G) in ethanol (EtOH; $\Phi_{F,ref} = 0.95$[7]). The concentrations for the reference and sample solutions were adjusted and, sequentially, excitations wavelengths were selected, as presented in **Figure S1**. The concentrations (*C*; diluted solutions, absorbance for the highest wavelength A < 0.1 a.u.) and selected excitation wavelengths (λ_{ex}) were as follows:

- $C_{R6G} = 9 \cdot 10^{-7}$ M.
- $C_{\mathbf{3}} = 2 \cdot 10^{-7}$ M; $\lambda_{ex} = 511$ nm.
- $C_{\mathbf{4}} = 2 \cdot 10^{-6}$ M; $\lambda_{ex} = 502$ nm.
- $C_{\mathbf{5}} = 1 \cdot 10^{-6}$ M; $\lambda_{ex} = 504$ nm.

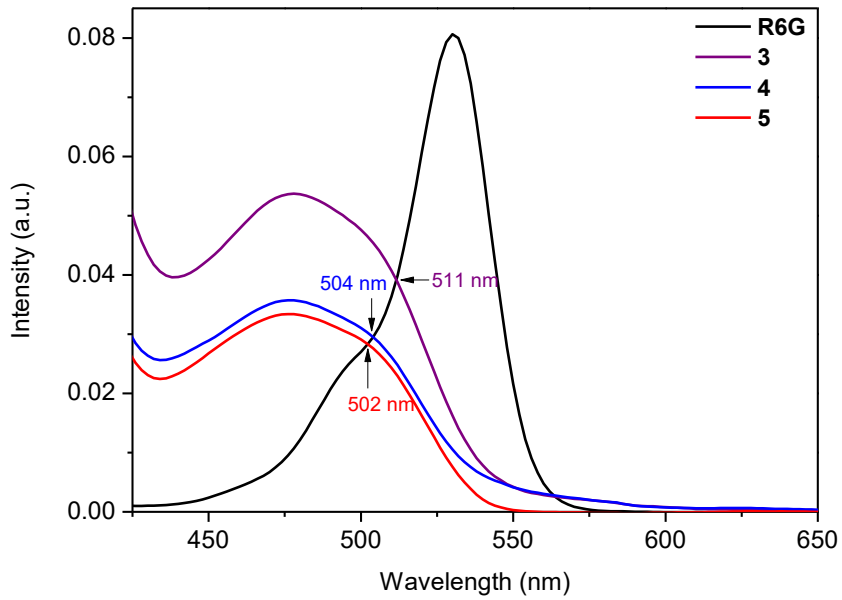

Figure S1. UV-vis spectra of compounds **3** ($CHCl_3$; $2{\cdot}10^{-7}$ M), **4** ($CHCl_3$; $2{\cdot}10^{-6}$ M), **5** ($CHCl_3$; $1{\cdot}10^{-6}$ M), and R6G (EtOH; $9{\cdot}10^{-7}$ M), for the selection of λ_{ex} regarding the fluorescence quantum yield (Φ_F) measurements.

The following formula was used for the calculation of Φ_F:

$$\phi_F = \phi_{F,ref} \cdot \frac{F_{compound}}{F_{reference}} \cdot \frac{n^2_{compound}}{n^2_{reference}}$$

where $\Phi_{F,ref}$ is the quantum yield for R6G (0.95[7]), F is the integral photon flux taken as integrated area under the fluorescence spectra, n is the refractive index of the solvent (1.3614 for EtOH, 1.4458 for $CHCl_3$), absorption factors component in the equation was omitted, since the determined absorbances for the sample and reference matched, see **Figure S1**).

S2. NMR spectra

S2.1. NMR spectra of compound 5 and discussion

The ^{1}H NMR (**Figure S4**) and {^{1}H}^{13}C NMR (**Figure S9**) spectra of compound **5** were relatively complex since compound **5** exists as a mixture of two diastereoisomers, a C_3-symmetrical and unsymmetrical one (see **Figure S2**). Overlapping of the signals coming from these diastereoisomers resulted in the multiplication of the signals in the NMR spectra.

The most direct conclusions could be drawn from ^{1}H NMR spectra analyzes. In the case of ^{1}H NMR spectra, 11 groups and 36 groups of signals shall be observed for the symmetrical and unsymmetrical diastereoisomer, respectively (see **Figure S3**). The signals found in the ^{1}H NMR spectra were carefully assigned to the given groups of protons, based on the spin-spin couplings observed on the ^{1}H-^{1}H COSY NMR spectrum (see **Figure S5** and **Figure S6**). The two multiplets labelled in pink (4.52-4.39 ppm) were ascribed to six protons of methylene (CH_2) groups bonded to nitrogen atoms. The two multiplets marked in light purple (1.48-1.36 ppm) corresponded to the nine protons of methyl (-CH_3) groups. The two multiplets located at 8.70-8.56 ppm were ascribed to 3H labelled in green. The multiplet at 8.18-8.13 ppm were ascribed to the 6H labelled in grey and red. The signals from the protons labelled yellow and orange were split, and formed multiplets at 7.75-7.66 ppm, 7.54-7.42 ppm and 7.29-7.21 ppm. These multiplets correspond to a total of 21H, including 6H from the aromatic positions of sumanene (orange), 3H from methidene (=CH-) groups (yellow). The remaining protons, *i.e.*, 3H marked in blue, 3H marked in dark purple, 3H marked in dark green, and 3H marked in dark blue, were further analyzed. **Figure S6** shows an inset of the ^{1}H-^{1}H COSY NMR spectrum of compound **5**. Correlations of protons labelled in dark purple with protons labelled in dark green and dark blue were observed. The correlations of protons labelled in dark blue with protons labelled in grey and dark purple were also detected. A long-range cross-correlation (through four bonds) was observed between the protons labelled in light green and red. This phenomenon was also confirmed with the ^{1}H-^{1}H COSY NMR experiment for the starting material (aldehyde **7**; **Figure S7**). The signal from the grey-labelled protons overlapped with the red-labelled signal, as determined by other correlations for protons coupled to the grey-labelled protons. The correlation of the grey-labelled protons and the protons marked with dark blue color was determined by comparing with the profile of the ^{1}H NMR spectrum of aldehyde **7**, see **Figure S8**. An analogy was concluded when assigning the correlation of the protons labelled with dark blue and dark violet, and when determining the correlation of the protons labelled with dark green and the dark violet. After assigning the above protons to their respective signals, nine protons (1.5H + 4.5H + 3H) remained. The first two (1.5+4.5H) give a total of 6H and were ascribed from the aromatic positions of sumanene (orange). The remaining 3H were ascribed to methidene protons (yellow).

The {^{1}H}^{13}C NMR spectrum (**Figure S9**) of compound **5** comprised the signals that were ascribed to the presence of carbon nuclei coming from sumanene and carbazole moieties, as well as linkers between these motifs. The multiplication of the signals (see

the inset of the {^{1}H}^{13}C NMR spectrum in **Figure S10**) was the result of the presence of diastereoisomers of **5** in the sample. Notably, signals coming from the methylene (CH_2) and methyl (CH_3) groups could be identified with the ^{1}H-^{13}C HSQC spectrum (see **Figure S11** and insets in **Figure S12**), by the presence of 38.3-38.0 ppm ↔ 4.52-4.38 ppm (CH_2) and 14.2-14.1 ppm ↔ 1.49-1.36 ppm (CH_3) cross-correlations.

ESI-HRMS (TOF) experiment (see spectrum in Section S3) ultimately supported the formation of **5**, *i.e.*, the calculated and measured spectra were consistent (m/z $[M]^+$ calcd. for $C_{66}H_{45}N_3$ 879.3608, found 879.3603). The purity of the **5** sample was also further supported with elemental analysis (Anal. Calcd for $C_{66}H_{45}N_3$: C, 90.07; H, 5.15; N. 4.77. Found: C, 89.52; H, 5.18; N, 5.12.).

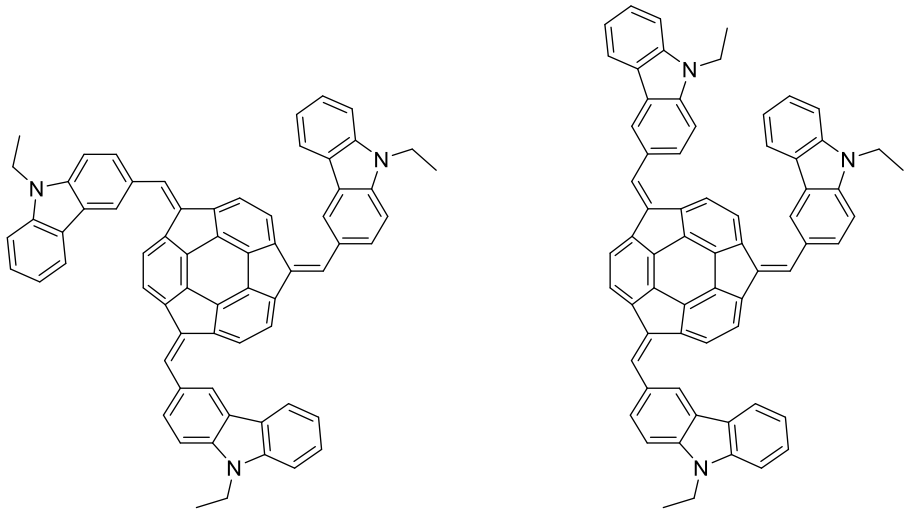

Figure S2. Diastereoisomers forming compound **5**. The DFT-optimized structures of those diastereoisomers are presented and discussed in Section S5.

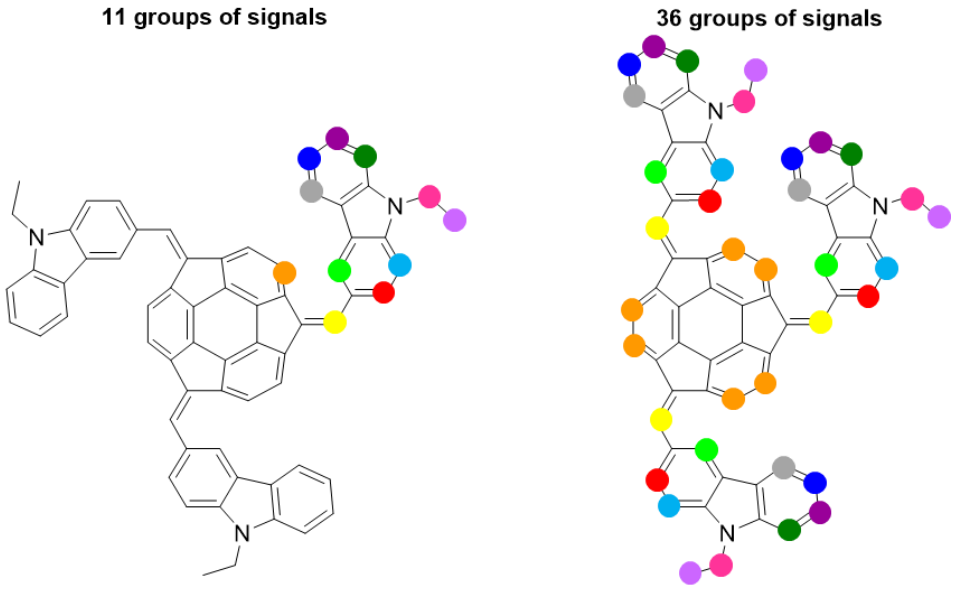

Figure S3. Graphical representation of the number and types of signals observed in the ^{1}H NMR spectrum of compound **5** (left – symmetrical diastereoisomer, right – unsymmetrical diastereoisomer). The same color does not correspond to the same chemical shift in the ^{1}H NMR spectrum.

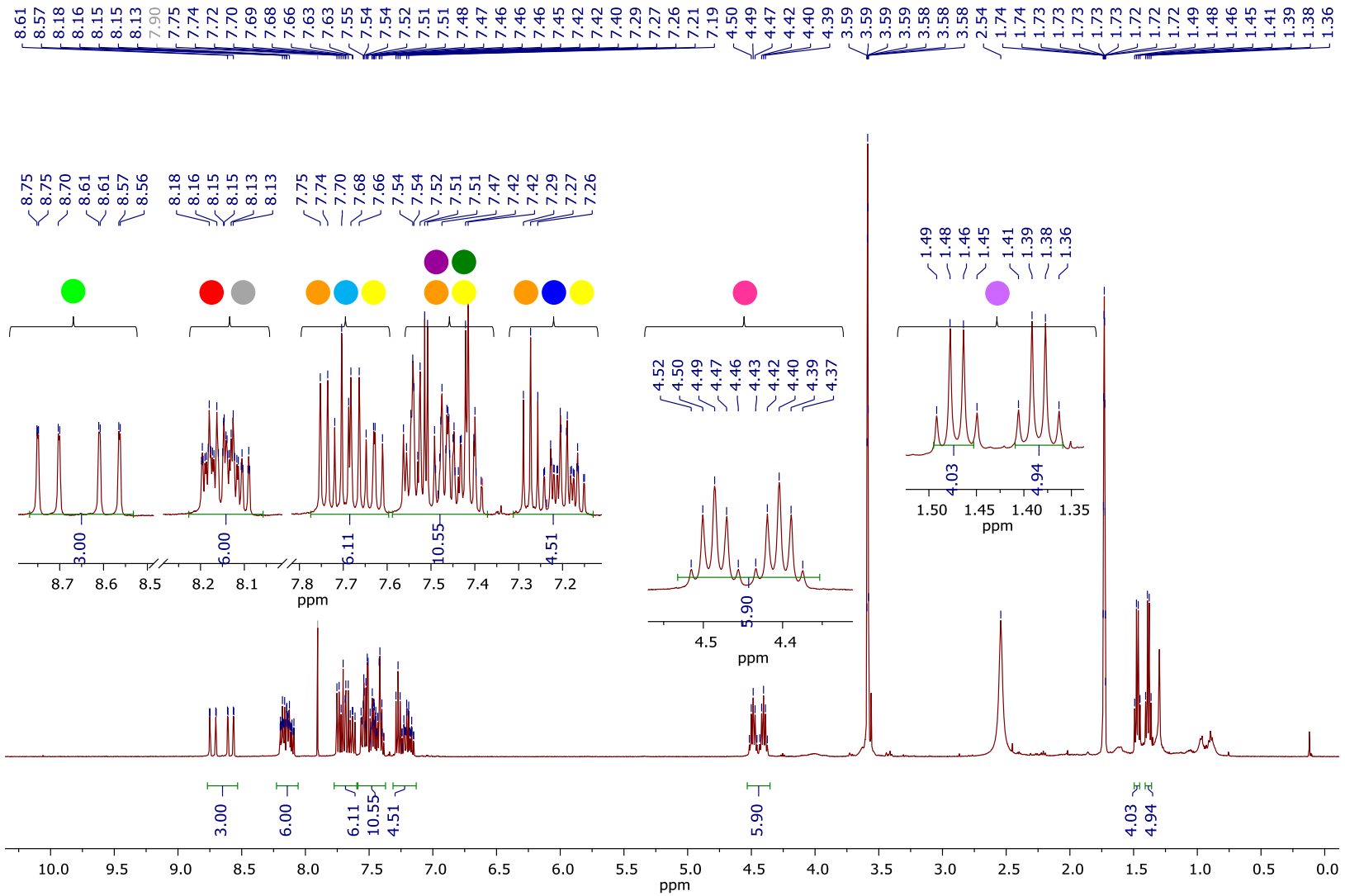

Figure S4. ^{1}H NMR (500 MHz, THF-d_8) spectrum of compound **5** together with the protons' assignations (for the labels, see **Figure S3**).

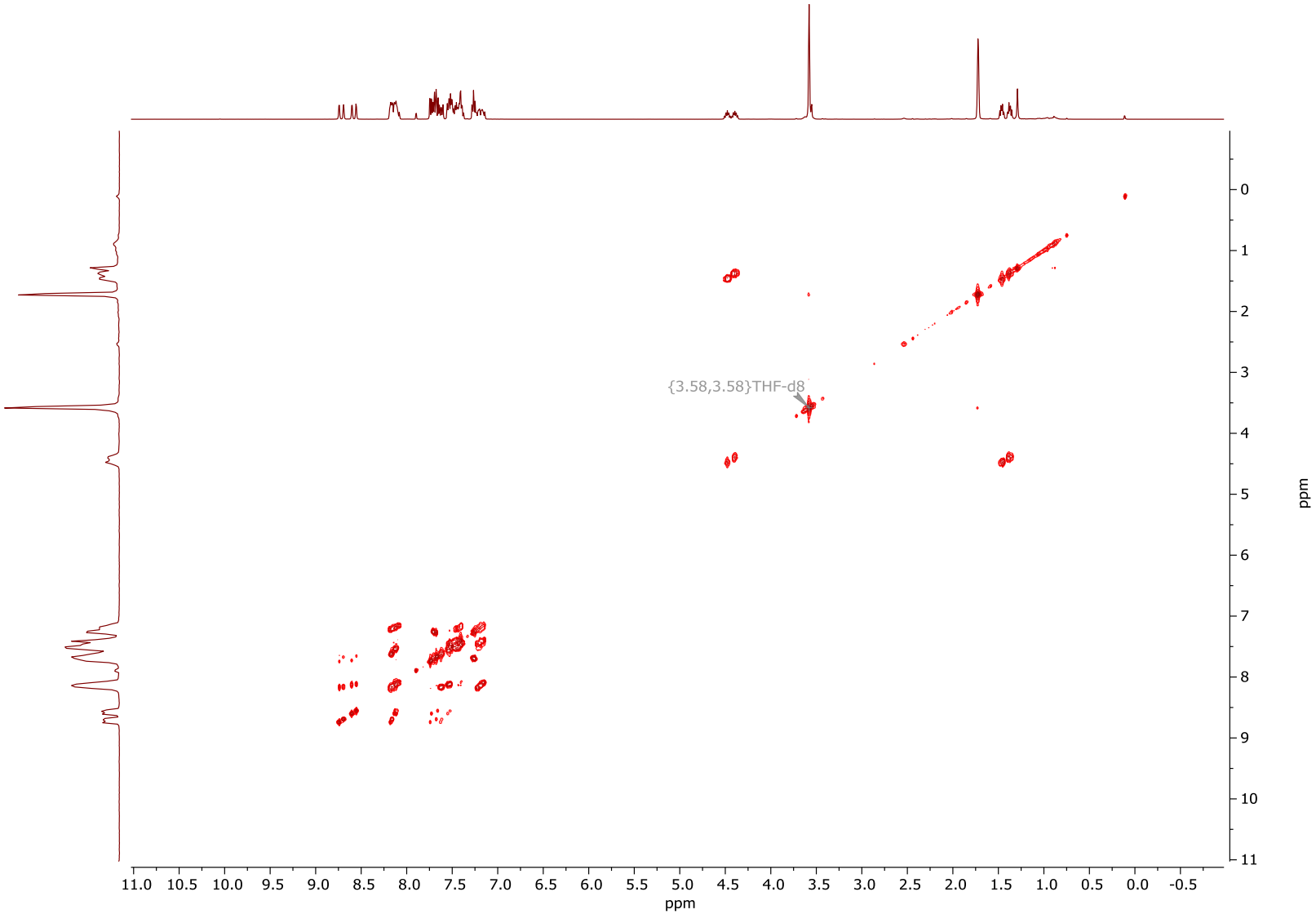

Figure S5. ^{1}H-^{1}H COSY NMR (500 MHz, THF-d_8) spectrum of compound **5**.

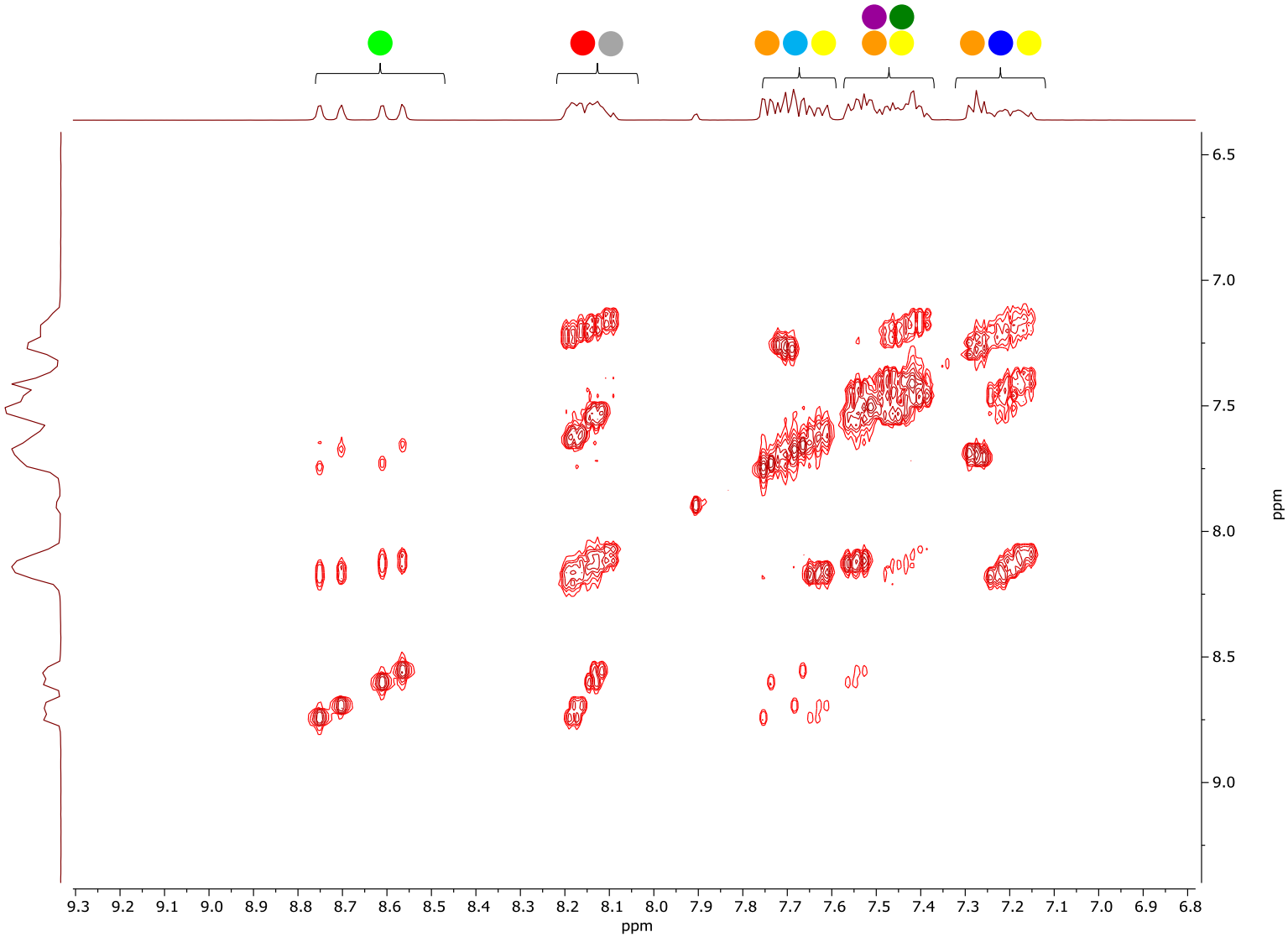

Figure S6. Inset (9.30-6.70 ppm) of the ^{1}H-^{1}H COSY NMR (500 MHz, THF-d_8) spectrum of compound **5** together with the protons' assignations (for the labels, see **Figure S3**).

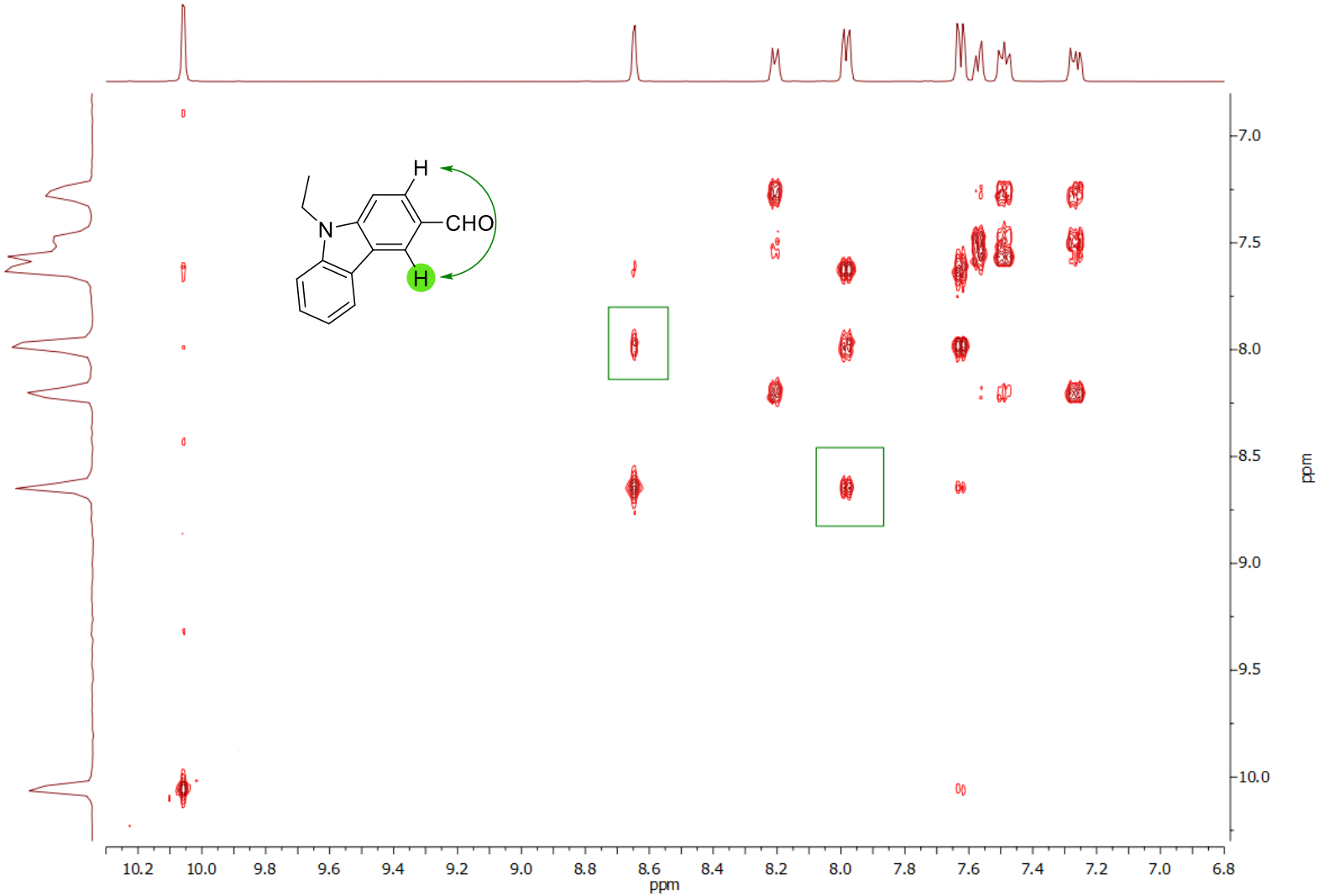

Figure S7. Inset (10.30-6.80 ppm) of the ^{1}H-^{1}H COSY NMR (500 MHz, THF-d_8) spectrum of the starting material (aldehyde) **7**. The green frame highlights the crucial long-range cross-correlation (through four bonds; the compound **7** structure is also presented).

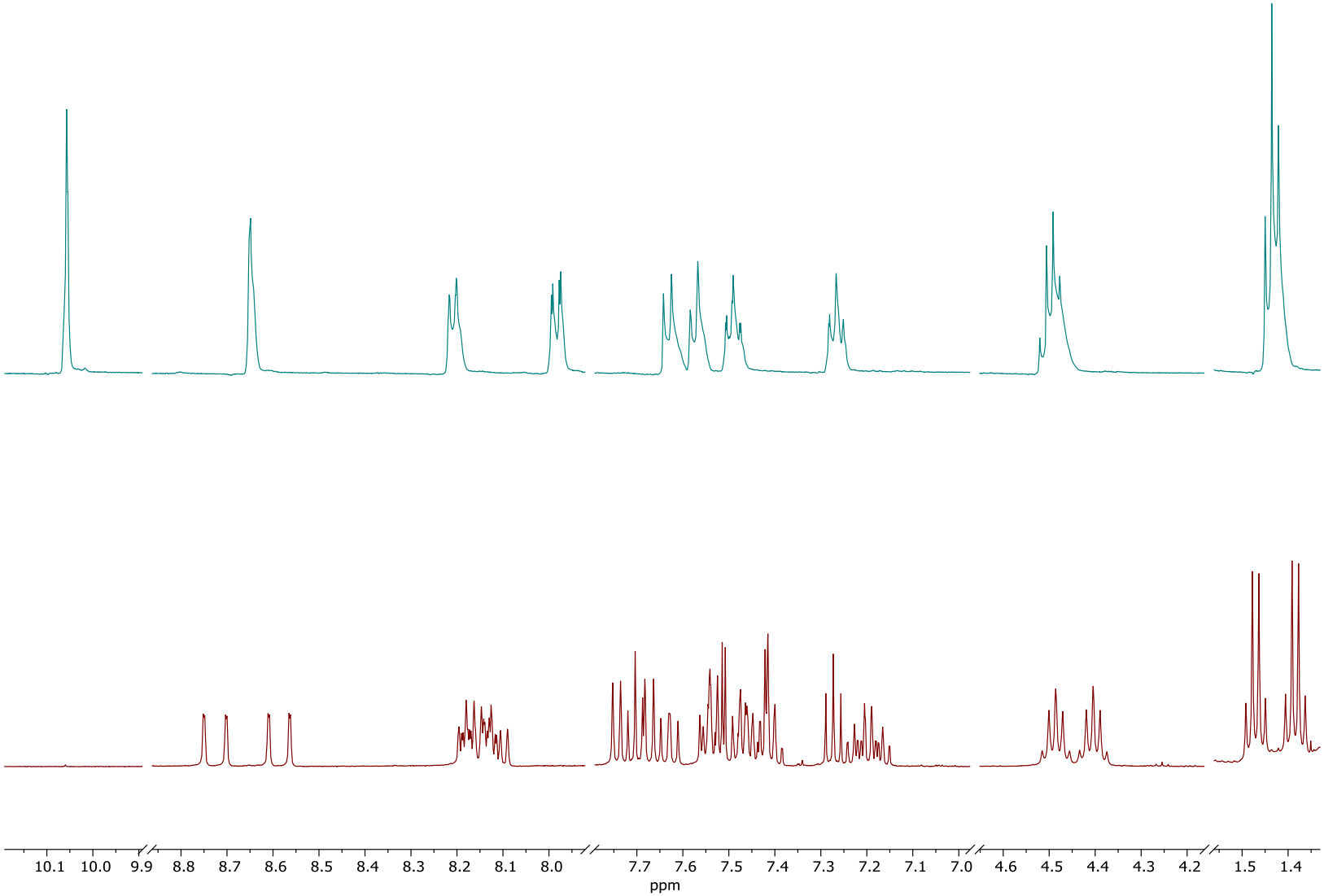

Figure S8. Comparison of the ^{1}H NMR (500 MHz, THF-d_8) spectra of starting material (aldehyde) **7** (top) and compound **5** (bottom).

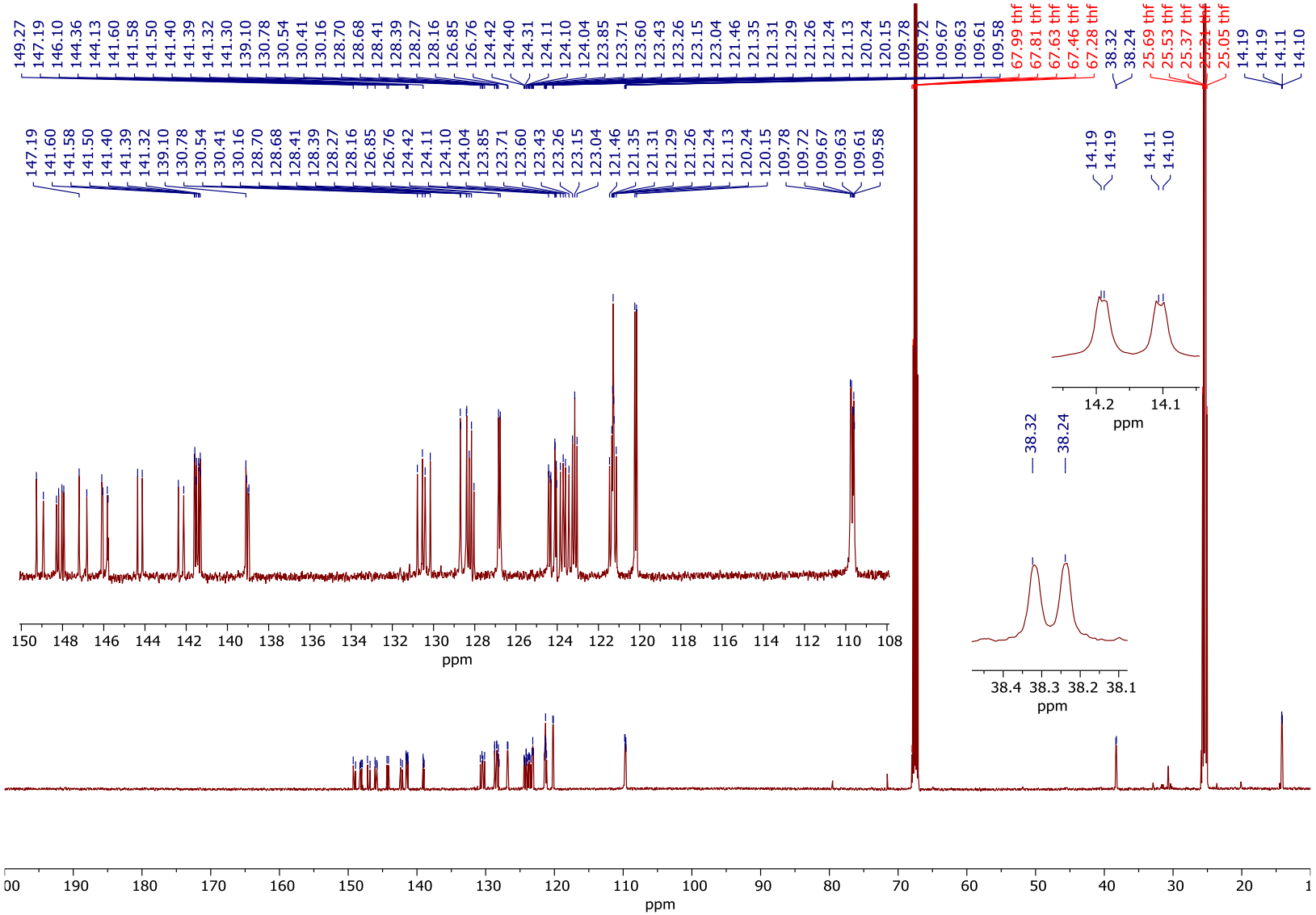

Figure S9. {^{1}H}^{13}C NMR (500 MHz, THF-d_8) spectrum of compound **5**.

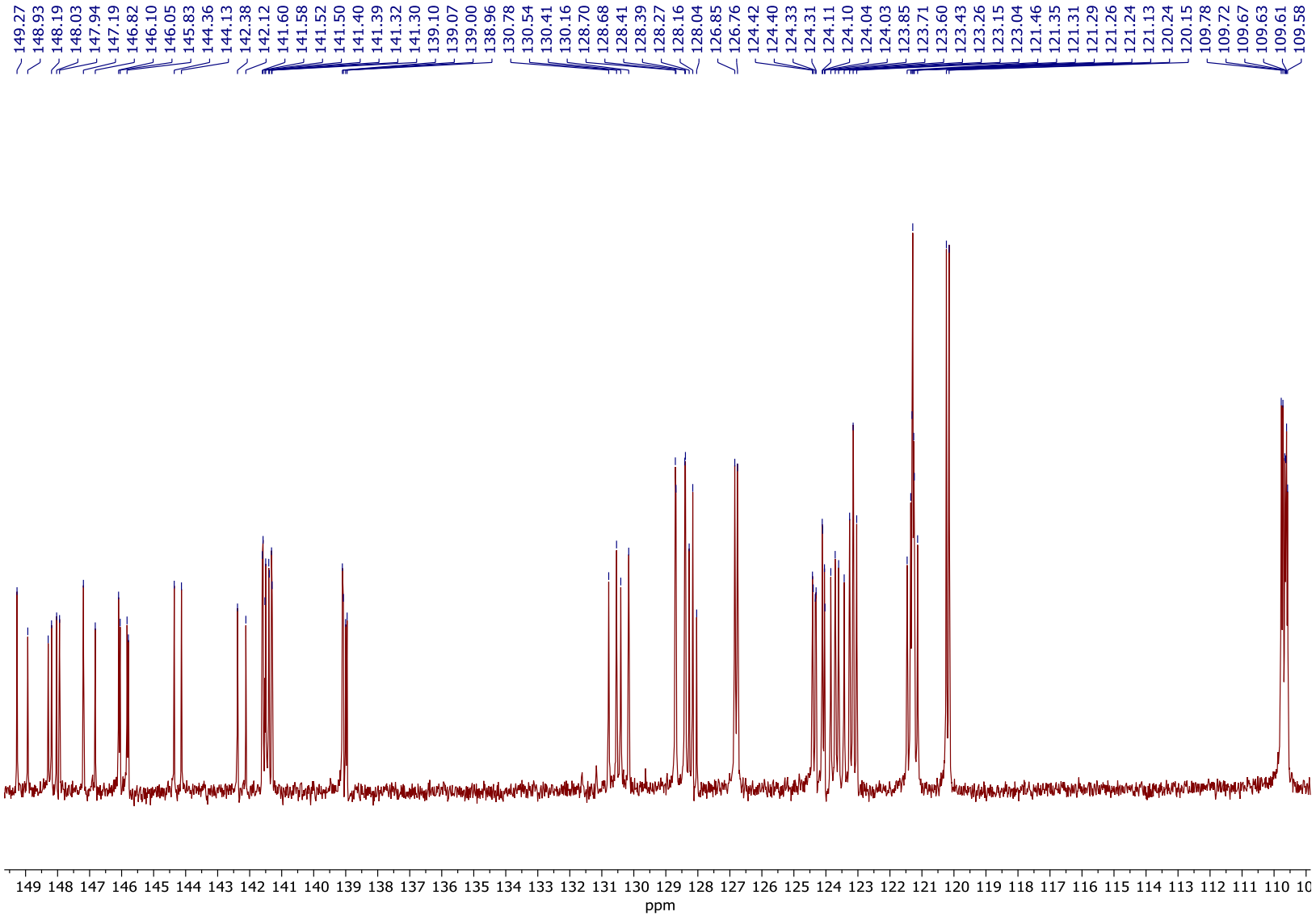

Figure S10. Inset (149.5-109.0 ppm) of the $\{^{1}H\}^{13}C$ NMR (500 MHz, THF-d_8) spectrum of compound **5**.

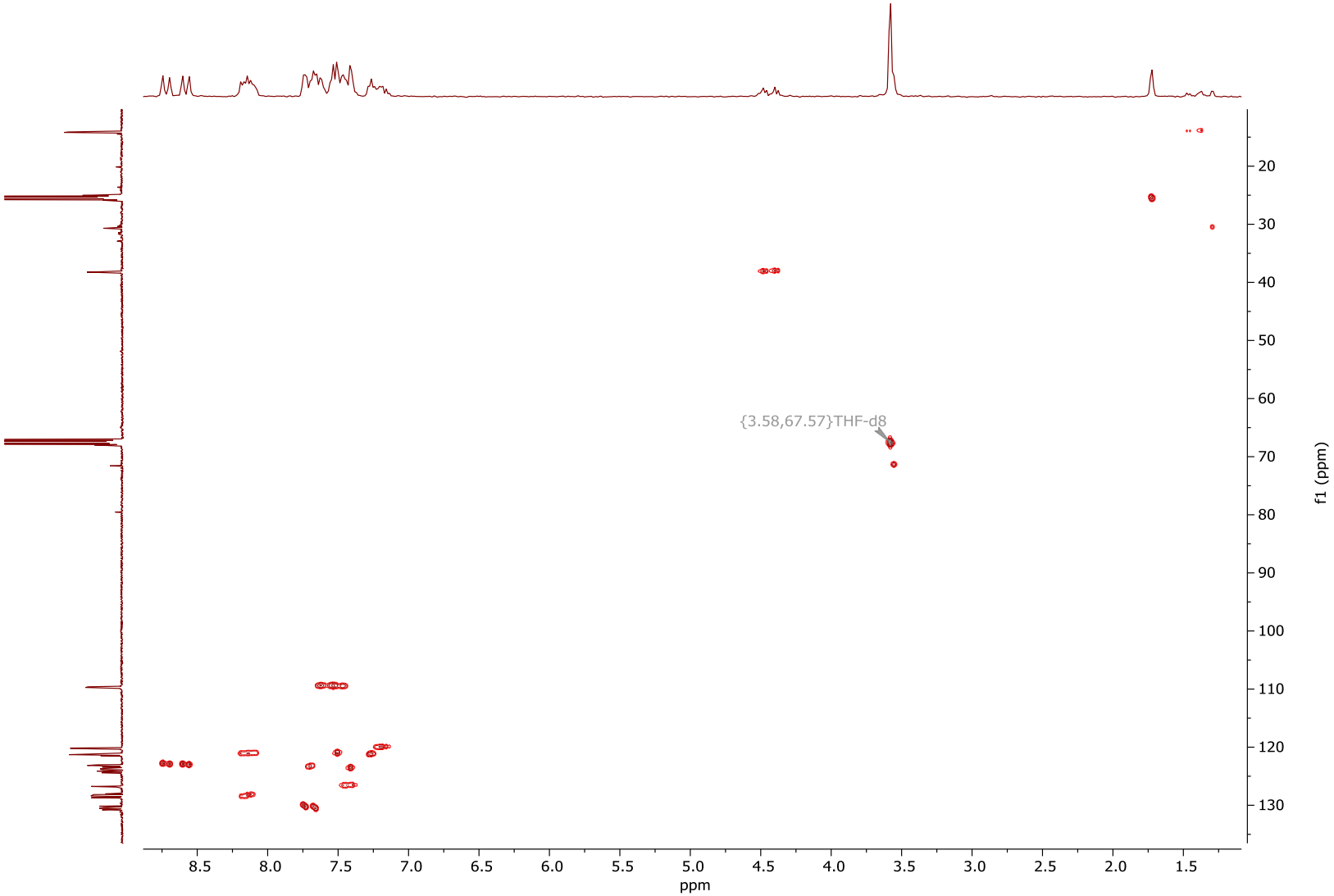

Figure S11. ^{1}H-^{13}C HSQC NMR (THF-d_8) spectrum of compound **5**.

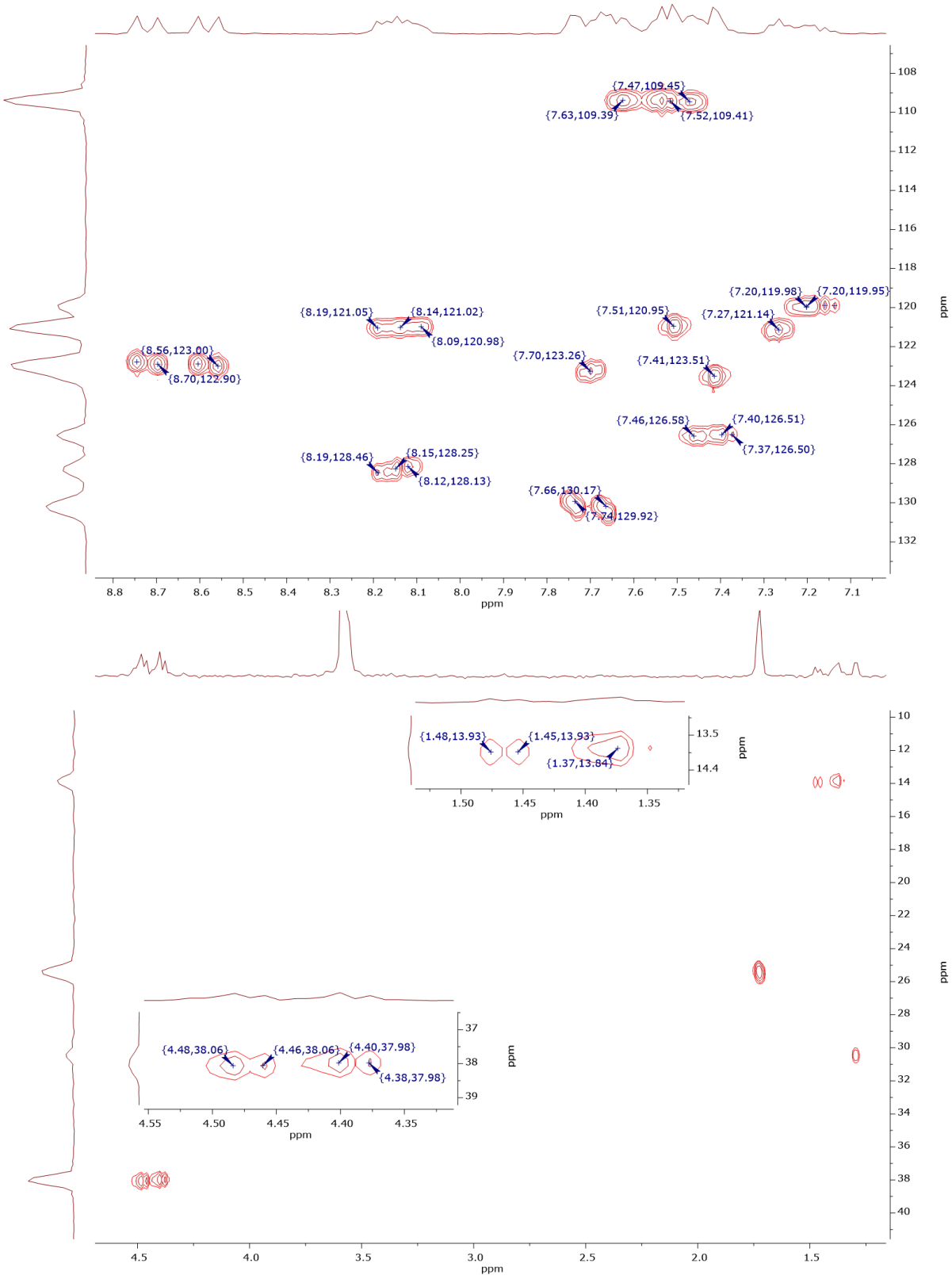

Figure S12. Insets of the ^{1}H-^{13}C HSQC NMR (THF-d_8) spectrum of compound **5**.

S2.2. NMR spectra of compound 4 and discussion

The ^{1}H NMR (**Figure S15**) and {^{1}H}^{13}C NMR (**Figure S18**) spectra of compound **4** are presented below. Similarly to the NMR spectra of compound **3**, the NMR spectra of compound **4** were relatively complex due to the presence of two diastereoisomers of compound **4** (see **Figure S13**). The signals' shifts for these diastereoisomers did not differ significantly. This overlapping resulted in the multiplication of the signals in the NMR spectra.

The most essential signals assignments were achieved for the ^{1}H NMR spectra. **Figure S14** shows the structure of compound **4** with the assignations of the protons in the ^{1}H NMR spectra. Signals in the ^{1}H NMR spectrum of **4** were assigned based on the spin-spin couplings observed in the ^{1}H-^{1}H COSY NMR spectrum (see **Figure S16** and **Figure S17**). In general, 8 groups of signals and 27 groups of signals shall be observed for the C_3-symmetrical and unsymmetrical diastereoisomer, respectively. The multiplets labelled in brown and blue (8.28-8.17 ppm) corresponded to a total of 12H and were ascribed to the protons of the phenylene rings from the linker and protons within the carbazole unit. Signals from protons labelled in yellow and orange were split and were found in the spectrum as multiplets located at 7.79-7.67 ppm, 7.59-7.52 ppm and 7.44-7.35 ppm. Among these, 6H was ascribed to the protons located at the aromatic positions of sumanene (orange), 3H were ascribed to the methidene (=CH-) moieties (yellow). The remaining 18H were ascribed to the latter protons coming from the introduced structural moieties, that is 6H protons labelled in dark green, 6H labelled in purple, and 6H labelled in light green. The multiplet (6H) labelled in pink (7.28-7.26 ppm) was ascribed to the protons of the phenylene rings closer to the methidene linkers.

The {^{1}H}^{13}C NMR spectrum (**Figure S18**) of compound **4** comprised the signals coming from the carbon nuclei of sumanene and carbazole moieties, as well as *p*-phenylene between these motifs. The presence of two diastereoisomers of **4** in the sample resulted in the multiplication of the signals, for clarity see the inset of the {^{1}H}^{13}C NMR spectrum in **Figure S19**. These findings were further with the ^{1}H-^{13}C HSQC experiment (see **Figure S20** and inset in **Figure S21**).

ESI-HRMS (TOF) experiment (see spectrum in Section S3) ultimately supported the formation of **4**, *i.e.*, the calculated and measured spectra were consistent (m/z [M]$^{+}$ calcd. for $C_{78}H_{45}N_3$ 1024.3686, found 1024.3801). The purity of the **4** sample was also further supported with elemental analysis (Anal. Calcd for $C_{78}H_{45}N_3$: C, 91.47; H, 4.43; N, 4.10. Found: C, 90.74; H, 4.46; N, 4.07).

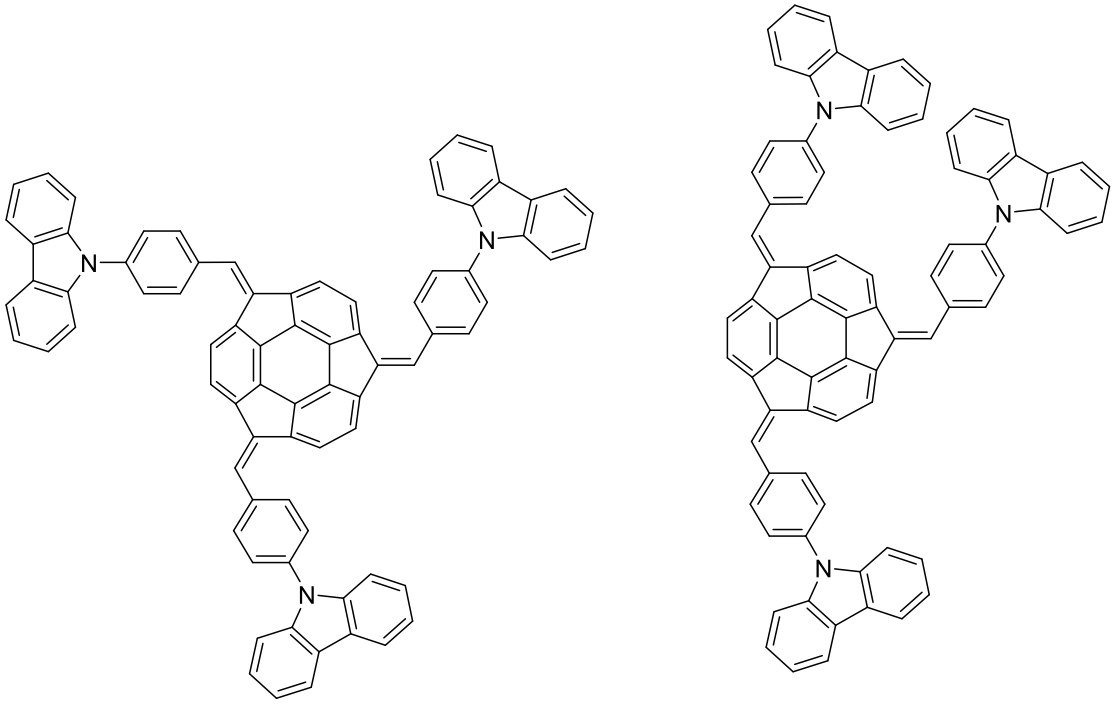

4 - symmetrical diastereoisomer

4 - unsymmetrical diastereoisomer

Figure S13. Diastereoisomers forming compound **4**. The DFT-optimized structures of those diastereoisomers are presented and discussed in Section S5.

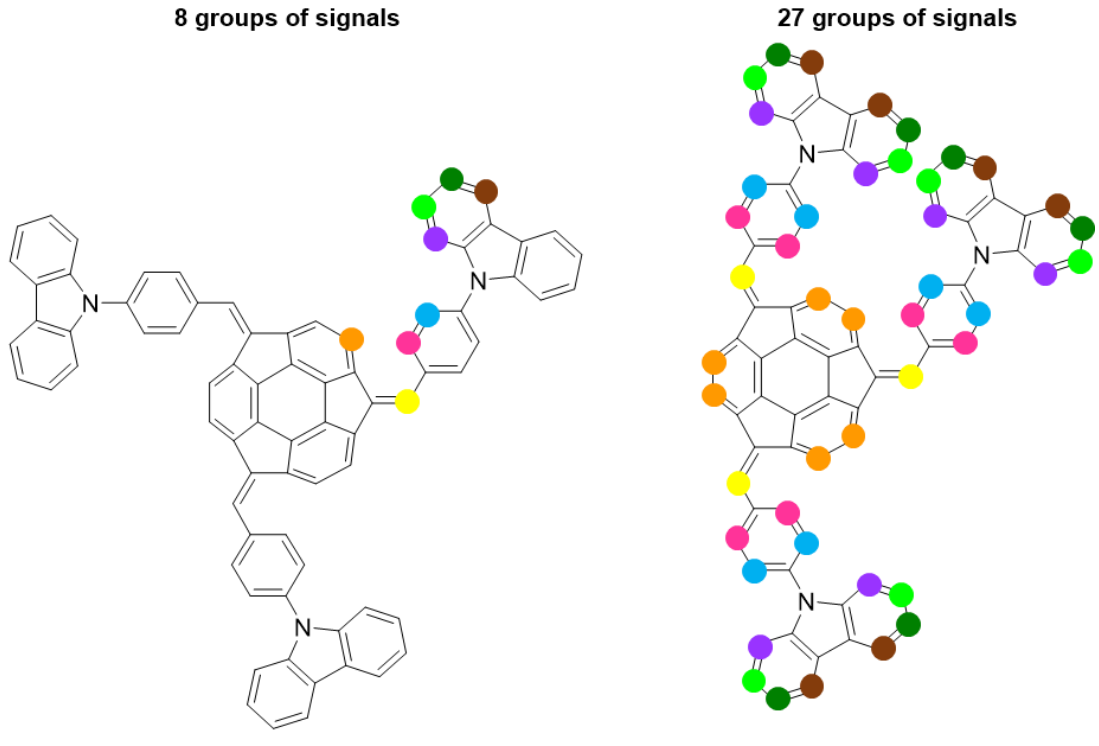

4 - symmetrical diastereoisomer

4 - unsymmetrical diastereoisomer

Figure S14. Graphical representation of the number and types of signals observed in the ^{1}H NMR spectrum of compound **4**. The same color does not correspond to the same chemical shift in the ^{1}H NMR spectrum.

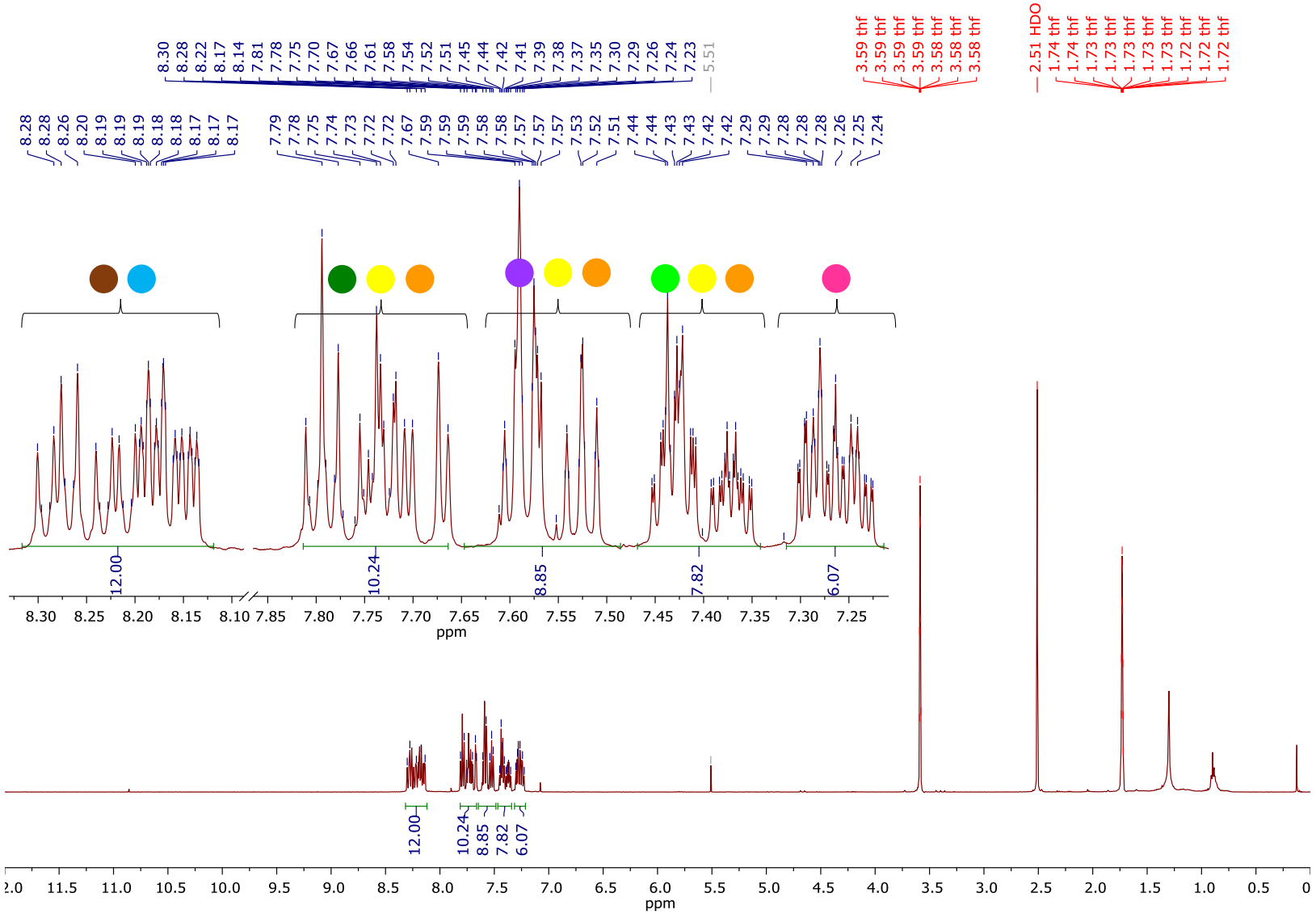

Figure S15. ^{1}H NMR (500 MHz, THF-d_8) spectrum of compound **4** together with the protons' assignations (for the labels, see **Figure S14**).

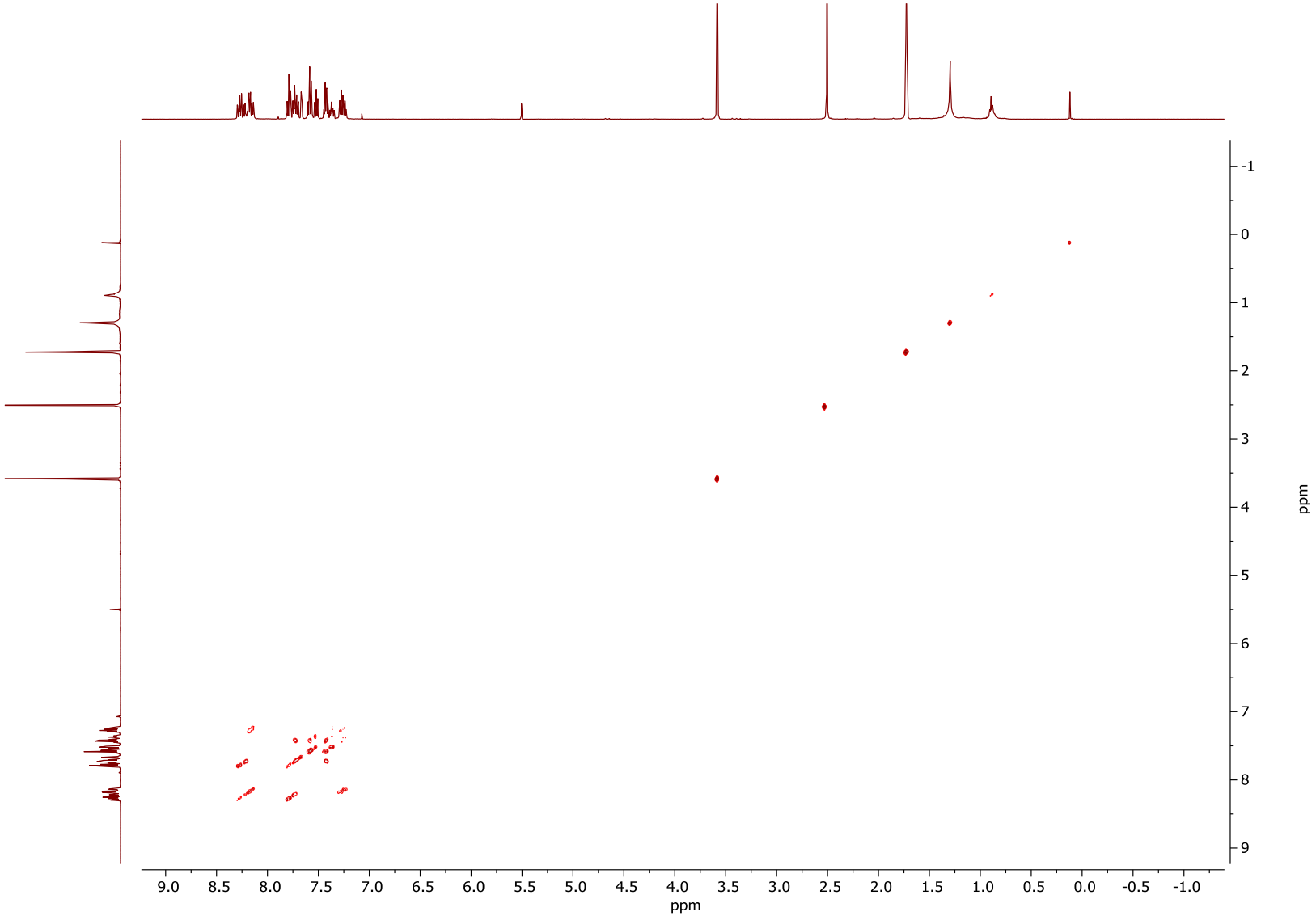

Figure S16. ^{1}H-^{1}H COSY NMR (500 MHz, THF-d_8) spectrum of compound **4**.

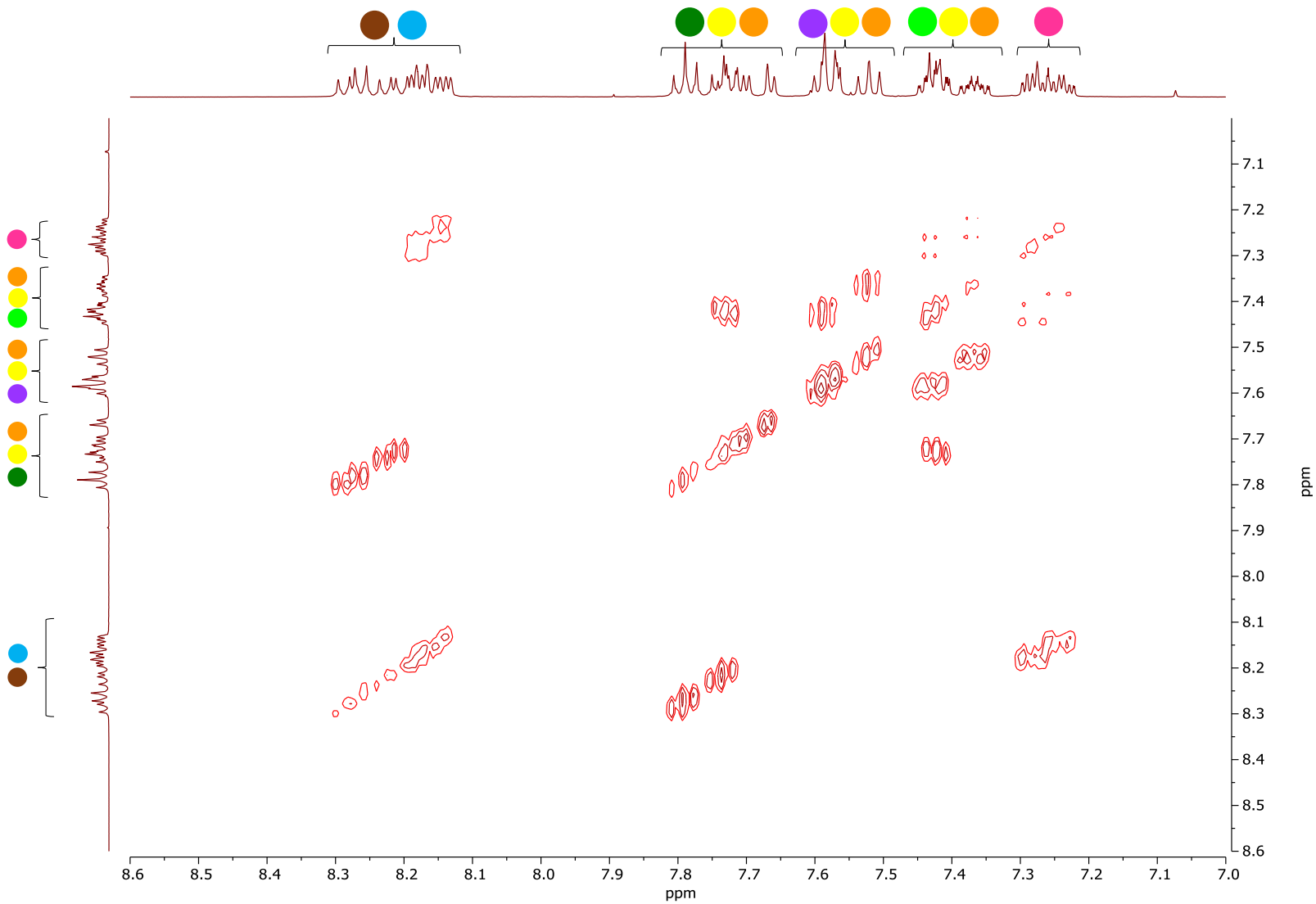

Figure S17. Inset (8.60-7.00 ppm) of the ^{1}H-^{1}H COSY NMR (500 MHz, THF-d_8) spectrum of compound **4** together with the protons' assignations (for the labels, see **Figure S14**).

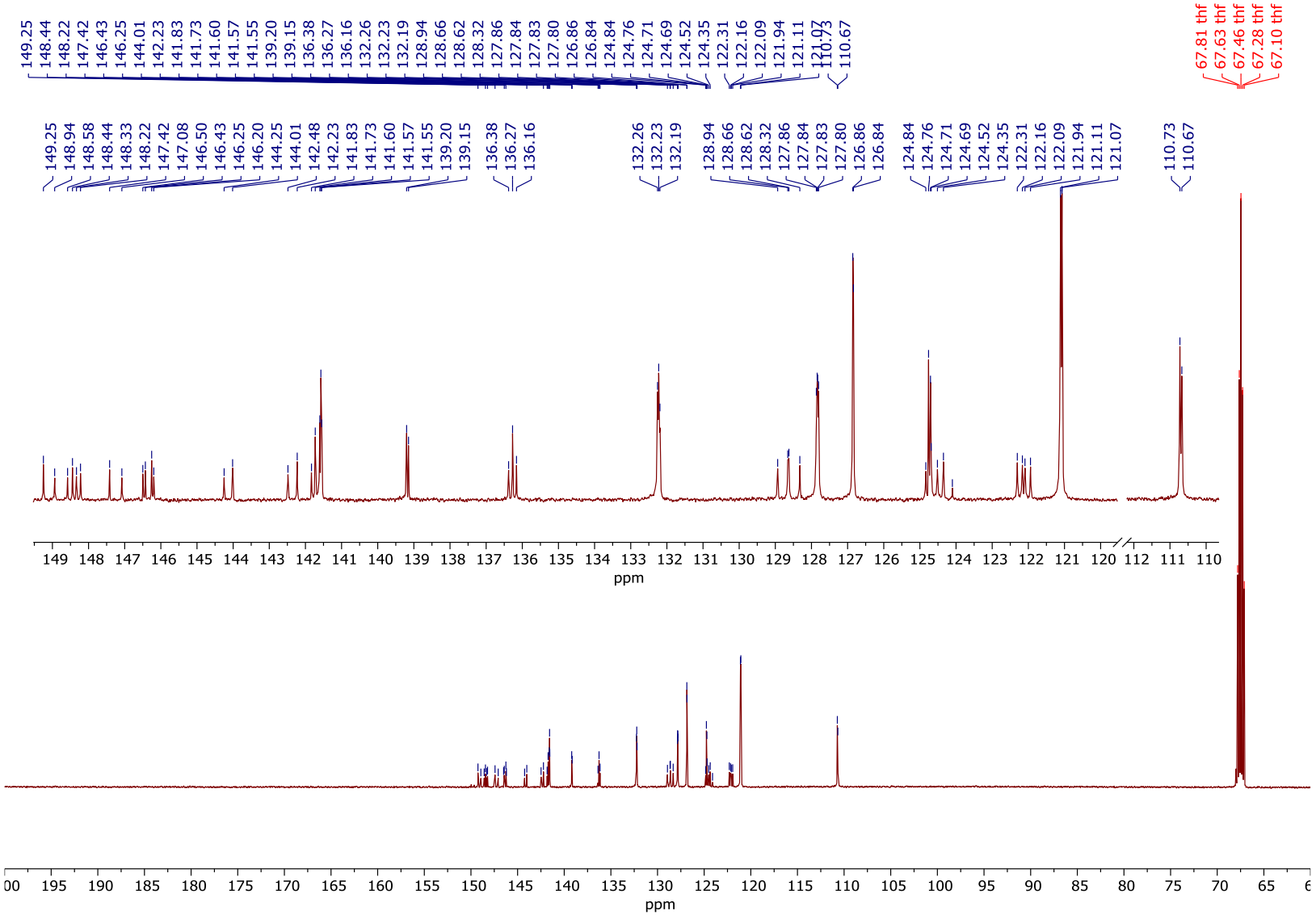

Figure S18. $\{^{1}H\}^{13}C$ NMR (125 MHz, THF-d_8) spectrum of compound **4**.

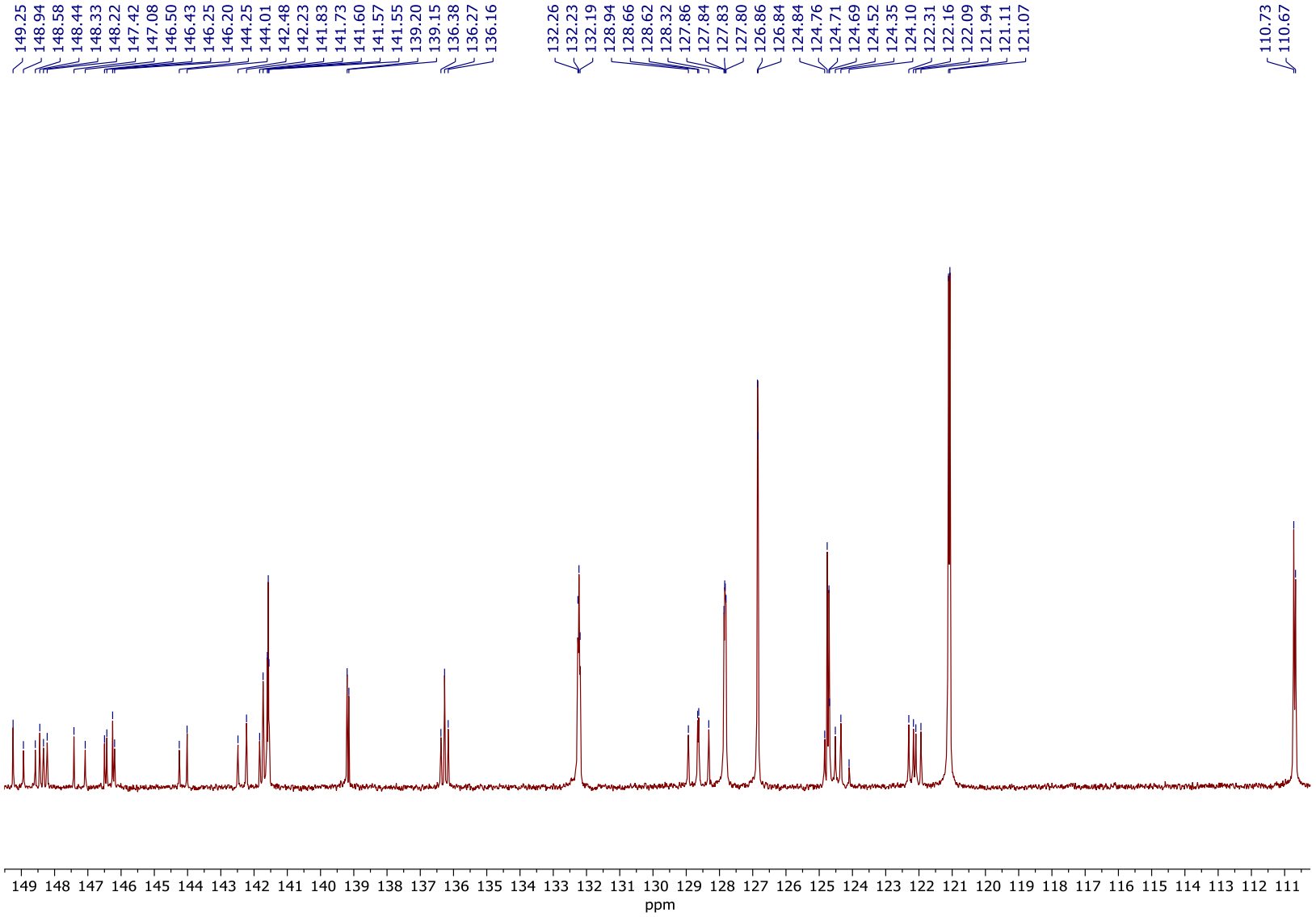

Figure S19. Inset (149.5-110.0 ppm) of the $\{^{1}H\}^{13}C$ NMR (125 MHz, THF-d_8) spectrum of compound **4**.

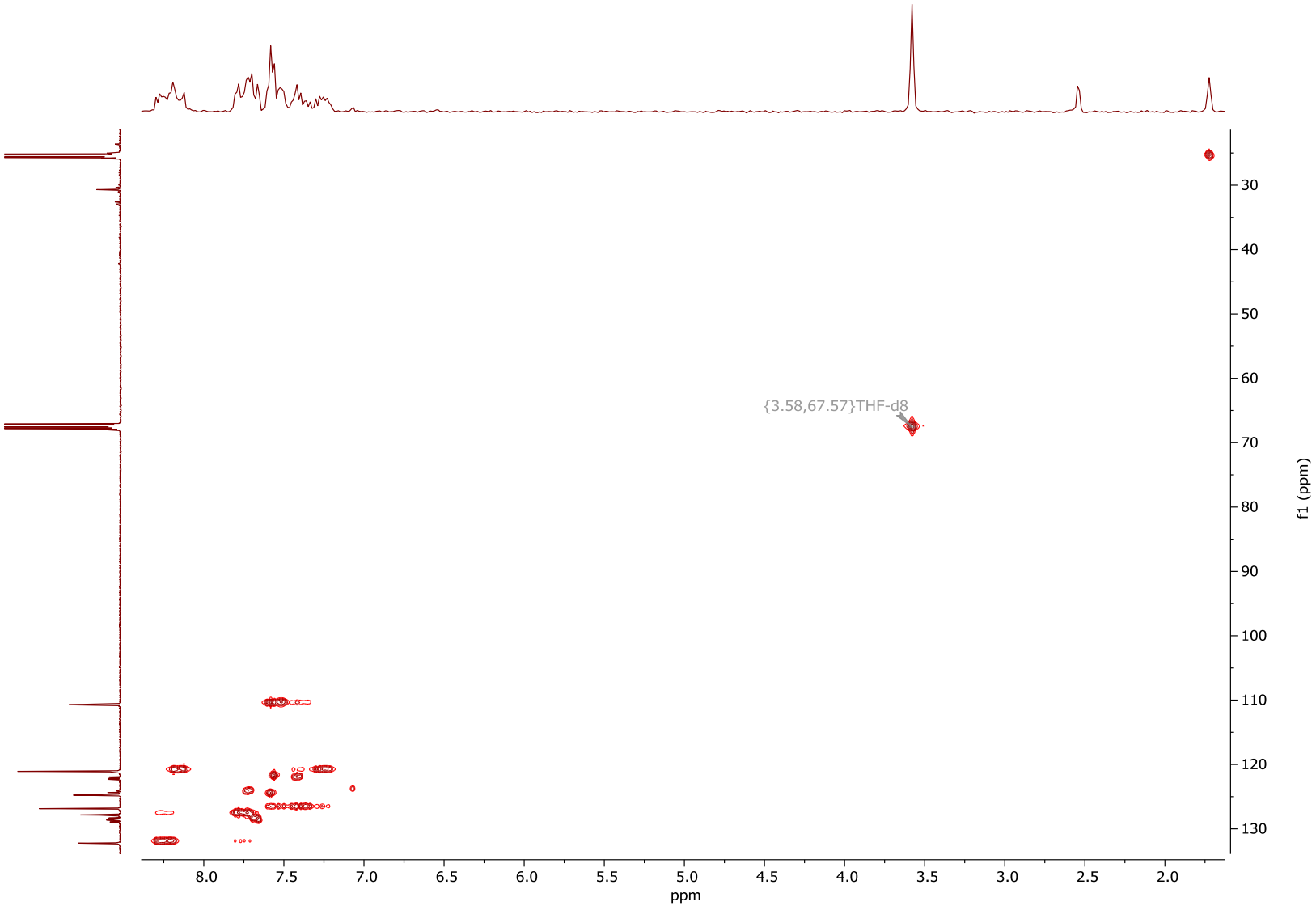

Figure S20. ^{1}H-^{13}C HSQC NMR (THF-d_8) spectrum of compound **4**.

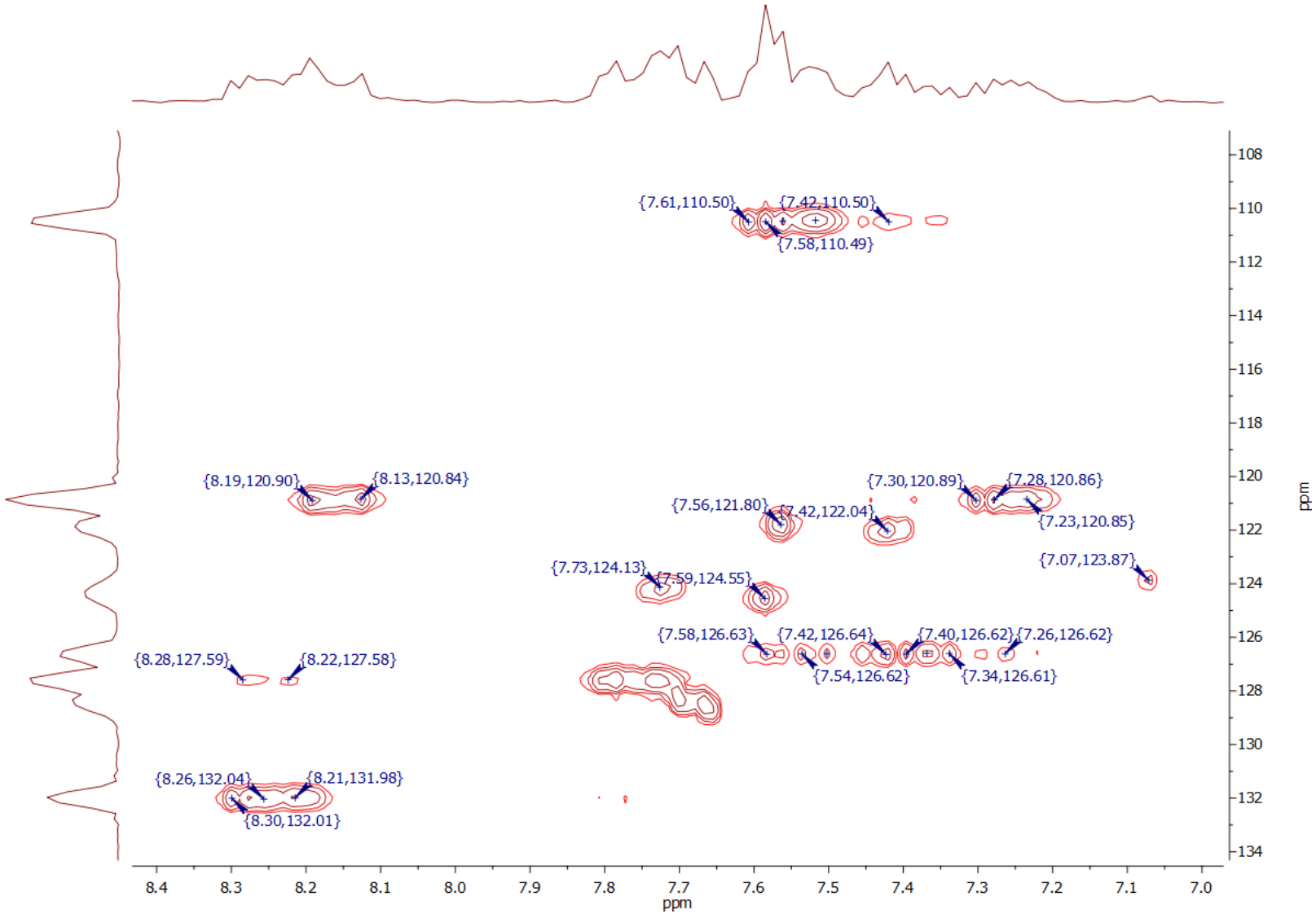

Figure S21. Inset of the ^{1}H-^{13}C HSQC NMR (THF-d_8) spectrum of compound **4**

S2.3. NMR spectra of compound 10

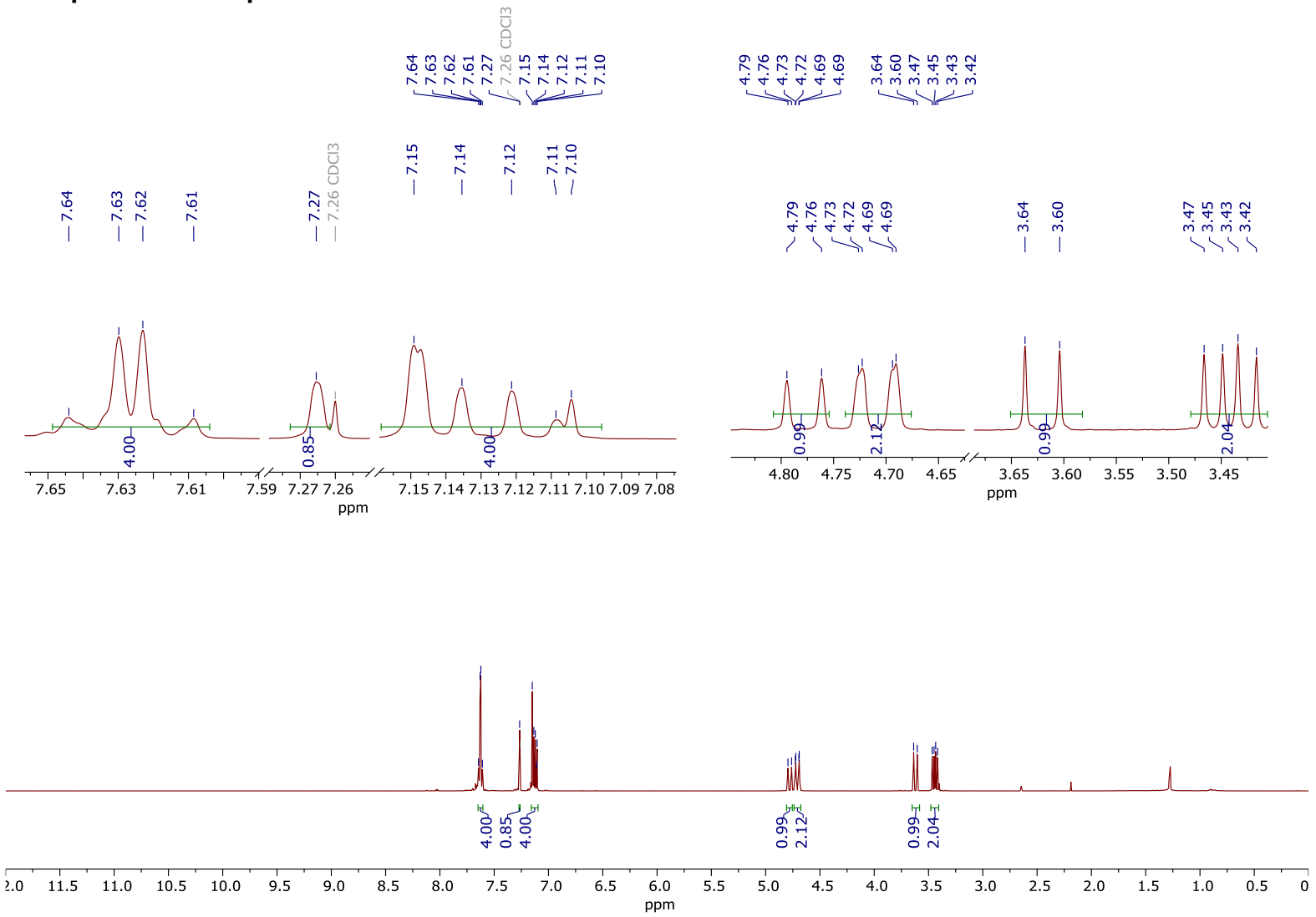

Figure S22. ^{1}H NMR (600 MHz, $CDCl_3$) spectrum of compound **10**.

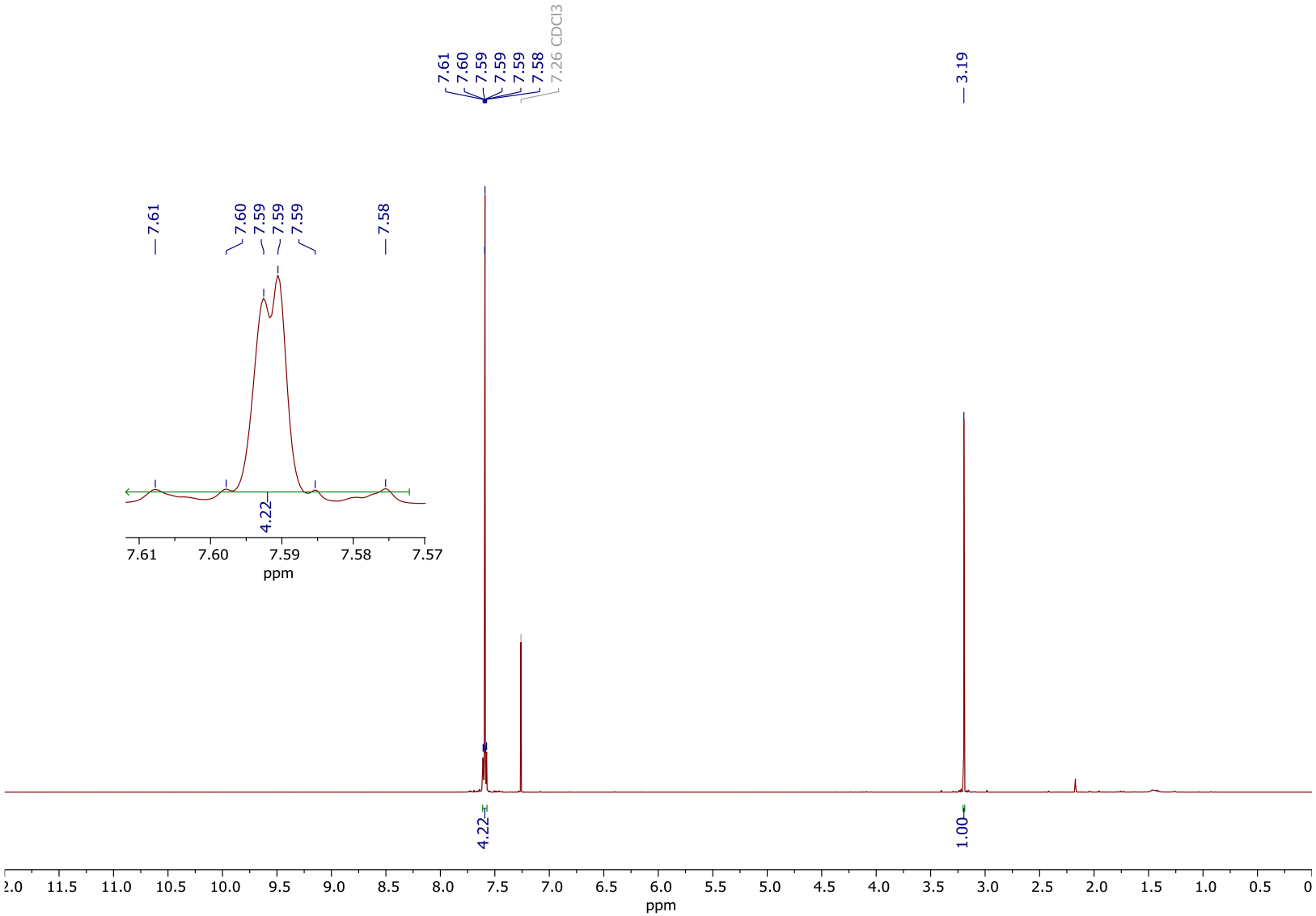

Figure S23. ^{1}H NMR (600 MHz, $CDCl_3$) spectrum of 1-ethynyl-4-(trifluoromethyl)benzene (**9**; commercial compound). This spectrum is presented to show the shape of the 7.61-7.58 ppm multiplet for the starting material in the synthesis of compound **10**.

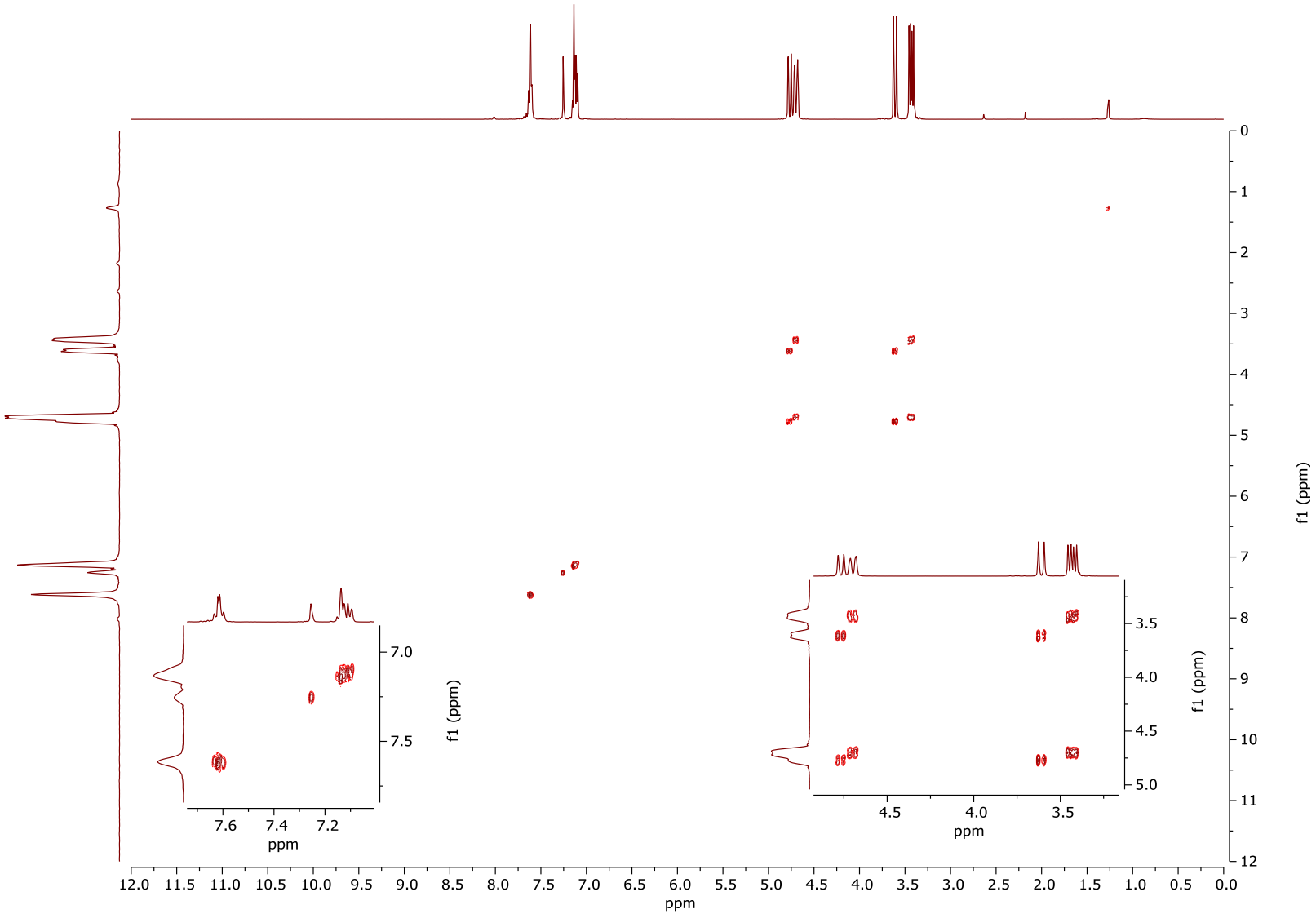

Figure S24. ^{1}H-^{1}H COSY NMR (600 MHz, THF-d_8) spectrum of compound **10**.

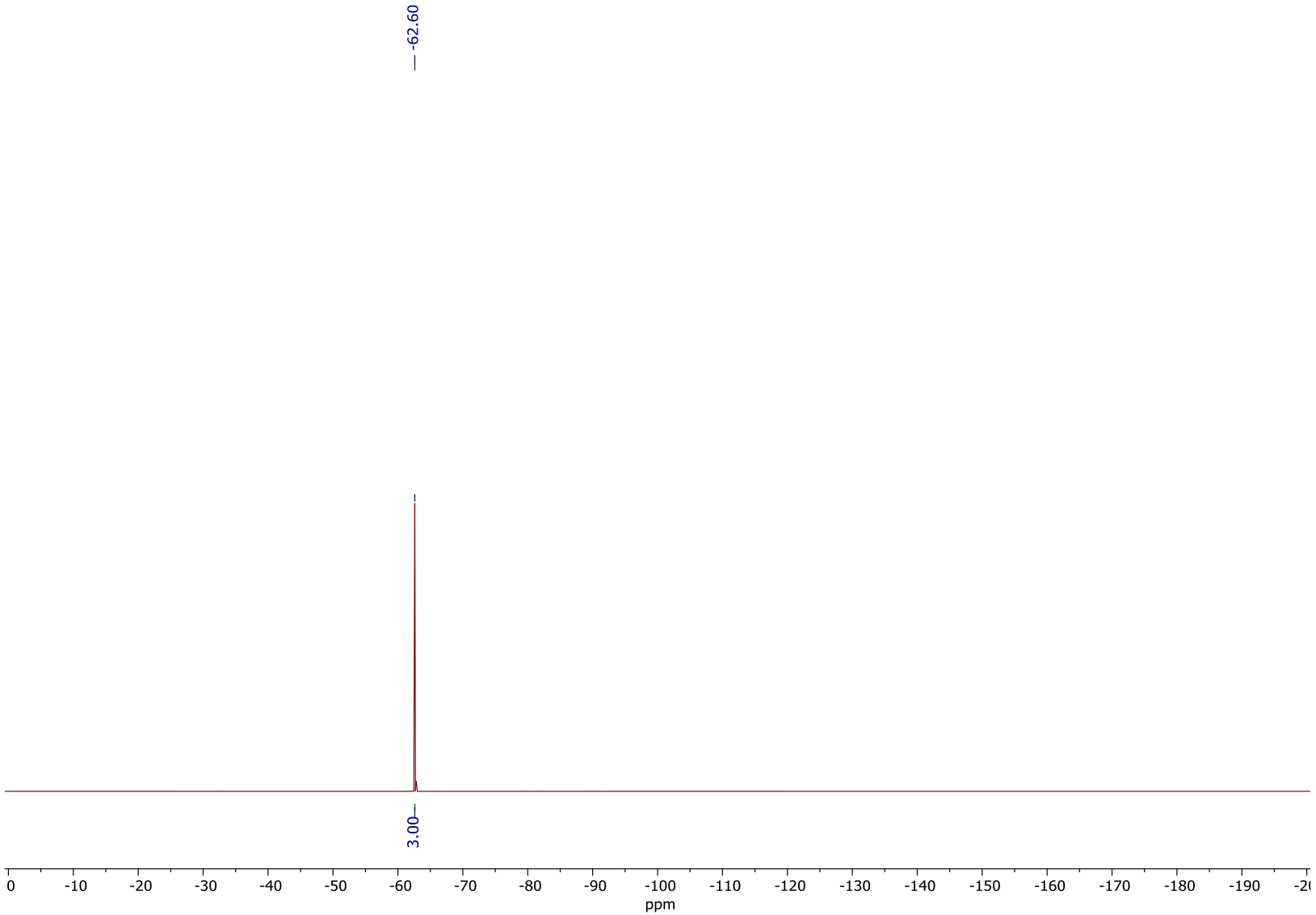

Figure S25. ^{19}F NMR (600 MHz, $CDCl_3$) spectrum of compound **10**.

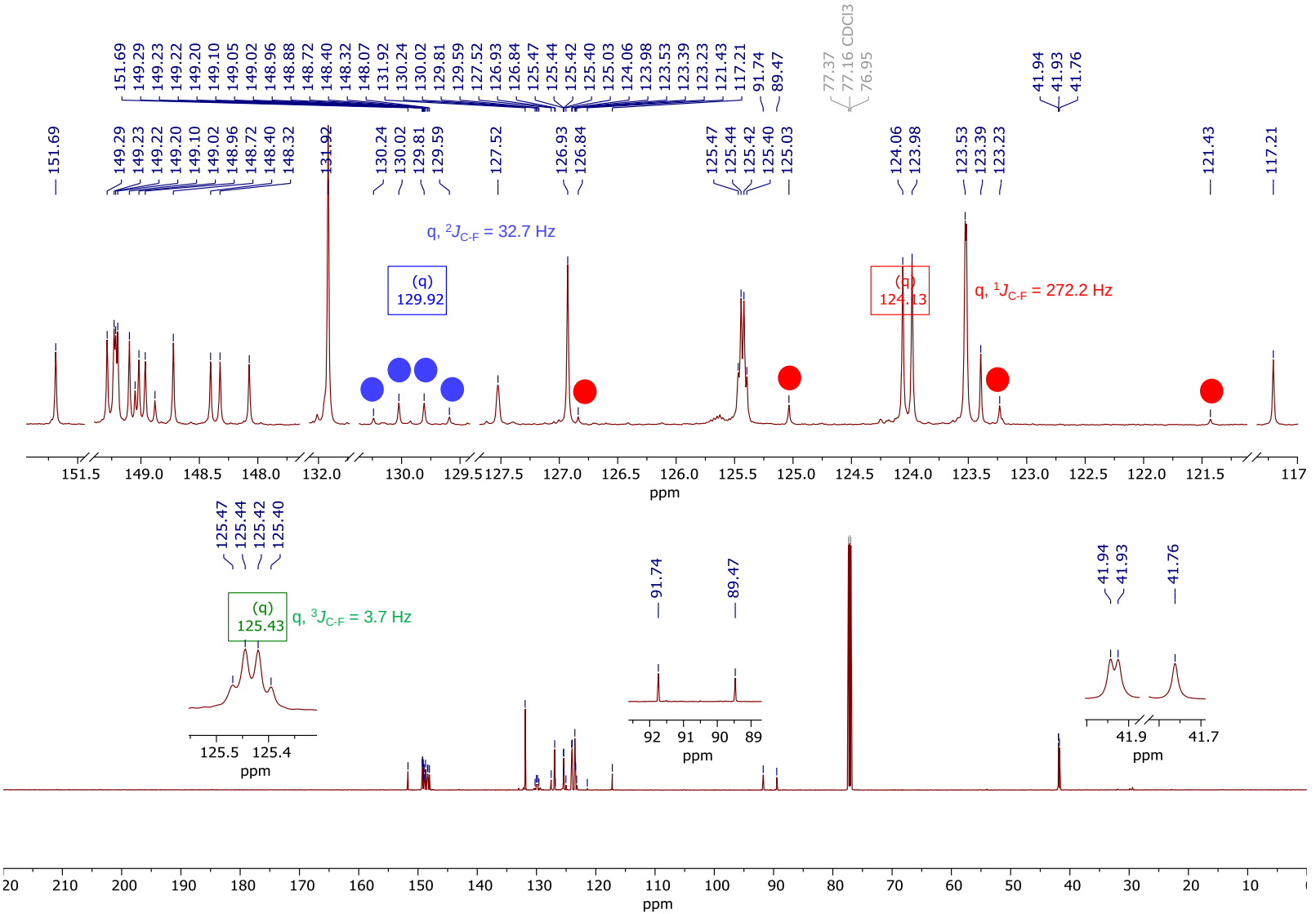

Figure S26. {^{1}H}^{13}C NMR (150 MHz, $CDCl_3$) spectrum of compound **10**. Insets present the signals included in the C-F couplings, together with the respective C-F *J*-coupling values.

S2.4. NMR spectra of compound 3 and discussion

The NMR spectra of compound **3** comprised the signals coming from the sumanene and carbazole moieties, as well as the linkers. The presence of multiplets in the spectra resulted from the existence of **3** as the mixture of diastereoisomers. While two diastereoisomers of compounds **4-5** were considered (see discussion in Subsections S2.1-S2.2), four diastereoisomers of compound **3** can be considered, see **Figure S27**.

^{1}H NMR spectrum of compound **3** (**Figure S28**) consisted of the multiplets located in the aromatic region, namely 8.33-7.06 ppm. Due to relatively complex structure of **3** and the existence of diastereoisomers od **3** in the sample, the straightforward assignment of these multiplets in the ^{1}H NMR spectrum of **3** to the given protons was hard to accomplish. The analysis of the spectrum of **3** was performed building on the ^{1}H NMR spectrum analyzes on reference compound **4** (see Section S2.2). The total number of protons in the ^{1}H NMR spectrum of **3** was 48H what conformed to the anticipated value. The multiplets could be split into two major groups. The first multiplet group at 8.33-8.01 ppm (12H), featuring the highest chemical shift values, were ascribed to the H-1, H-4, H-5 and H-8 protons (3x4H) within of the carbazole moiety (see the atom numbering in the presented image on the left). This hypothesis was supported with the ^{1}H-^{1}H COSY NMR experiment (**Figure S31**). The second multiplet group at 7.89-7.06 ppm comprised significant number of signals that can be grouped into several multiplets featuring the intensities between 3H and 11H. These signals were ascribed to the remaining 36H coming from the sumanene (5H), carbazole H-2, H-3, H-6, H-7 protons (3x4H=12H), *p*-phenylene (4x4H=16H) and methidene (3H) moieties. The content of each diastereoisomer in the sample was not the same what was the result of different integral values for their signals. However, the total intensity of these signals was 36H with the respect to the total intensity of the signals from the 8.33-7.06 ppm multiplet (12H), see inset of the spectrum in **Figure S29**. Finally, no signals in the sumanene benzylic region were detected in the ^{1}H NMR spectrum of compound **3**. This finding further confirmed the successful modification of sumanene skeleton at all benzylic positions. Notably, as expected, the profile of the ^{1}H NMR spectrum of **3** was similar to that of **4** with slight differences in the chemical shifts and relative intensities of the respective signals, see stacked ^{1}H NMR spectra of **3** and **4** in **Figure S30**. This finding also supported the presence of 2-substituted sumanene backbone in compound's **3** structure in comparison to compound **4** containing sumanene skeleton non-substituted at the aromatic position. Therefore, taking into account all the above-listed outcomes from the ^{1}H NMR spectra, tetra-substitution of sumanene at aromatic and benzylic positions was achieved in **3**.

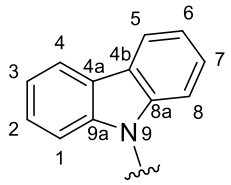

The presence of fluorine in the form of trifluoromethyl (CF_3) group in compound **3** structure was confirmed with the ^{19}F NMR experiment (**Figure S32**). The multiplet (δ_F from −63.45 to −63.48 ppm) in this spectrum resulted from the presence diastereoisomers of compound **3** (**Figure S27**) in the sample.

The {^{1}H}^{13}C NMR spectrum (**Figure S33**, **Figure S34**) of compound **3** comprised the multiplicated signals (due to the presence of diastereoisomers) coming from the sumanene and carbazole moieties, what supported successful tetra-substitution of the

sumanene skeleton. Notably, compound **3** had relatively high molar mass and features limited solubility as for the $\{^1H\}^{13}C$ NMR experiment. This fact made it hard to localize and distinguish all the signals from each one of low-intensity quaternary carbons of sumanene skeleton and -C≡C-*p*-C_6H_4-CF_3 group, as well as to directly analyze signals from quaternary carbons included in C-F couplings (expected as quartets, similarly to the $\{^1H\}^{13}C$ NMR spectrum of starting material in the synthesis of **3**, *i.e*., compound **10**, see **Figure S26**). These signals additionally overlapped with signals coming from the carbazole and *p*-phenylene moieties (three of each moiety in compound **3** structure). Nevertheless, by means of the long-time acquisition (more than 60 hours) of the ^{13}C decoupled ^{19}F-^{13}C HSQC experiment with **3** we were able to distinguish that the chemical shift for the ^{13}C nuclei signals coming from the **C**F_3 group were 125.3-125.2 ppm, see **Figure S35**. Additionally, the signals in the $\{^1H\}^{13}C$ NMR spectrum of **3** were also tracked based on the ^1H-^{13}C HMBC NMR spectrum (long-time acquisition), see **Figure S36**. Despite the complexity of the ^1H-^{13}C HMBC NMR spectrum of **3** mostly due to the presence of diastereoisomers and significant number C-H couplings by two, three or four bonds, important outcomes from this analysis were found related to the confirmation of the presence of low-intensity quaternary carbons in the $\{^1H\}^{13}C$ NMR spectrum. First, it was possible to confirm the presence of low-intensity quaternary carbons coming from the sumanene skeleton between 150-120 ppm, see **Figure S36**. Secondly, it was possible to confirm the presence of low-intensity quaternary carbons coming from the -C≡C- (93.4-92.3 ppm) within the -C≡C-*p*-C_6H_4-CF_3 group, see inset in **Figure S37**.

ESI-HRMS (TOF) experiment (see spectrum in Section S3) ultimately supported the successful formation of **3**, *i.e*., the calculated and measured spectra were consistent (m/z $[M]^+$ calcd. for $C_{87}H_{48}F_3N_3$ 1191.3795, found 1191.3778). The purity of the **3** sample was also further supported with elemental analysis (Anal. Calcd for $C_{87}H_{48}F_3N_3$: C, 87.64; H, 4.06; N, 3.52. Found: C, 87.20; H, 4.08; N, 3.50).

Importantly, one value of diffusion coefficient in the ^1H DOSY NMR spectrum of compound **3** (**Figure S38**) further supported that the sample is composed of one type of molecule. The hydrodynamic radii ($r_{H,solv}$) was estimated using the unmodified Stokes-Einstein equation[9,10]:

$$r_{H,solv} = \frac{k_B T}{6\pi\eta D}$$

where D is the measured diffusion coefficient for **3** ($4.78 \cdot 10^{-10}$ m^2s^{-1}), k_B is the Boltzmann constant ($1.3806485 \cdot 10^{-23}$ $kg \cdot s^{-2}K^{-1}$), T is the temperature for the ^1H DOSY NMR spectrum acquisition (298 K), $r_{H,solv}$ is the hydrodynamic radius of **3**, η is the viscosity of the solvent (THF) at temperature T (0.00048 $kg \cdot m^{-1}s^{-1}$). The approximate hydrodynamic radius for compound **3** equaled to *ca.* 0.96 nm. ^{19}F DOSY NMR experiment also supported that the sample is composed of one type of molecule, see **Figure S39**. Notably, the measured diffusion coefficient values from ^1H DOSY NMR ($4.78 \cdot 10^{-10}$ m^2s^{-1}) and ^{19}F DOSY NMR ($4.76 \cdot 10^{-10}$ m^2s^{-1}) were highly consistent.

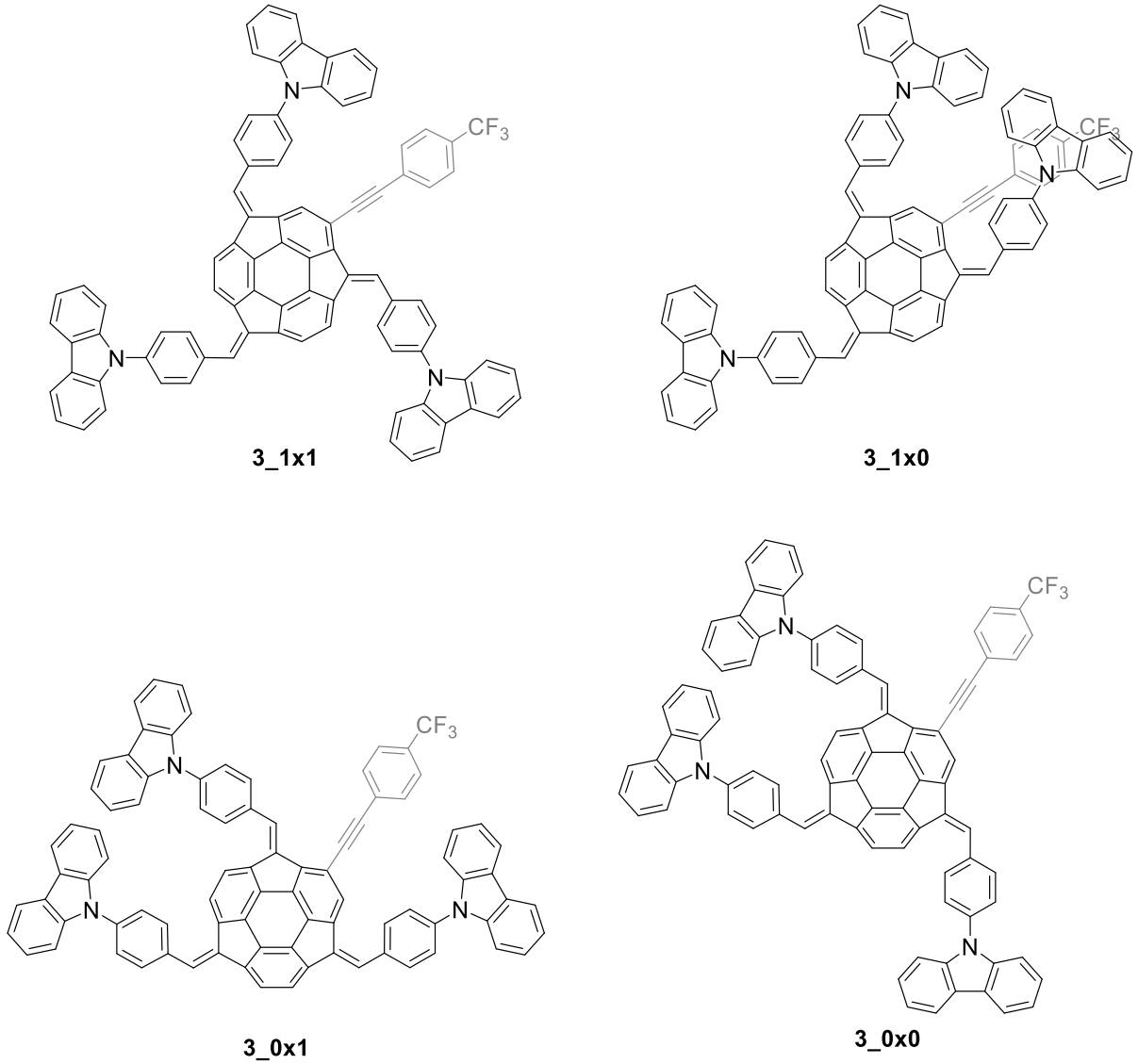

Figure S27. Representative, possible diastereoisomers of compound **3**. The DFT-optimized structures of those diastereoisomers are presented and discussed in Section S5. The presented diastereoisomers' numbers conform to that presented in Section S5.

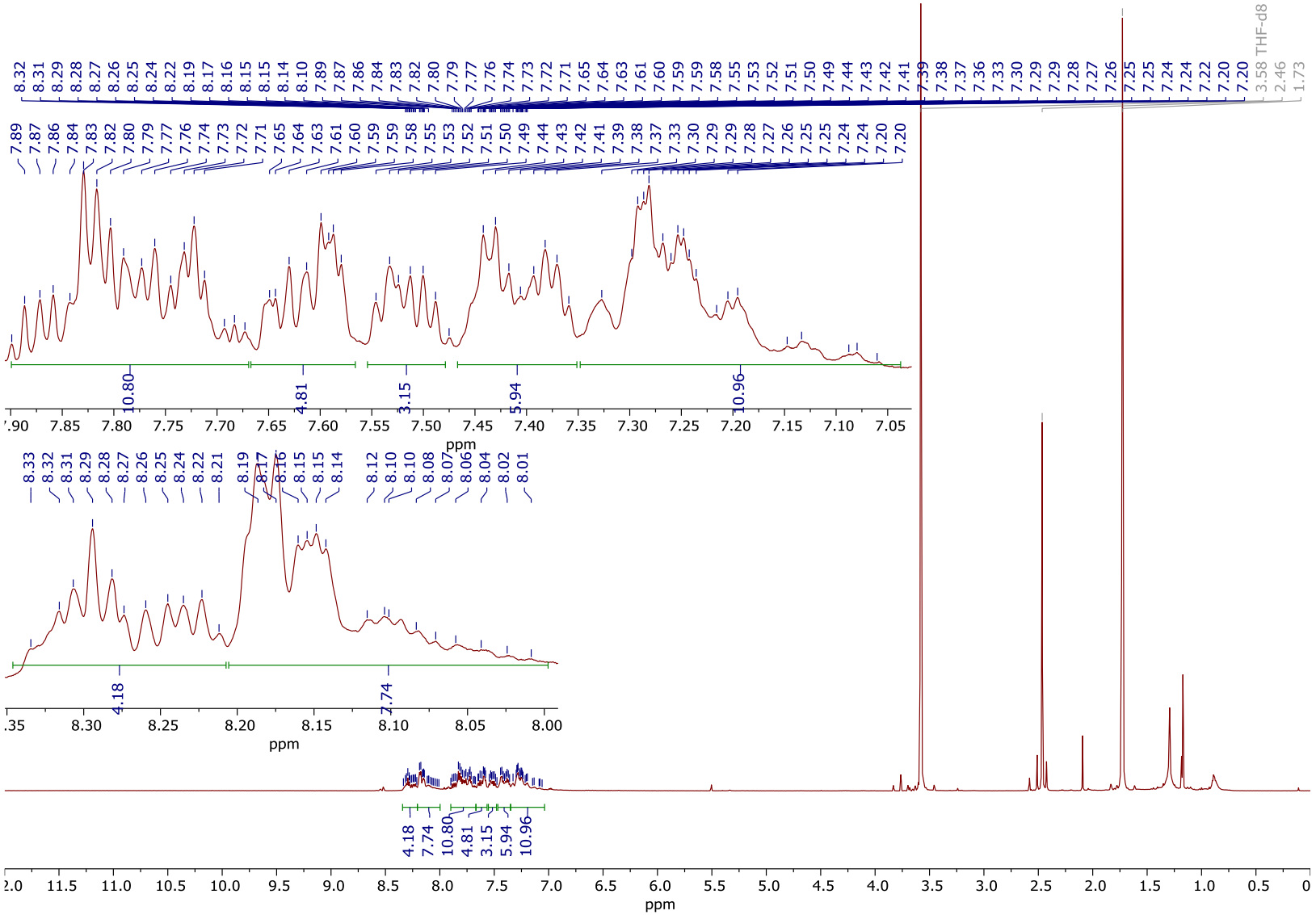

Figure S28. ^{1}H NMR (600 MHz, THF-d_8) spectrum of compound **3.**

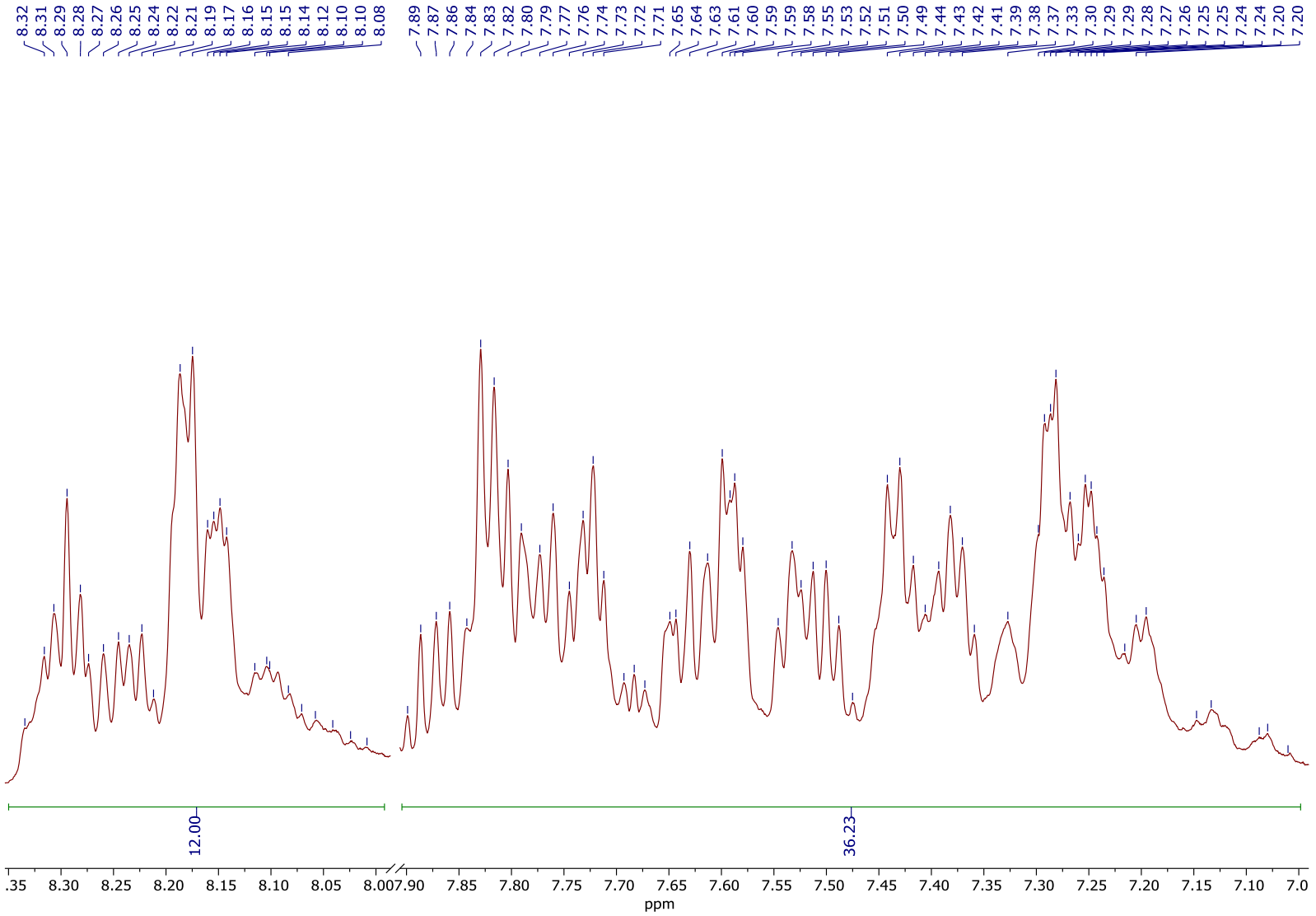

Figure S29. 8.35 ppm–7.05 ppm inset of the ^{1}H NMR (600 MHz, THF-d_8) spectrum of compound **3**, showing the relative integral values of the multiplets in the areas 8.33-8.01 ppm (12H) and 7.89-7.06 ppm (36H), total 48H.

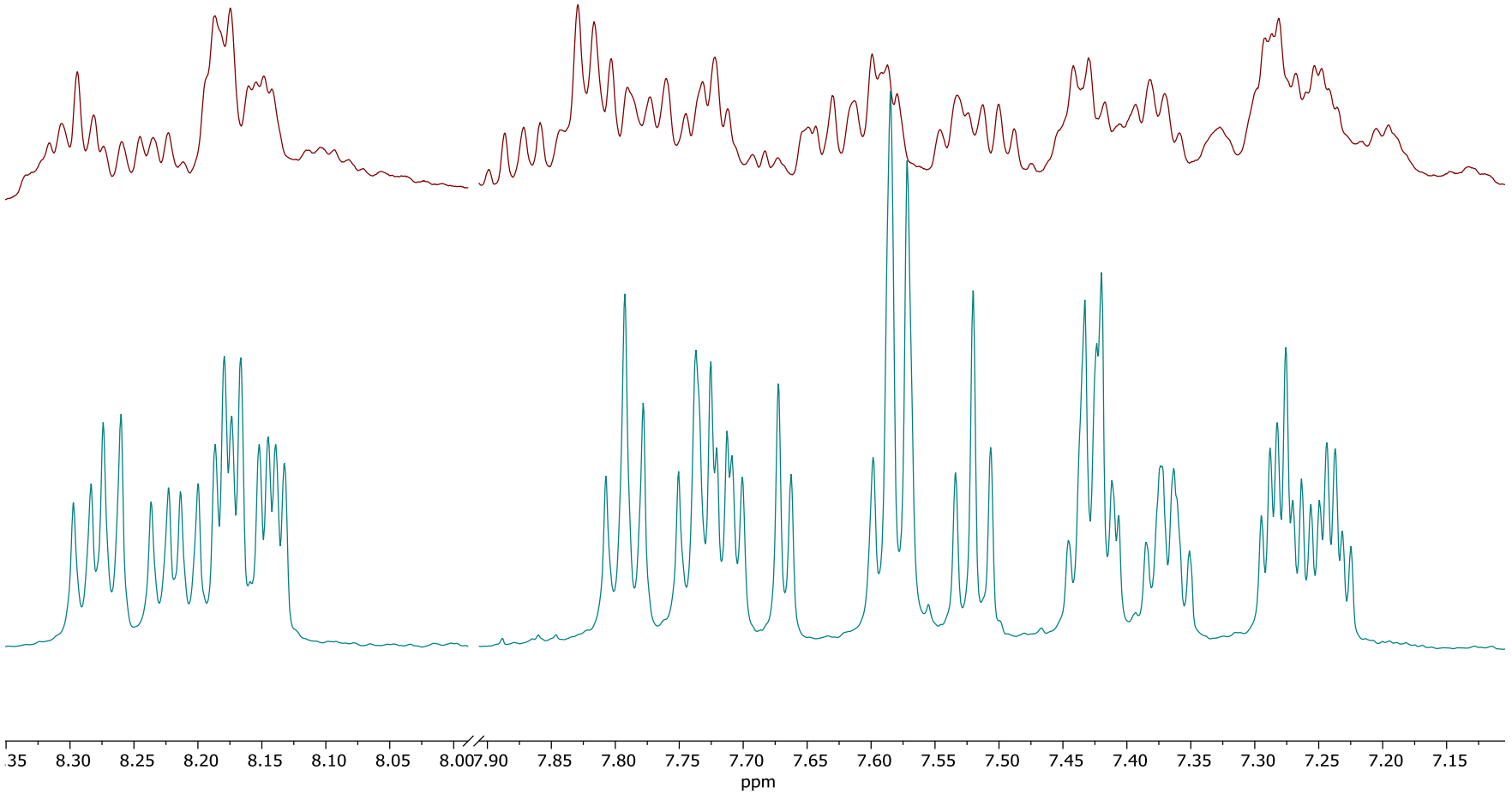

Figure S30. Comparison of the ^{1}H NMR (600 MHz, THF-d_8) spectra of compounds **3** (top) and **4** (bottom).

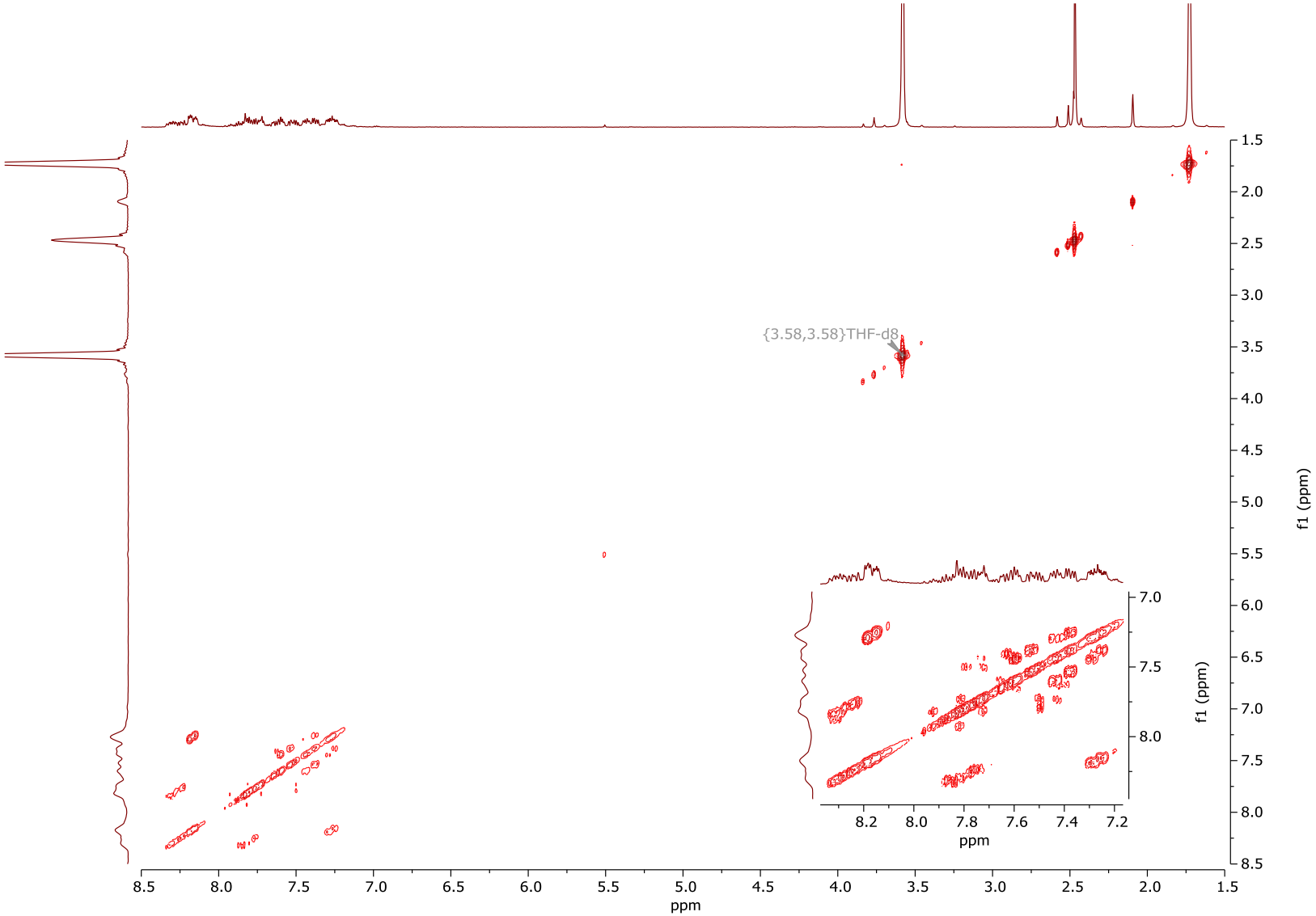

Figure S31. ^{1}H-^{1}H COSY NMR (600 MHz, THF-d_8) spectrum of compound **3**.

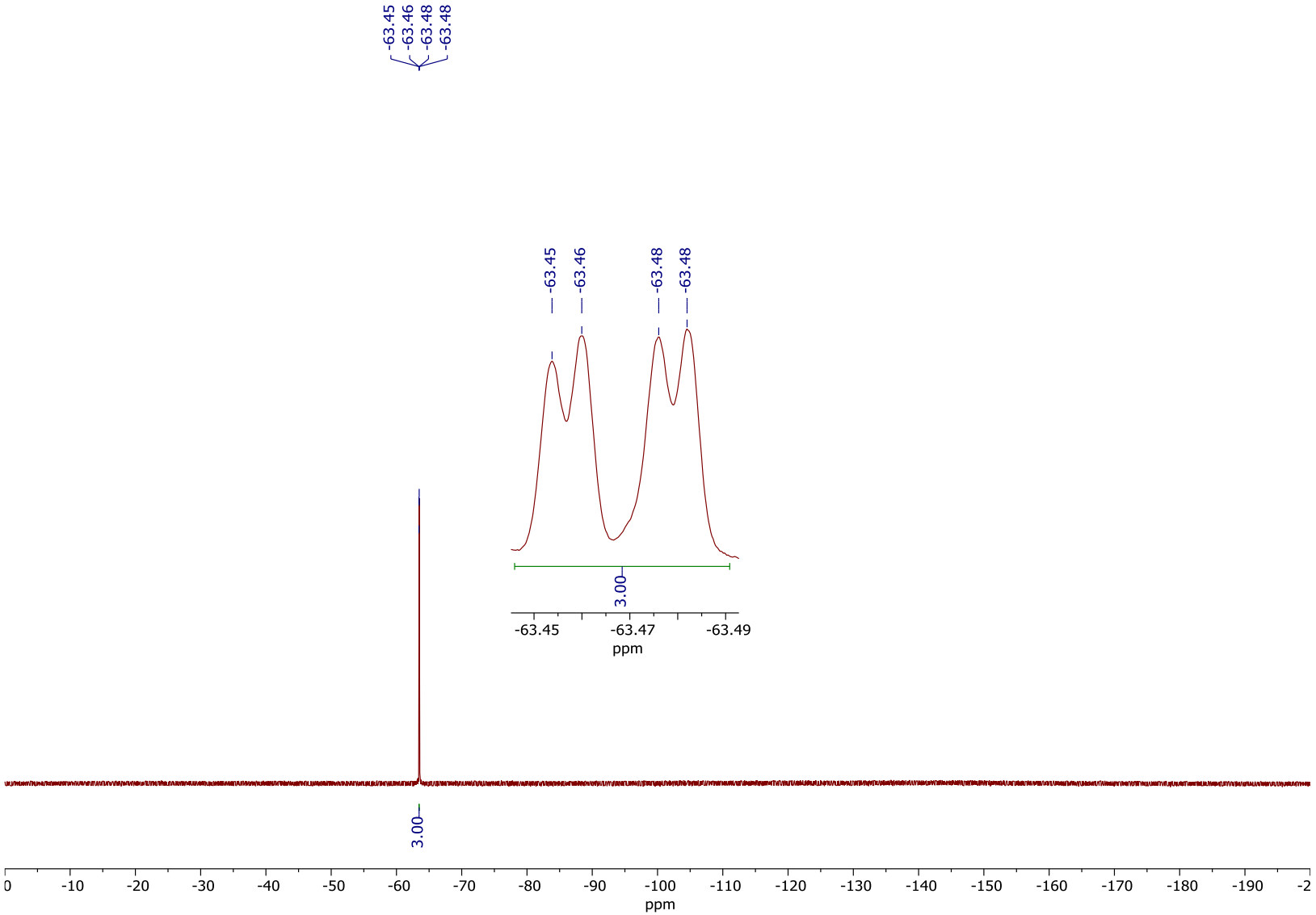

Figure S32. ^{19}F NMR (600 MHz, THF-d_8) spectrum of compound **3**.

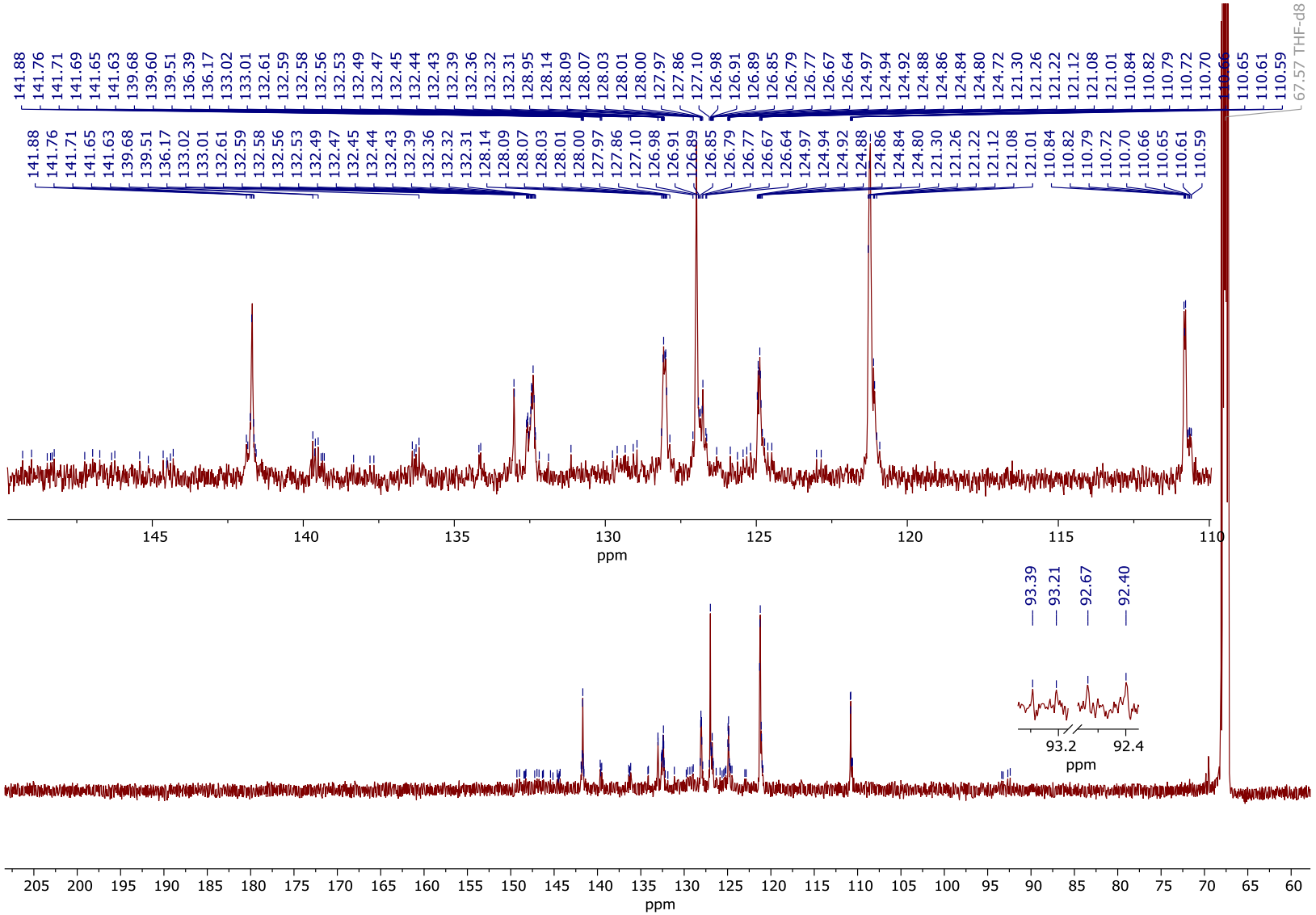

Figure S33. $\{^{1}H\}^{13}C$ NMR (150 MHz, THF-d_8) spectrum of compound **3**.

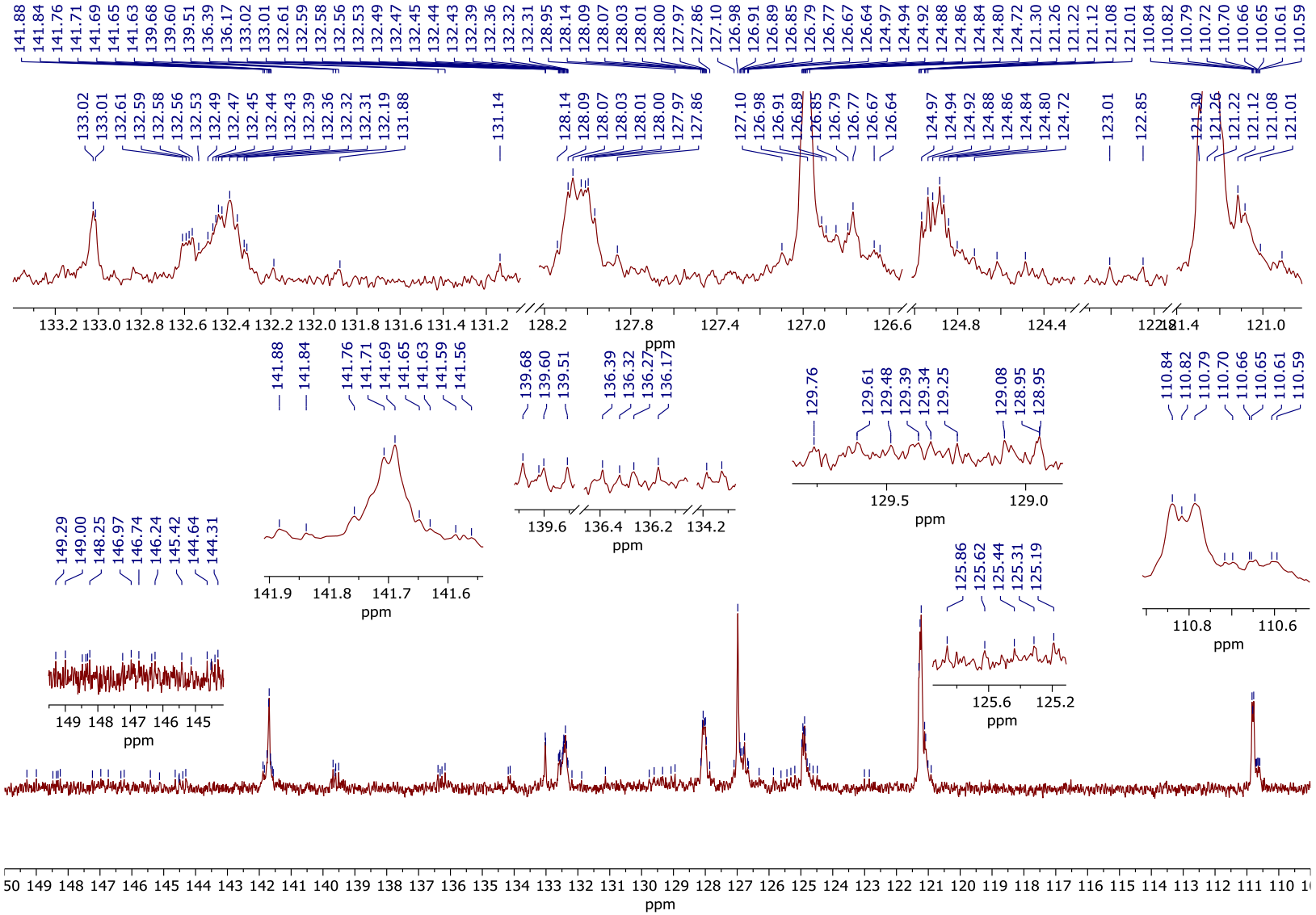

Figure S34. 150.0 ppm – 109.0 ppm inset of the {^{1}H}^{13}C NMR (150 MHz, THF-d_8) spectrum of compound **3**.

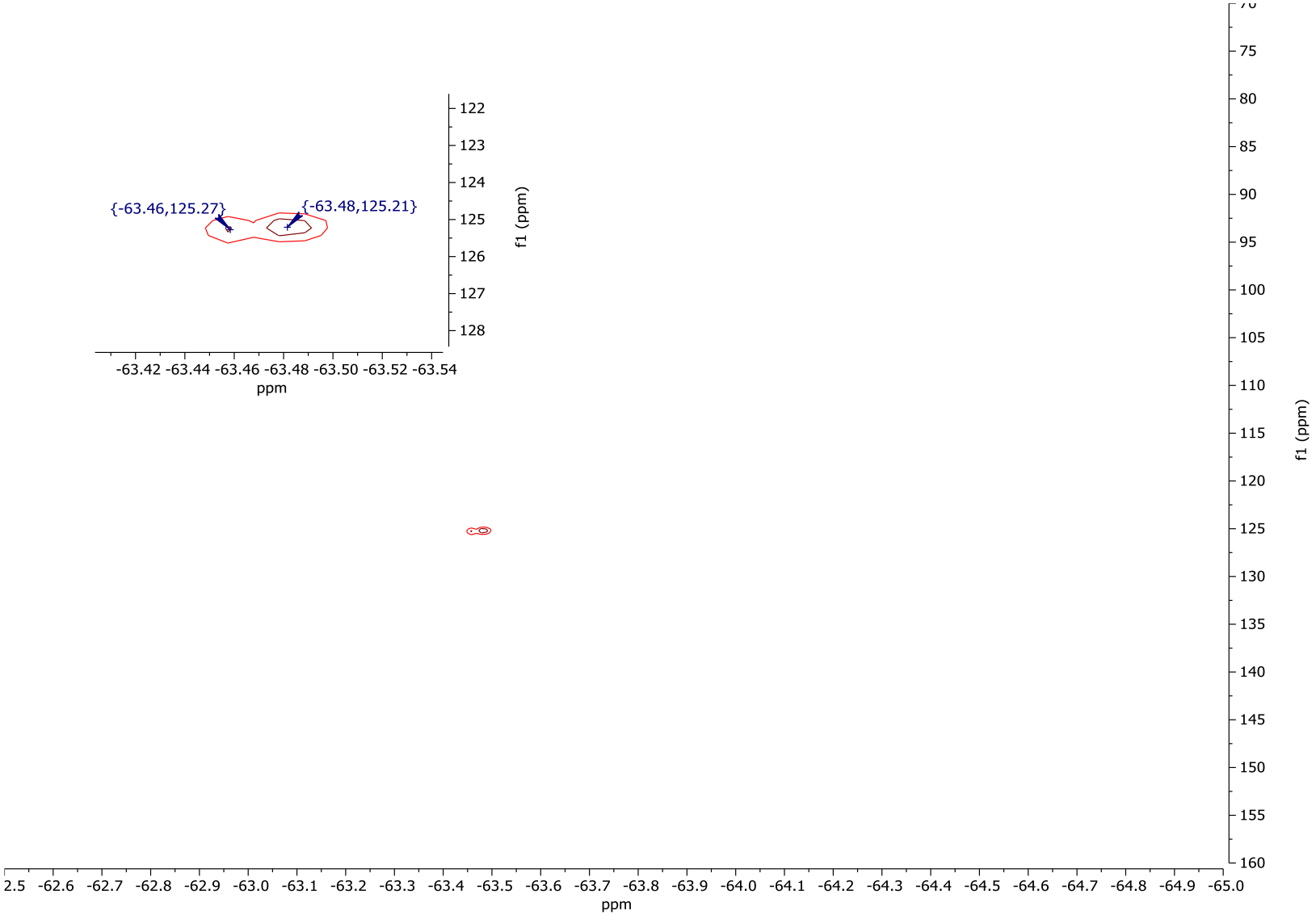

Figure S35. ^{13}C decoupled ^{19}F-^{13}C HSQC (THF-d_8) spectrum of compound **3** ($^{1}J_{C\text{-}F}$ of 270 Hz was set for the experiment, 96 scans).

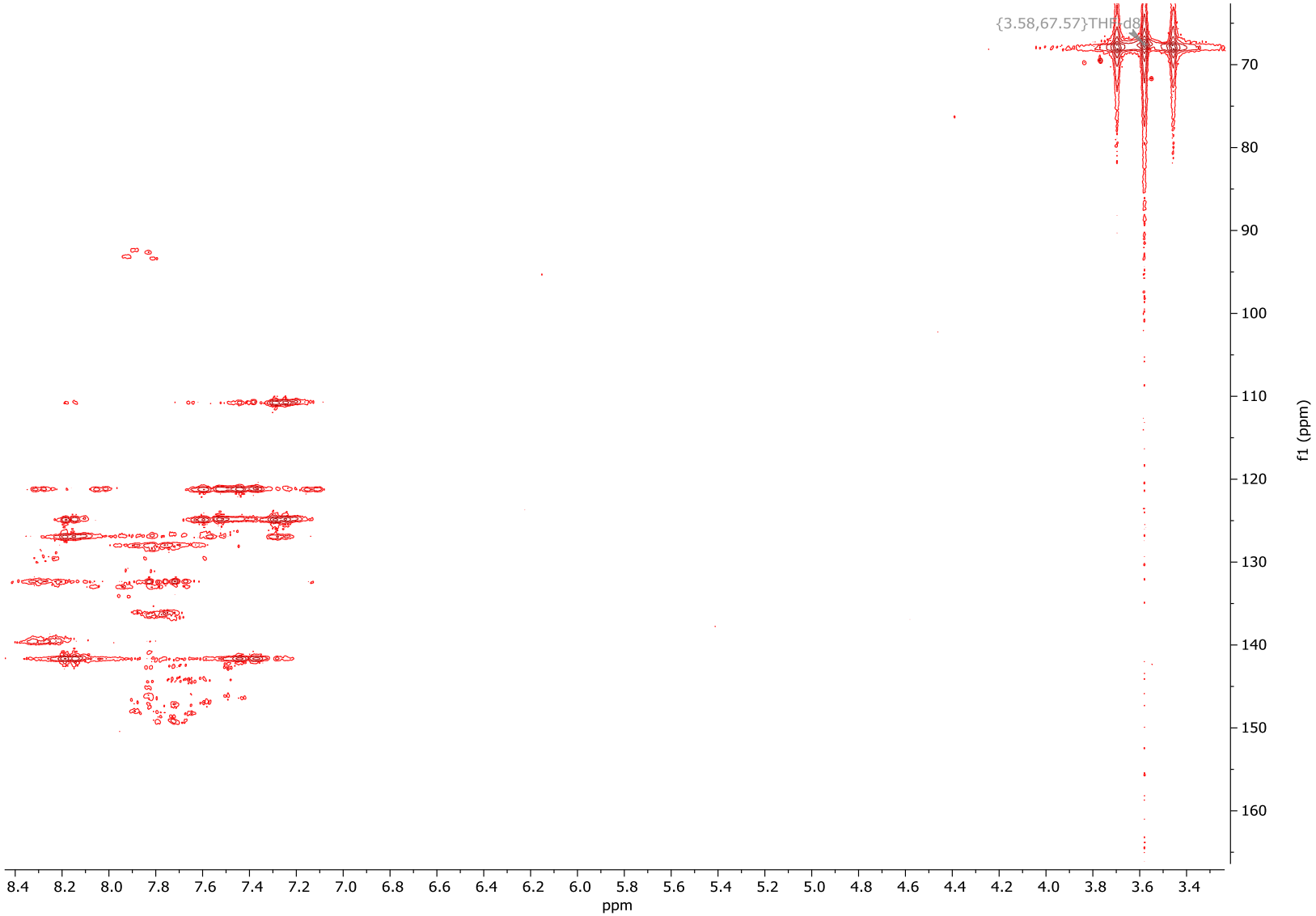

Figure S36. ^{1}H-^{13}C HMBC (THF-d_8) spectrum of compound **3**.

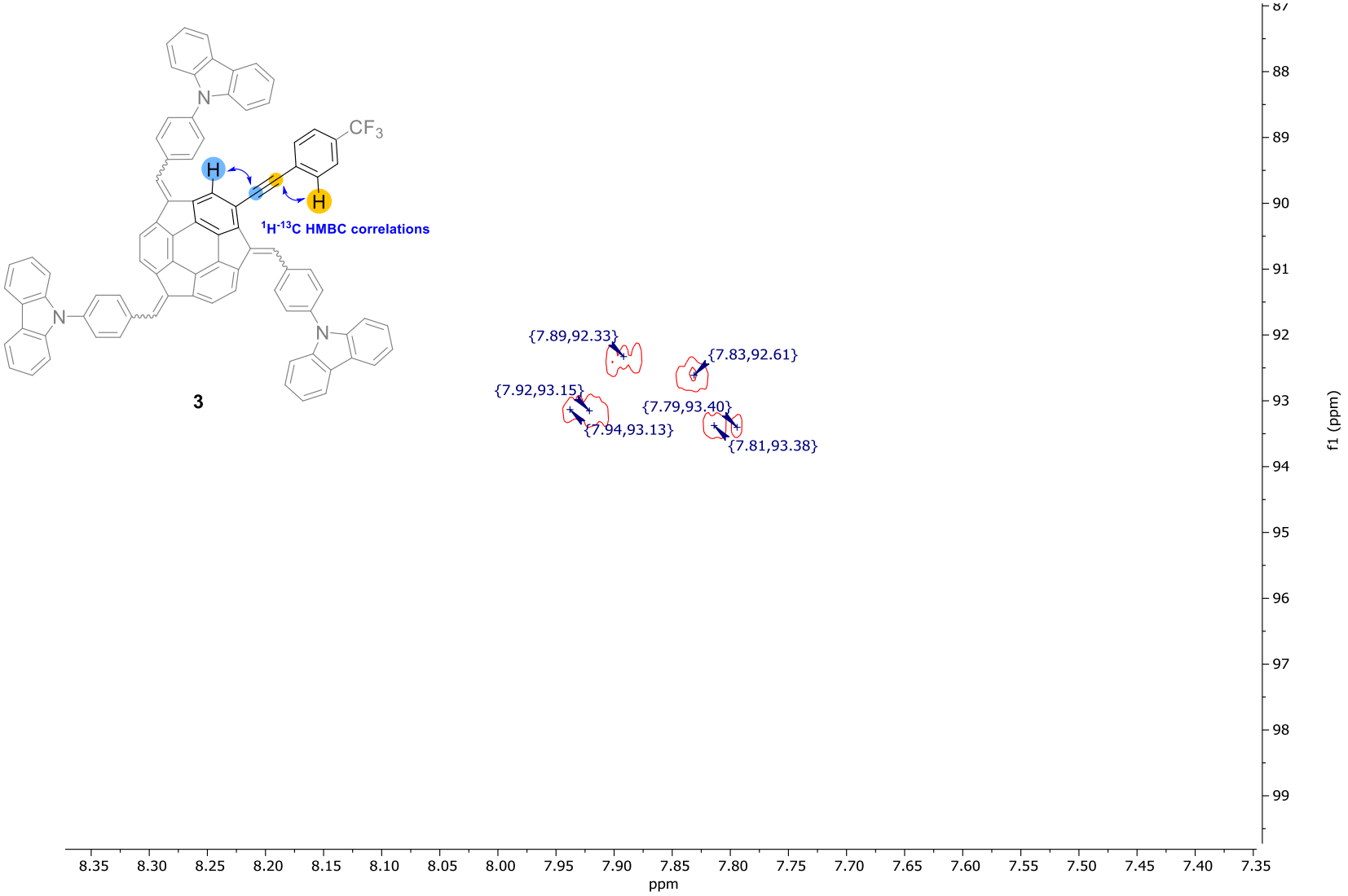

Figure S37. Inset of the ^{1}H-^{13}C HMBC (THF-d_8) spectrum of compound **3** regarding the confirmation of the presence of the signals from low-intensity quaternary carbons coming from the -C≡C- (within the -C≡C-*p*-C_6H_4-CF_3 group). The structure of compound **3** showing the discussed C-H couplings regarding this analysis is also presented for clarity.

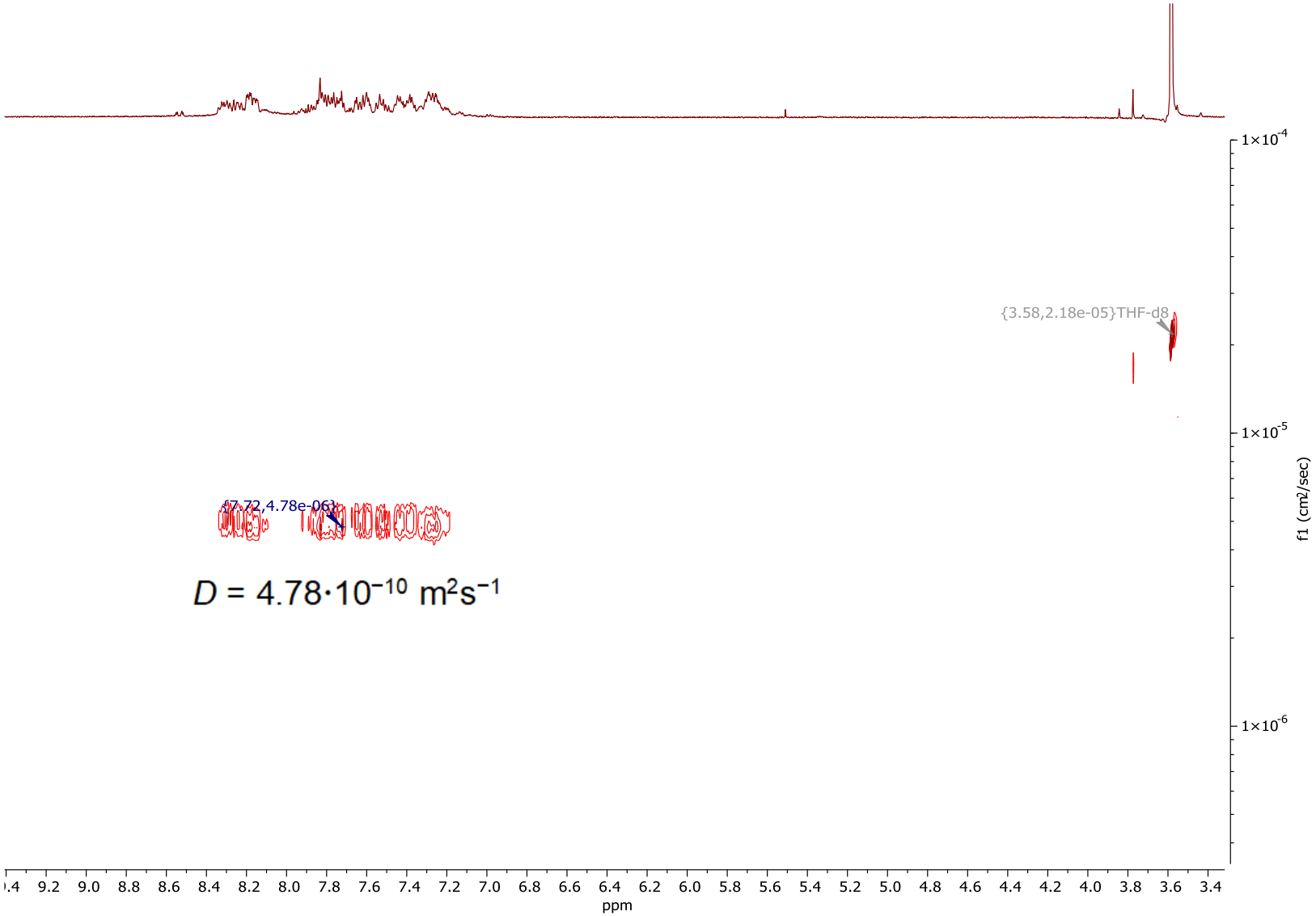

Figure S38. ^{1}H DOSY NMR (500 MHz, THF-d_8) spectrum of compound **3**.

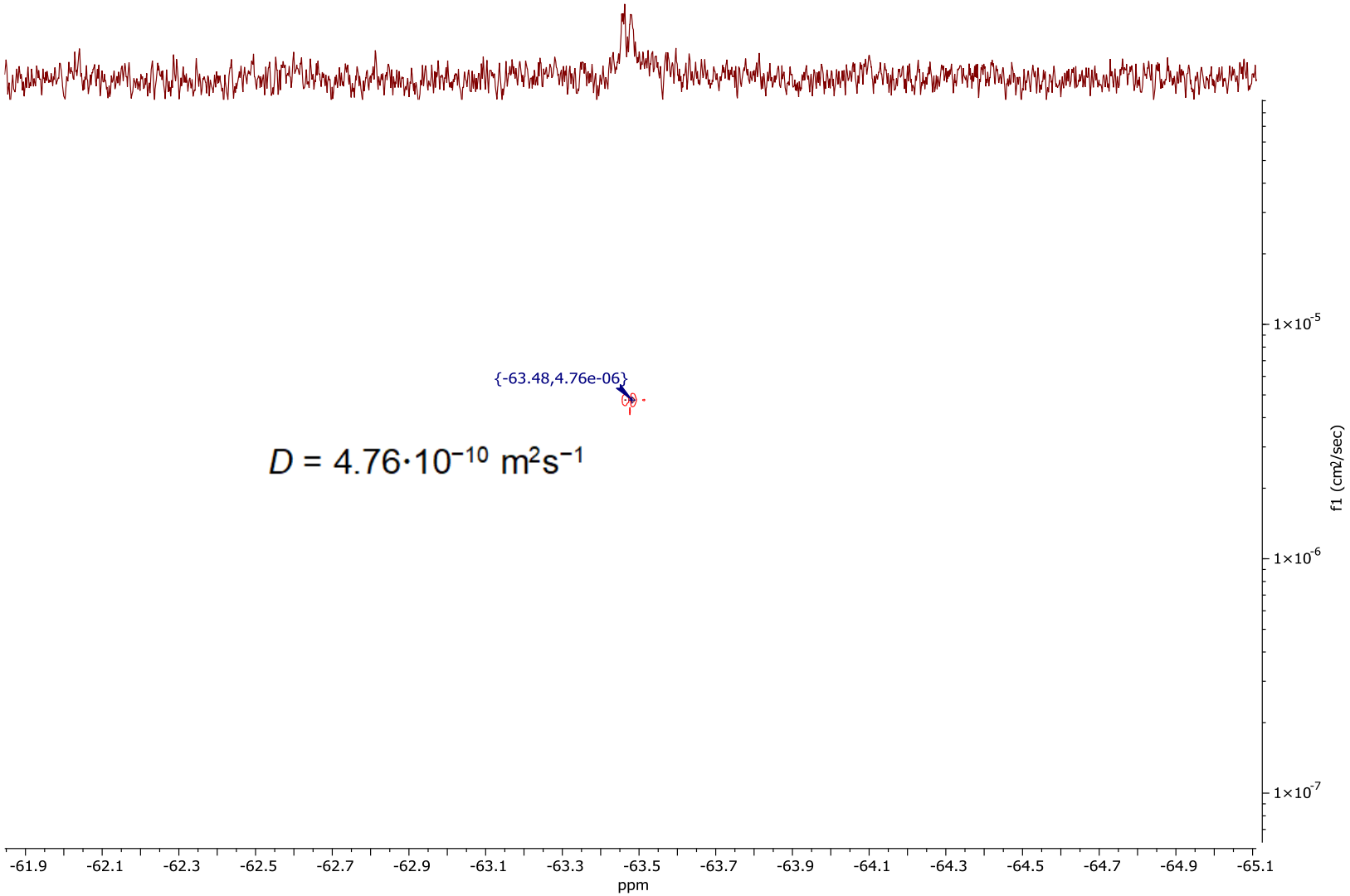

Figure S39. ^{19}F DOSY NMR (500 MHz, THF-d_8) spectrum of compound **3**.

S3. ESI-HRMS spectra

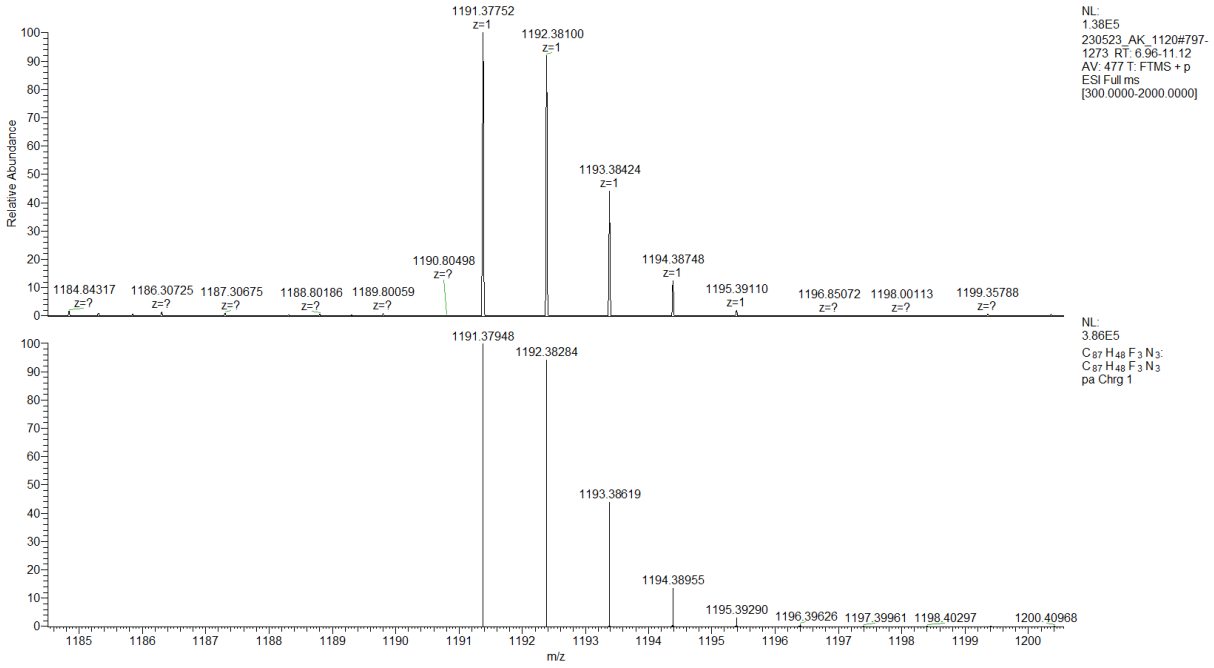

Figure S40. ESI-HRMS (TOF) spectrum of compound **3**.

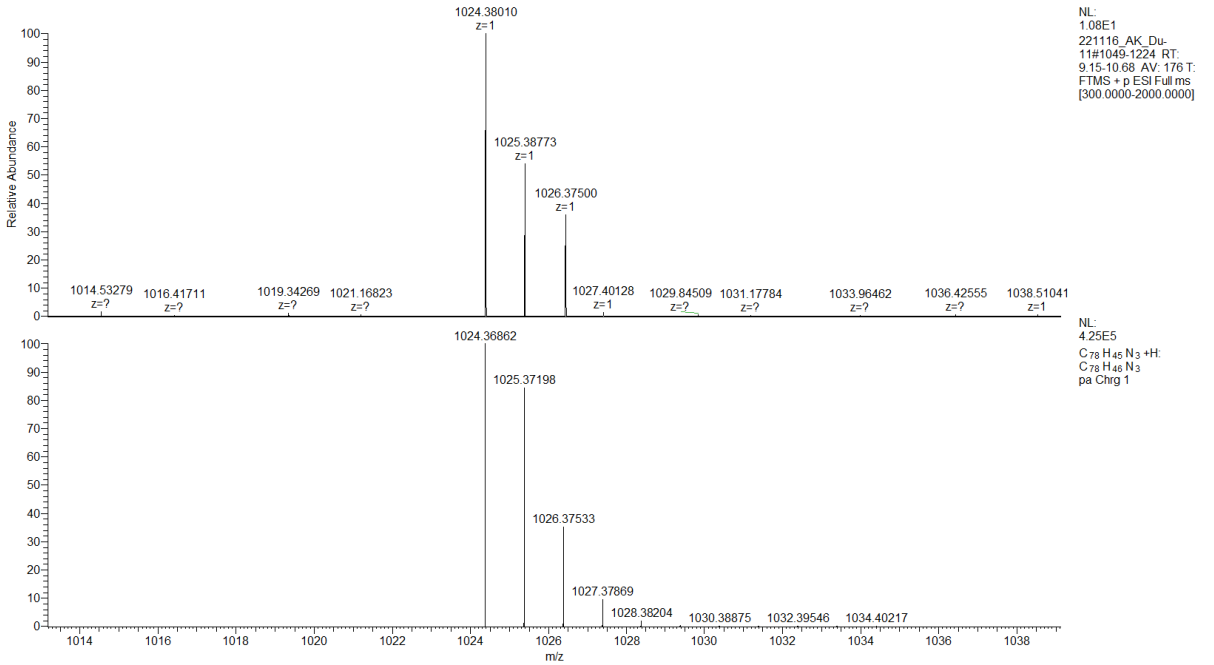

Figure S41. ESI-HRMS (TOF) spectrum of compound **4**.

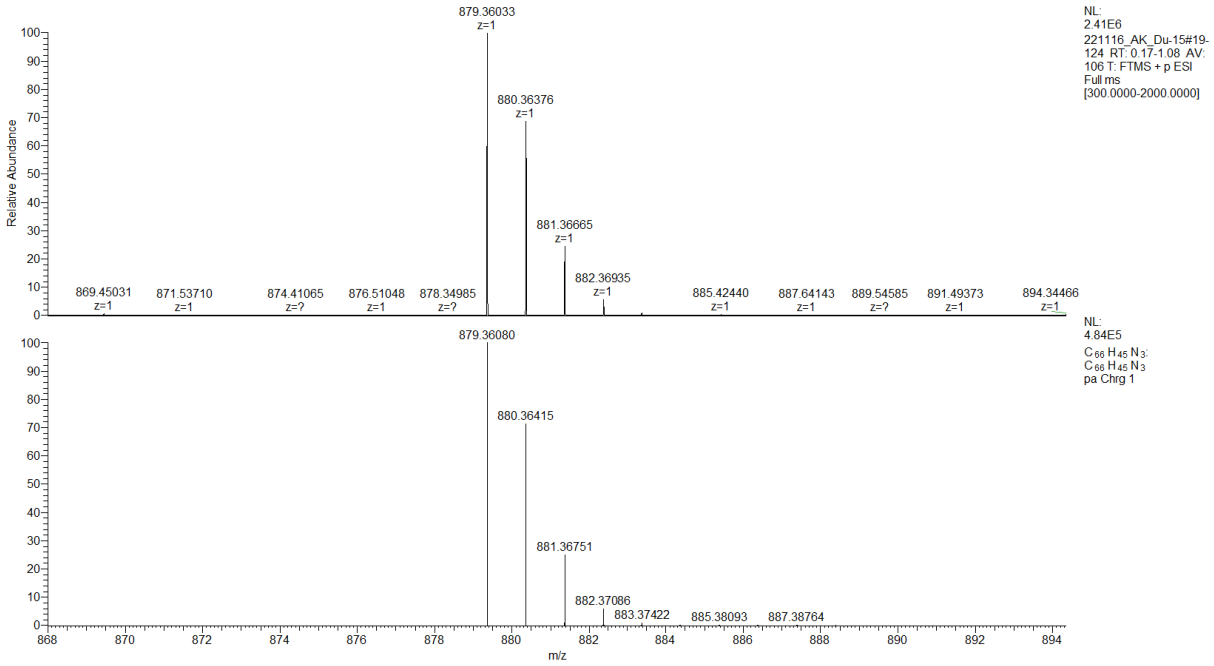

Figure S42. ESI-HRMS (TOF) spectrum of compound **5**.

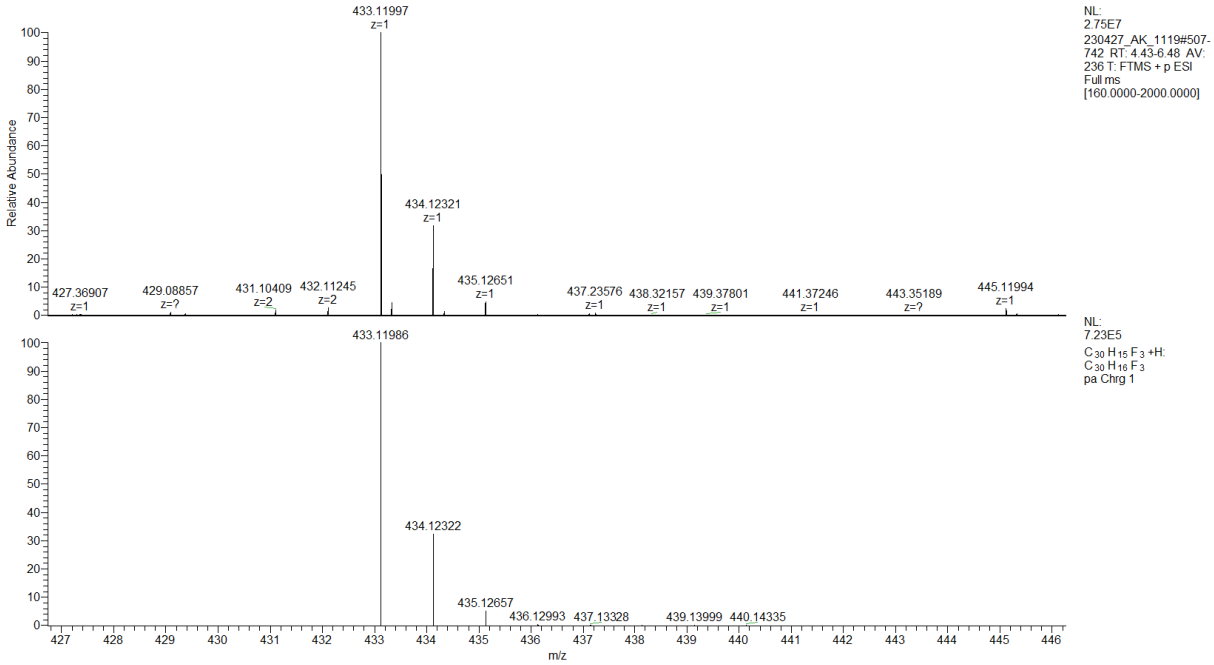

Figure S43. ESI-HRMS (TOF) spectrum of compound **10**.

S4. Absorption and emission spectra

The color of compounds **4-5** solution was orange-red (see **Figure 44a**). The UV-vis spectra ($2 \cdot 10^{-5}$ M; $CHCl_3$) of compounds **4-5** are presented in **Figure S44c**. The spectra featured three major absorption maxima (λ_{abs}) located at 243-251 nm, 368-395 nm and 474-490 nm. Notably, the spectra of **4-5** were red-shifted in comparison to the parent sumanene (**1**; λ_{abs} = 280 nm). These changes were ascribed to the presence of three carbazole units in the molecule and to the expansion of π-electron network. Additionally, the spectra of compounds **4-5** were significantly red-shifted in comparison to 1,3,5-tri(9*H*-carbazol-9-yl)benzene **11**[2] (λ_{abs} = 255, 290 nm), as the respective C_3-symmetrical derivative comprising three carbazole units in the formula. It elucidated the importance of the presence of sumanene skeleton in compounds **4-5** structure toward providing their beneficial optical properties.

The emission spectra ($2 \cdot 10^{-5}$ M in $CHCl_3$) of compounds **4-5** are presented in **Figure S44d**. Compounds **4-5** were found to be yellow-orange light emitters, as graphically presented in **Figure S44**. Emission maximum (λ_{max}) for **4-5** were located between 549 nm and 558 nm and they are significantly red-shifted in comparison to the native sumanene (**1**) (λ_{max} = 375 nm[11]) and compound **11** (λ_{max} = 361 nm; **Figure S45**). The reason for this is that for the π-extended compounds **4-5**, such π-π* transitions occur at longer wavelengths than in the case of native sumanene. Hence, such direct comparison only further proves the successful emergence of the extended π-system. Emission maximum for compound **5** (558 nm) was slightly red-shifted in comparison to **4** (549 nm). This change in the position of λ_{max} resulted in the visible change in the light emission properties, as representatively visualized for compounds **4-5** in **Figure S44d**. Emission intensity for **4** was *ca*. 12-fold higher in comparison to **5**. It was further visualized with the 3-D emission spectra experiments on compounds **4-5** (**Figures S46-48**). The solid-state spectra **5** (**Figure S44**, dashed lines). were *ca*. 25-35 nm red-shifted (λ_{max} between 575 and 595 nm) in comparison to the spectra measured in $CHCl_3$ solutions.

The spectra of compound **3** in different solvents ($CHCl_3$, DMF, PhMe) are presented in **Figure S49**.

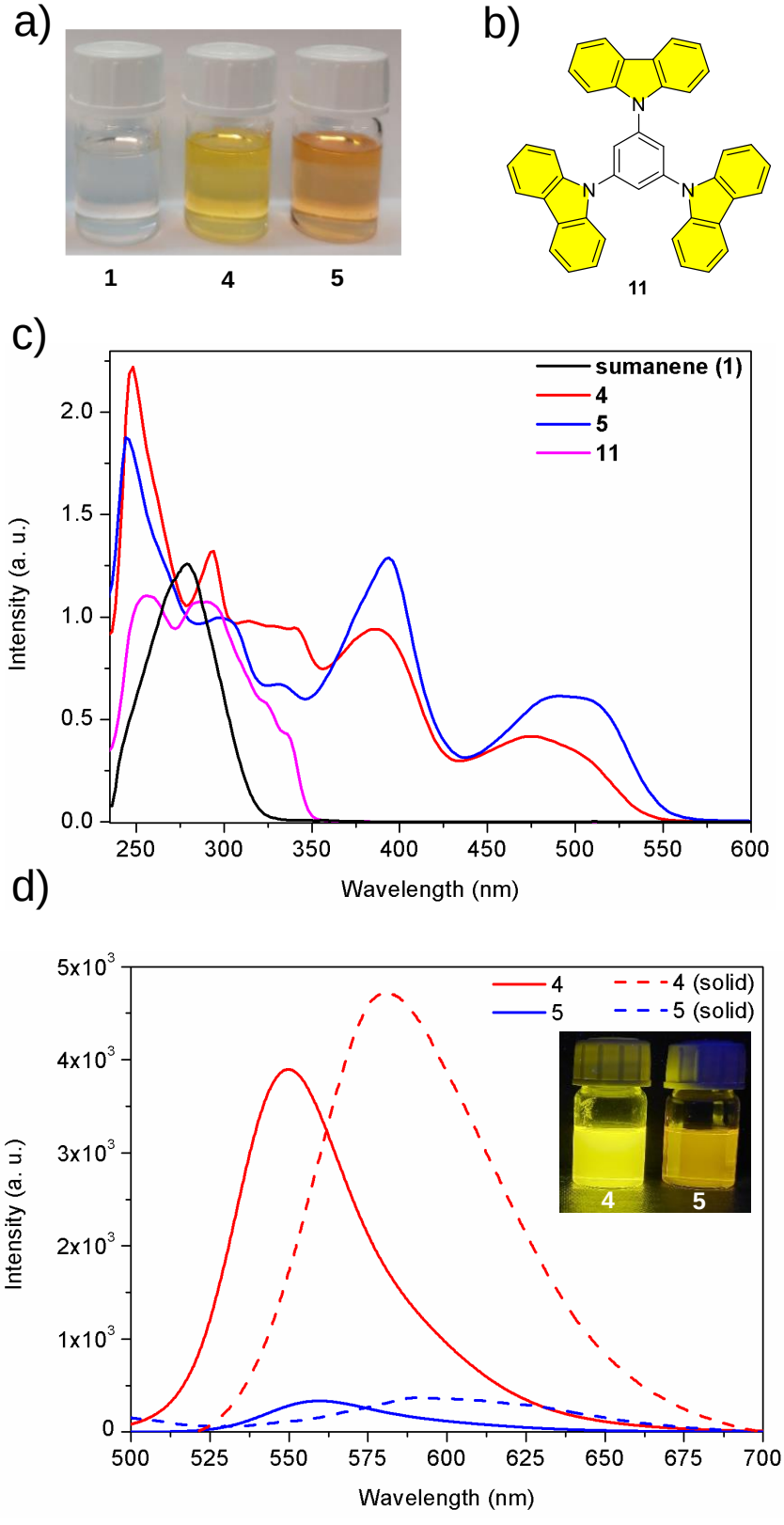

Figure S44. (**a**) Solution of sumanene (**1**) and compounds **4**-**5** in $CHCl_3$ ($2 \cdot 10^{-5}$ M); (**b**) Structure of compound **11**; (**c**) UV-vis spectra ($2 \cdot 10^{-5}$ M; $CHCl_3$) of compounds **1**, **4-5** and **11**; (**d**) Solution ($2 \cdot 10^{-5}$ M; $CHCl_3$, solid lines) and solid-state (dashed lines) emission spectra of compound **4** (λ_{ex} = 380 nm) and **5** (λ_{ex} = 390 nm. The inset image presents the light emission of compounds **4-5** ($2 \cdot 10^{-5}$ M; $CHCl_3$, λ_{ex} = 365 nm).

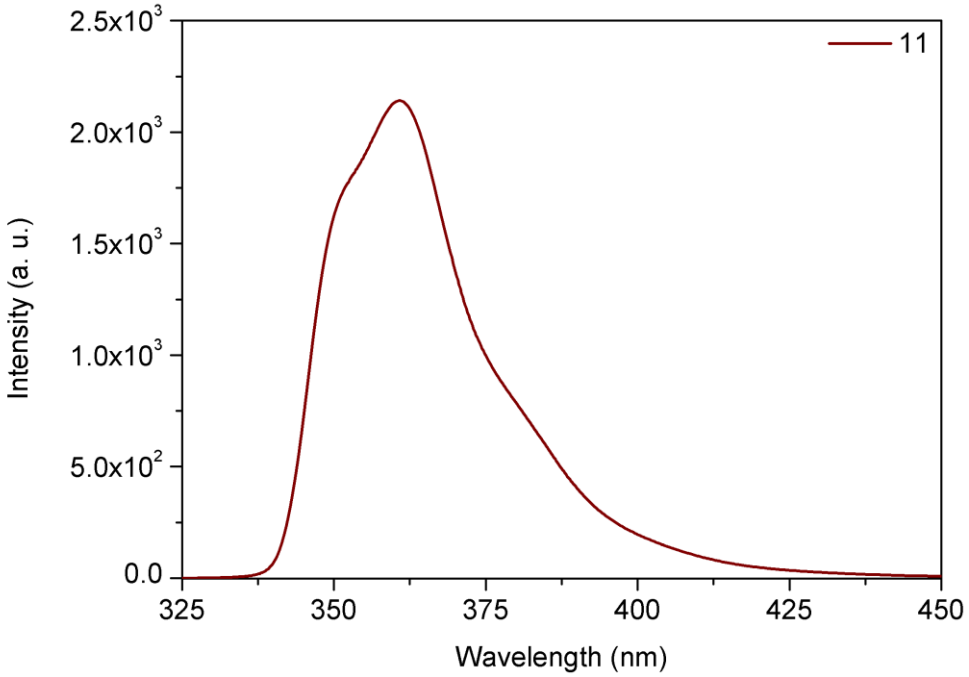

Figure S45. Emission spectrum ($2 \cdot 10^{-5}$ M; $CHCl_3$) compound **11** (λ_{ex} = 325 nm).

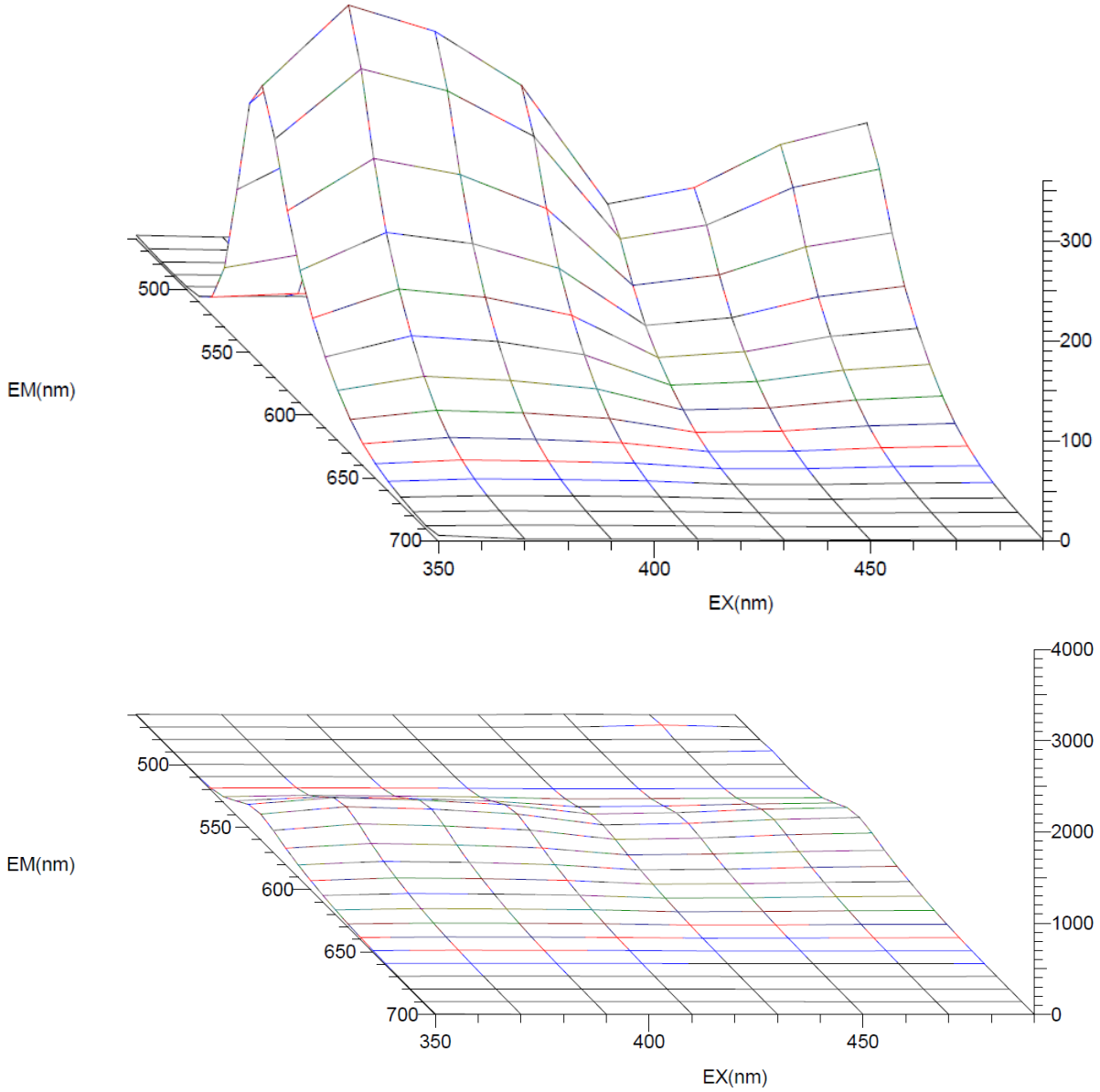

Figure S46. 3-D Emission spectrum ($2 \cdot 10^{-5}$ M; $CHCl_3$) of compound **5**. The spectra with two different scales are presented. The bottom spectrum can be used for the direct comparison of the emission intensity of compound **5** with the emission intensity of compound **4** (see **Figure S47**).

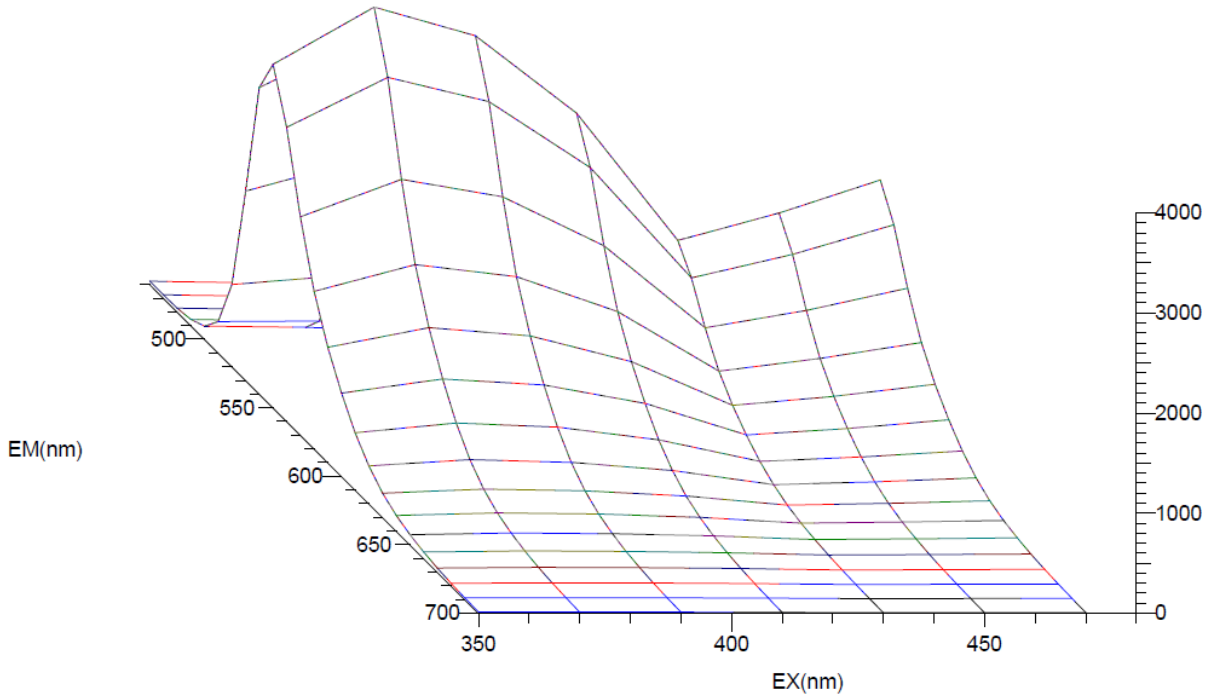

Figure S47. 3-D Emission spectrum ($2 \cdot 10^{-5}$ M; $CHCl_3$) compound **4**.

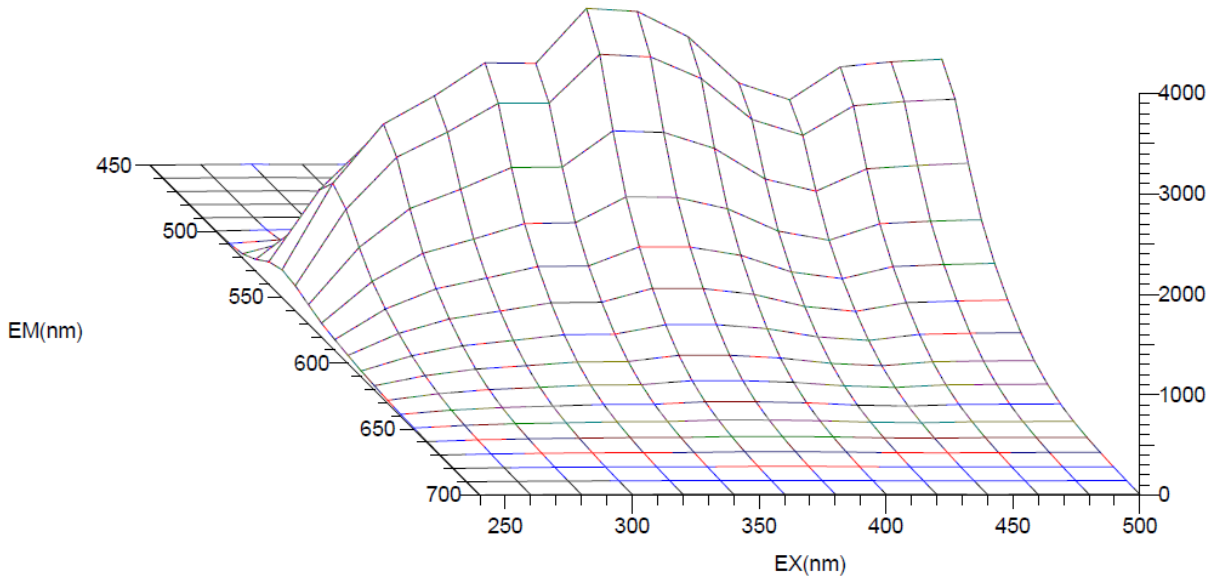

Figure S48. 3-D Emission spectrum ($2 \cdot 10^{-6}$ M; $CHCl_3$) compound **3**.

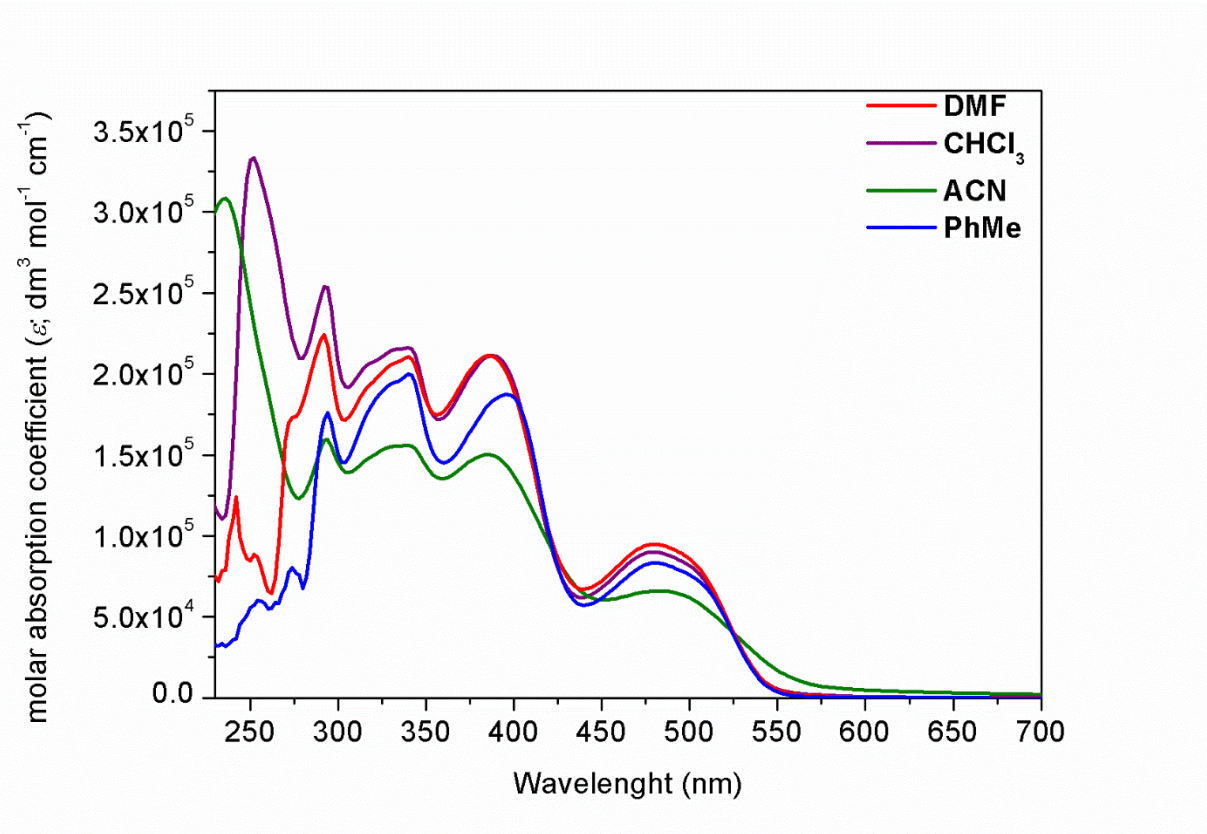

Figure S49. UV-vis spectra of compound **3** ($2 \cdot 10^{-6}$ M) measured in different solvents (DMF = *N*,*N*'-dimethylformamide, ACN = acetonitrile, PhMe = toluene).

S5. DFT calculations

The starting geometries were adopted from the crystal structure of sumanene, which was further modified using Avogadro software.[12] The generated structures were initially optimized using B3LYP functional with simple 3-21G basis set, which is not computationally expensive. This was followed by the optimization at B3LYP-D3[13–16]/6-31+G(d,p)[17] level of theory. It should be stressed that the applied level of theory includes Grimme's empirical dispersion correction, which accounts for the long-range interactions between pendant carbazole units. After proper structure optimization was completed, the vibrational frequencies were calculated, which in turn provided the thermal free energy correction to the electronic energy. It also confirmed that all optimized molecules are stable geometric structures (no imaginary frequencies). All the optimized geometries can be found in the XYZ file attached as part of the Supporting Information. TD-DFT calculations were performed at B3LYP/6-31+G(d,p) level of theory. For UV-vis spectra calculations, it is appropriate to incorporate the solvent effect, as the UV-vis measurements were conducted in $CHCl_3$. Consequently, Integral Equation Formalism Polarizable Continuum Model (IEFPCM)[18] was used with $CHCl_3$ solvent. The calculated electronic transitions for absorption and emission spectra are provided in **Tables S1** and **S2**.

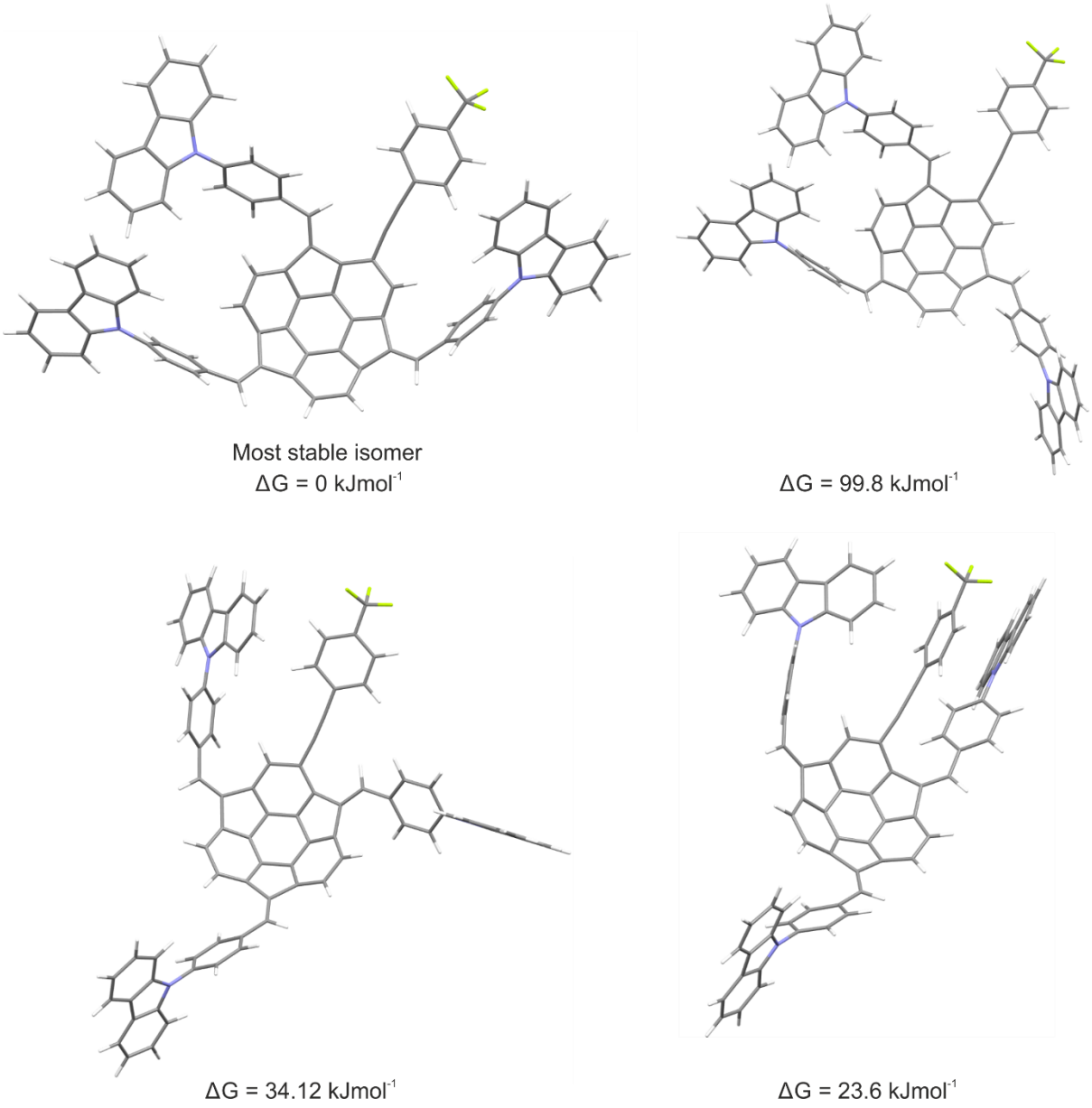

Figure S50. Molecular structures of four possible isomers of **3** and free enthalpy values related to the most stable form.

4

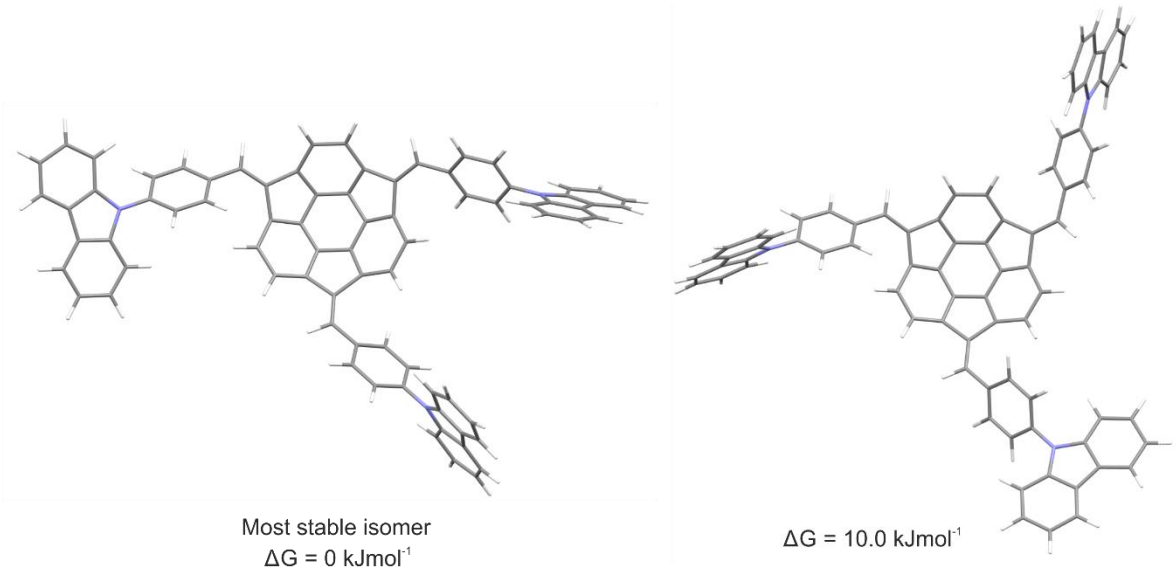

5

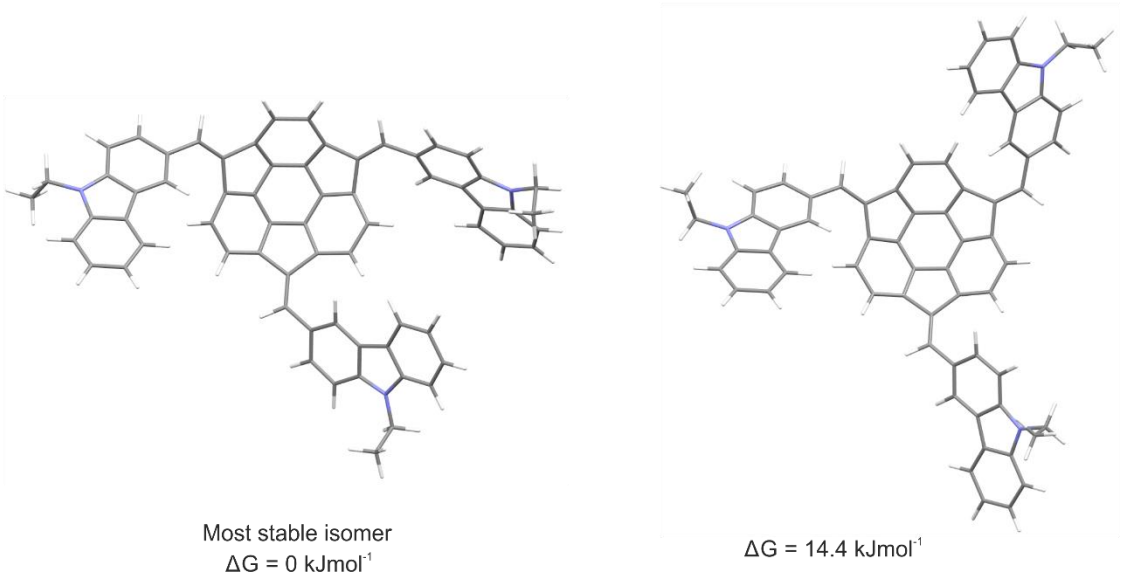

Figure S51. Molecular structures of two possible isomers of **4** and **5** along with the free enthalpy values related to the most stable forms.

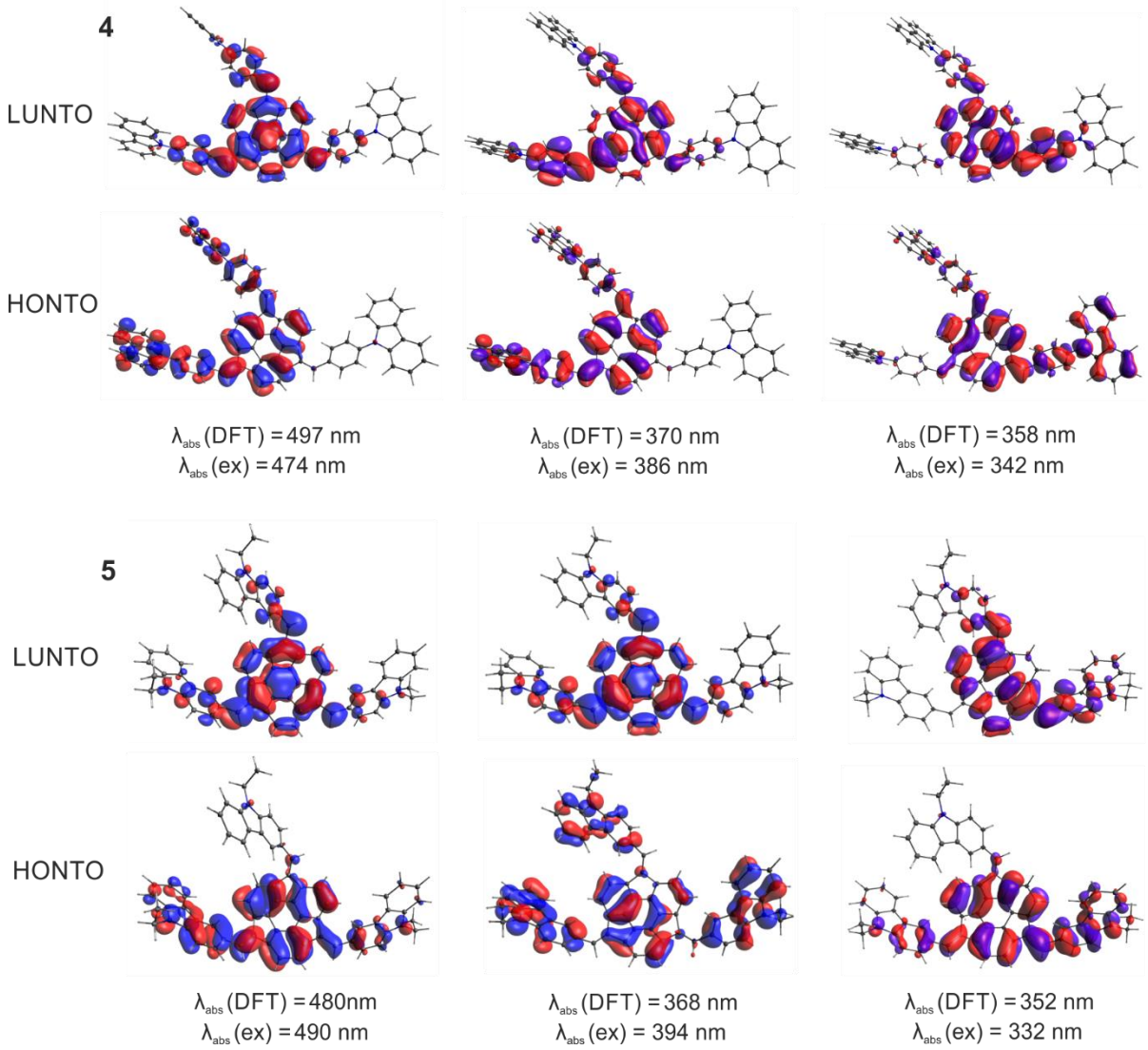

Figure S52. Graphical representation of highest-occupied and lowest unoccupied natural transition orbitals (HONTO and LUNTO, respectively) responsible for observed absorption bands in UV-Vis spectra of **4** and **5**.

Table S1. Calculated values of λ_{abs} for **3**-**5**.

	3		**4**		**5**	
	λ_{abs} / nm	*f*	λ_{abs} / nm	*f*	λ_{abs} / nm	*f*
S_1	523	0.0556	497	0.2618	481	0.3561
S_2	493	0.3272	492	0.3654	469	0.1687
S_3	462	0.0258	442	0.0413	376	0.0523
S_4	449	0.0366	428	0.0672	372	0.0741
S_5	431	0.0263	427	0.0052	369	0.2268
S_6	421	0.0041	384	0.0000	366	0.1546
S_7	401	0.2857	384	0.0000	363	0.0794
S_8	387	0.0788	378	0.0000	352	0.6486
S_9	386	0.0001	376	0.0399	348	0.1510
S_{10}	383	0.0012	371	0.4320	342	0.0123
S_{11}	379	0.1235	367	0.3088	340	0.0008
S_{12}	375	0.0218	358	0.3583	337	0.0051
S_{13}	363	0.0502	352	0.0005	336	0.0069
S_{14}	360	0.3078	336	0.0007	325	0.0972
S_{15}	356	0.1220	331	0.0163	325	0.1364

Table S2. Calculated values of λ_{em} for **3**-**5**.

	3		**4**		**5**	
	λ_{em} / nm	*f*	λ_{em} / nm	*f*	λ_{em} / nm	*f*
S_1	553	0.0546	527	0.2616	590	0.4073
S_2	531	0.4086	522	0.3650	542	0.1590
S_3	492	0.0156	472	0.0413	444	0.1863
S_4	485	0.0479	458	0.0674	441	0.0922
S_5	467	0.0210	457	0.0052	423	0.0448

S6. Cation binding experiments

In the Job's plots, *x* stands for the mole fraction of Cs^+.

The apparent binding constant (K_{app}) values were estimated using the Benesi-Hildebrand method[19,20], given by the equation:

$$\frac{1}{I - I_0} = \frac{1}{a} + \frac{1}{a \cdot K_{app} \cdot C(\mathrm{Cs^+})}$$

where I_0 and I are the fluorescence intensities of sumanene derivative in the absence and presence of Cs^+, respectively, a is a constant, and $C(Cs^+)$ is the concentration of Cs^+ in solution. K_{app} were determined as a ratio of intercept-to-slope of $1/(I - I_0)$ vs. $1/C(Cs^+)$ linear plots.

The data (for the estimation of K_{app} and system stoichiometry – Job's plot method) for the studied systems were collected from the following emission maxima (λ_{em}):

- Compound **5**, λ_{em} = 567 nm (λ_{ex} = 390 nm).
- Compound **4**, λ_{em} = 552 nm (λ_{ex} = 395 nm).
- Compound **3**, λ_{em} = 557 nm (λ_{ex} = 390 nm). For this compound, UV-vis experiments were also performed, and the data were collected for λ_{max} = 395 nm.

The limit of detection (LOD) values were estimated from the intercept and slope of the linear plots[21–23] of $(I\text{-}I_{min})/(I_{max}\text{-}I_{min})$ *versus* $\log(C_{Cs+})$ for compounds **3-4** (lowering of the emission intensity) or $(I_{max}\text{-}I)/(I_{max}\text{-}I_{min})$ *versus* $\log(C_{Cs+})$ for compound **5** (increase in the emission intensity). The *x* value for *y* =1 was calculated (value x(y=1)), and LOD was taken as $10^{x(y=1)}$.

The selectivity studies were performed for representative triscarbazolyl derivative **4** and tetra-substituted derivative **3** using PF_6^- salts of Na^+, K^+, Li^+ and Ca^{2+}. No interfering effects of Na^+ and K^+ were found. As compared to the Cs^+ titration experiments, the changes after the addition of Li^+ to the solutions were slight. Thus, the designed sumanene-carbazole conjugates were characterized by satisfactory selectivity toward the recognition of Cs^+.

All the spectra and plots are presented below.

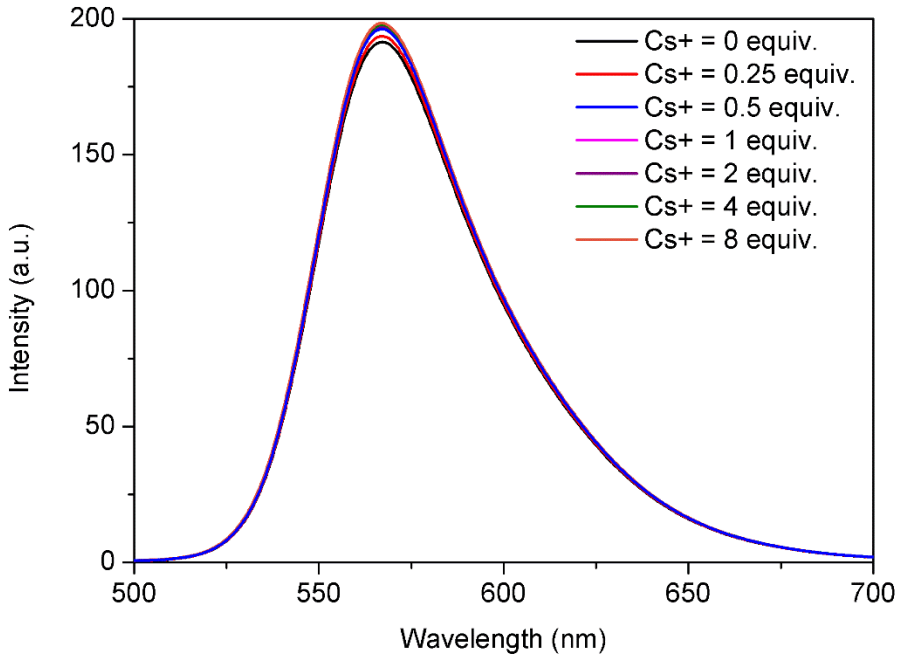

Figure S53. Emission spectra of **5** in the presence of various molar equivalents of Cs^+ (THF:water = 1:1 *vol*/*vol*, λ_{ex} = 390 nm, C_5 = $2 \cdot 10^{-5}$ M).

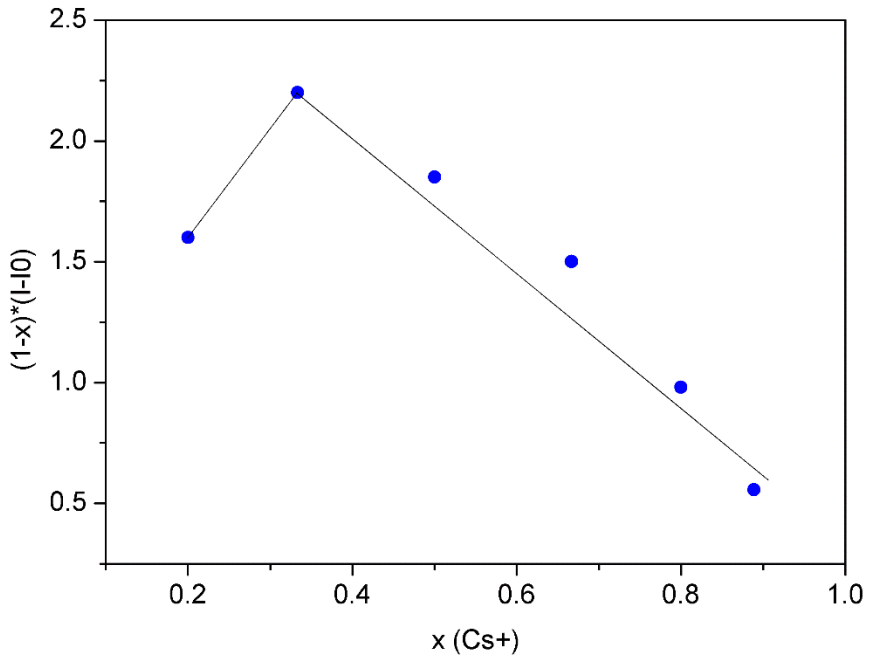

Figure S54. Job's plot regarding the interactions between **5** and Cs^+ (data were collected for, λ_{em} = 567 nm).

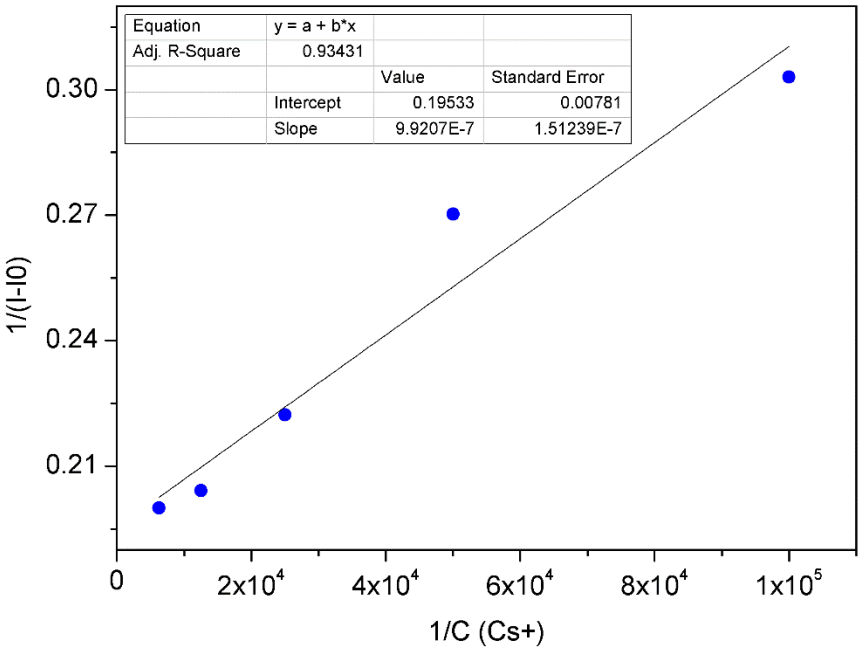

Figure S55. Benesi-Hildebrand plots regarding the interactions between **5** and Cs^+ (data were collected for, λ_{em} = 567 nm). The data for the linear plot are also presented.

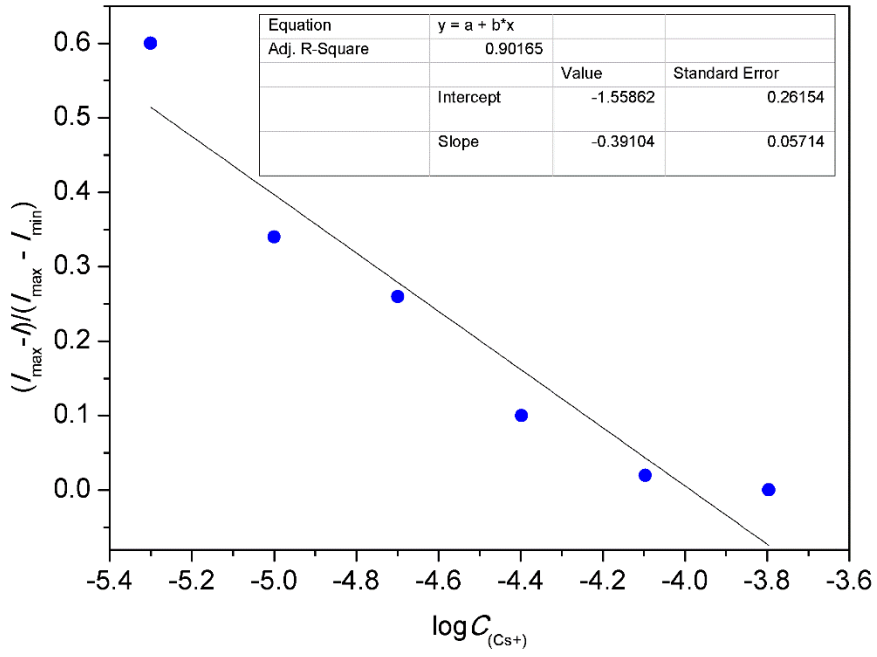

Figure S56. Plot of $(I_{max}-I)/(I_{max}-I_{min})$ *versus* $\log(C_{Cs+})$ regarding the interactions between **5** and Cs^+ (data were collected for, λ_{em} = 567 nm). The data for the linear plot are also presented.

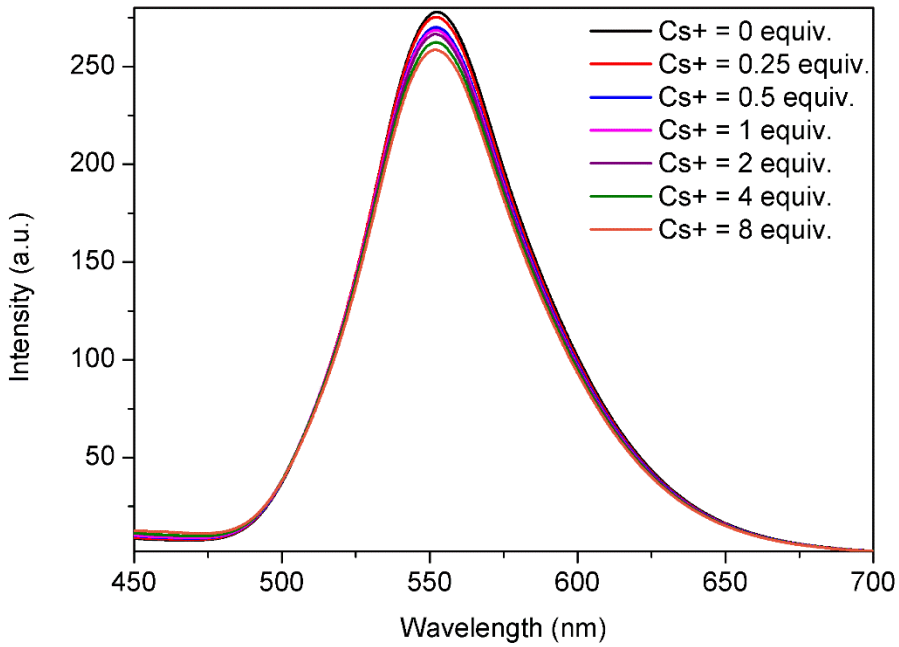

Figure S57. Emission spectra of **4** in the presence of various molar equivalents of Cs^+ (THF:water = 1:1 *vol*/*vol*, λ_{ex} = 395 nm, C_4 = $2 \cdot 10^{-5}$ M).

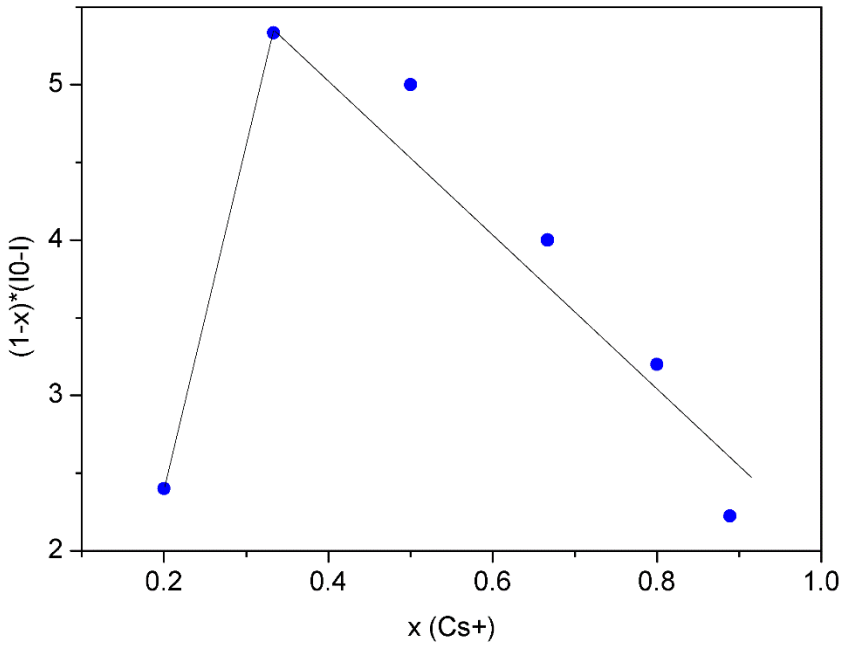

Figure S58. Job's plot regarding the interactions between **4** and Cs^+ (data were collected for, λ_{em} = 552 nm).

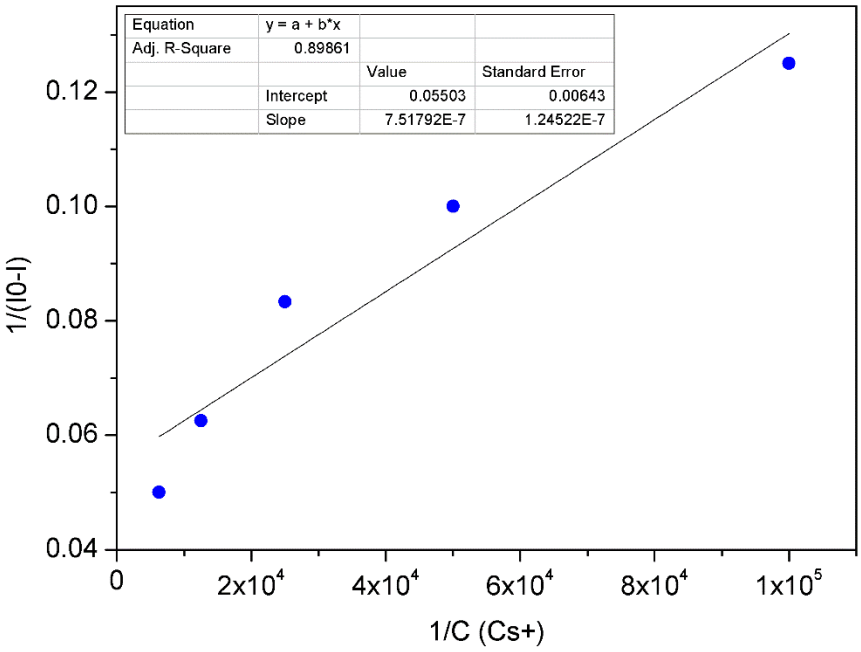

Figure S59. Benesi-Hildebrand plots regarding the interactions between **4** and Cs^+ (data were collected for, λ_{em} = 552 nm). The data for the linear plot are also presented.

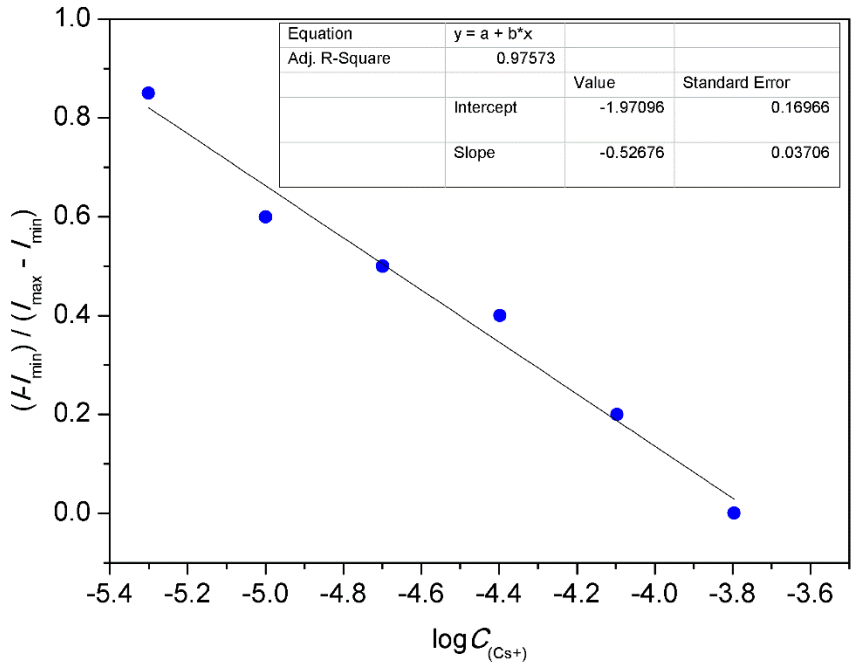

Figure S60. Plot of $(I\text{-}I_{min})/(I_{max}\text{-}I_{min})$ *versus* $\log(C_{Cs+})$ regarding the interactions between **4** and Cs^+ (data were collected for, λ_{em} = 552 nm). The data for the linear plot are also presented.

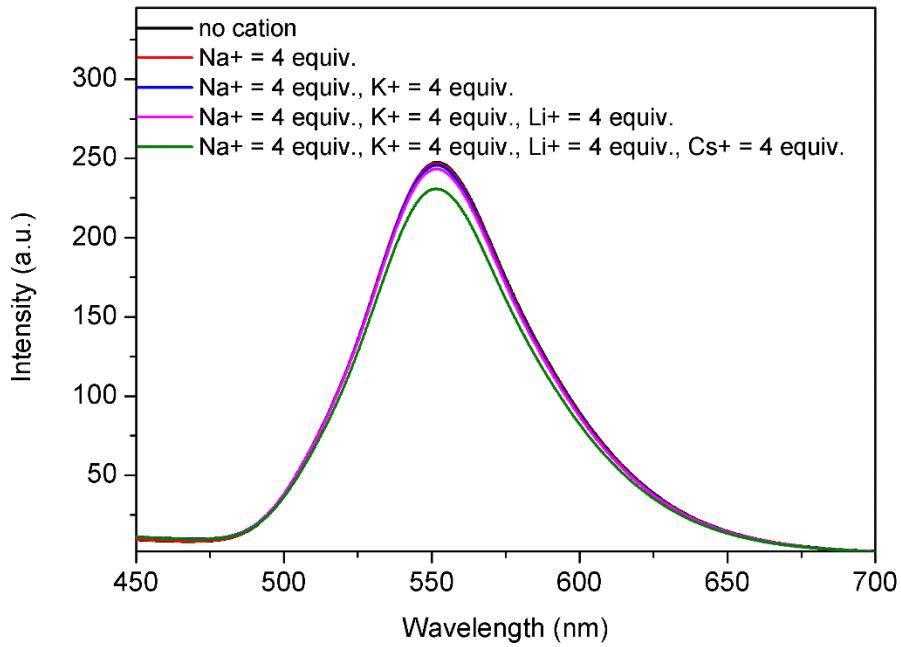

Figure S61. The results of selectivity studies with **4**.

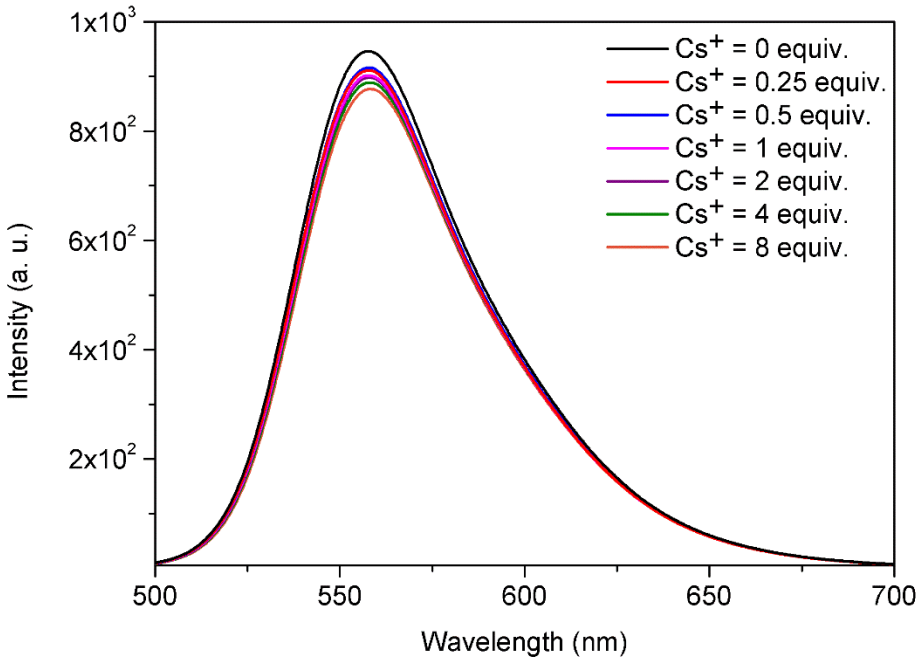

Figure S62. Emission spectra of **3** in the presence of various molar equivalents of Cs^+ (THF:water = 1:1 *vol*/*vol*, λ_{ex} = 390 nm, $C_3 = 2 \cdot 10^{-6}$ M).

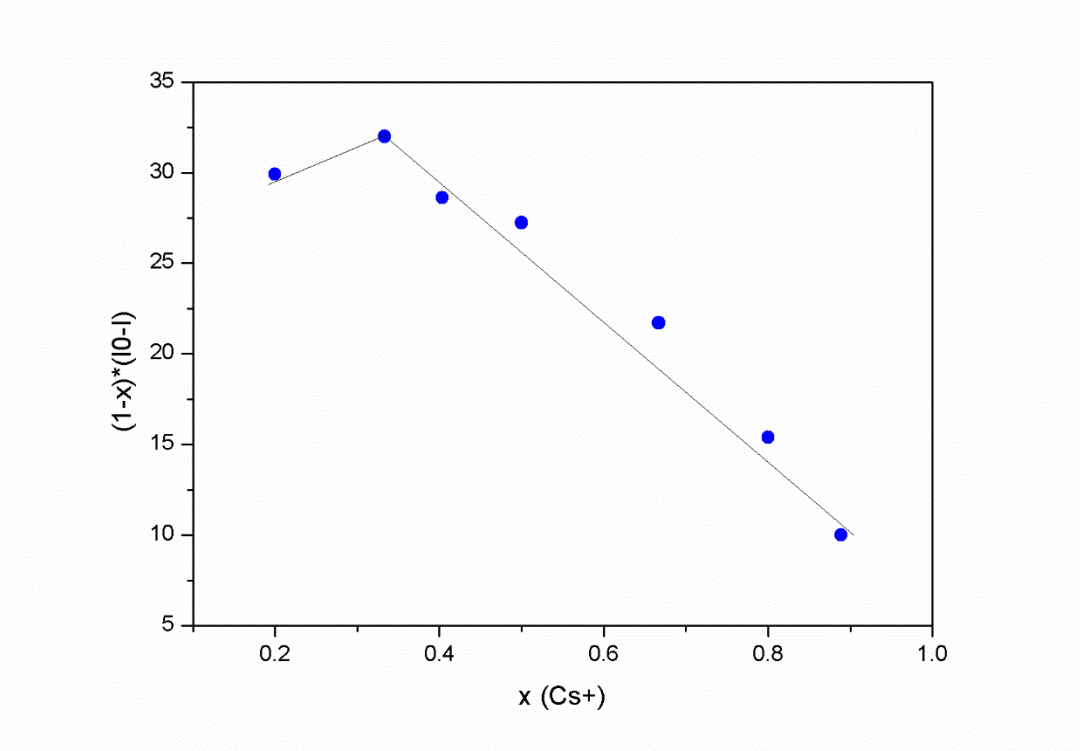

Figure S63. Job's plot regarding the interactions between **3** and Cs^+ using emission spectroscopy (data were collected for, λ_{em} = 557 nm).

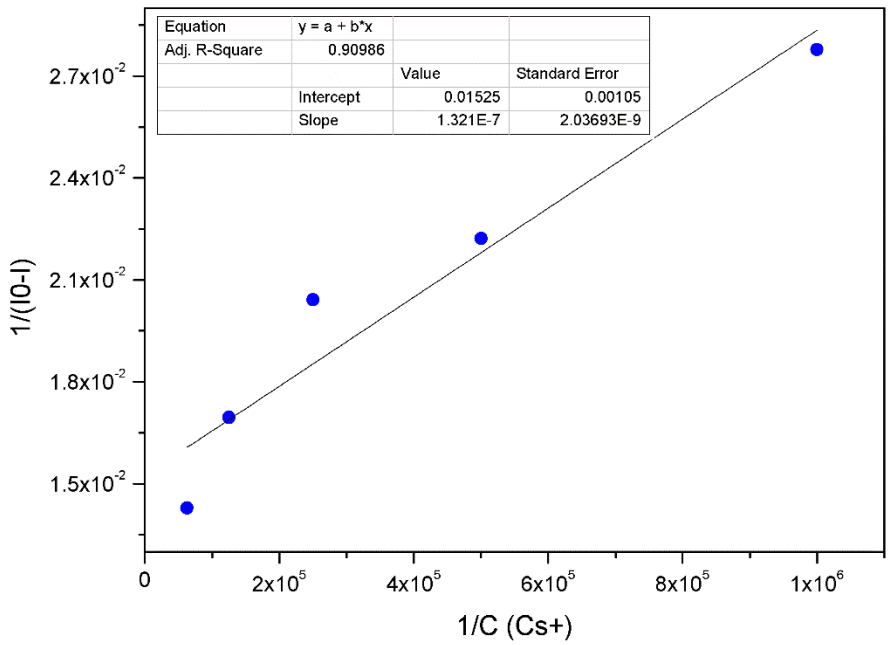

Figure S64. Benesi-Hildebrand plots regarding the interactions between **3** and Cs^+ using emission spectroscopy (data were collected for, λ_{em} = 557 nm). The data for the linear plot are also presented.

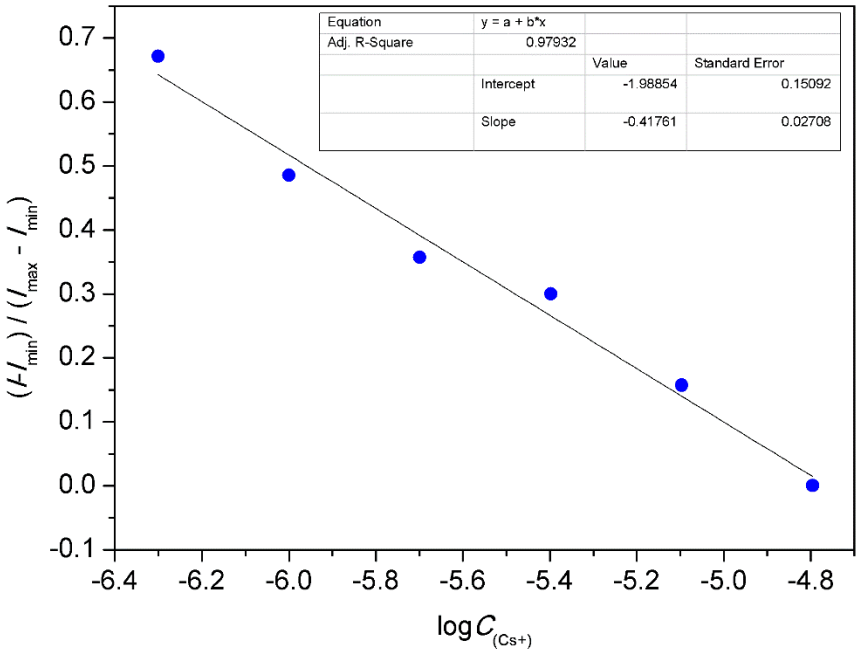

Figure S65. Plot of $(I\text{-}I_{min})/(I_{max}\text{-}I_{min})$ *versus* $\log(C_{Cs+})$ regarding the interactions between **3** and Cs^+ using emission spectroscopy (data were collected for, λ_{em} = 557 nm). The data for the linear plot are also presented.

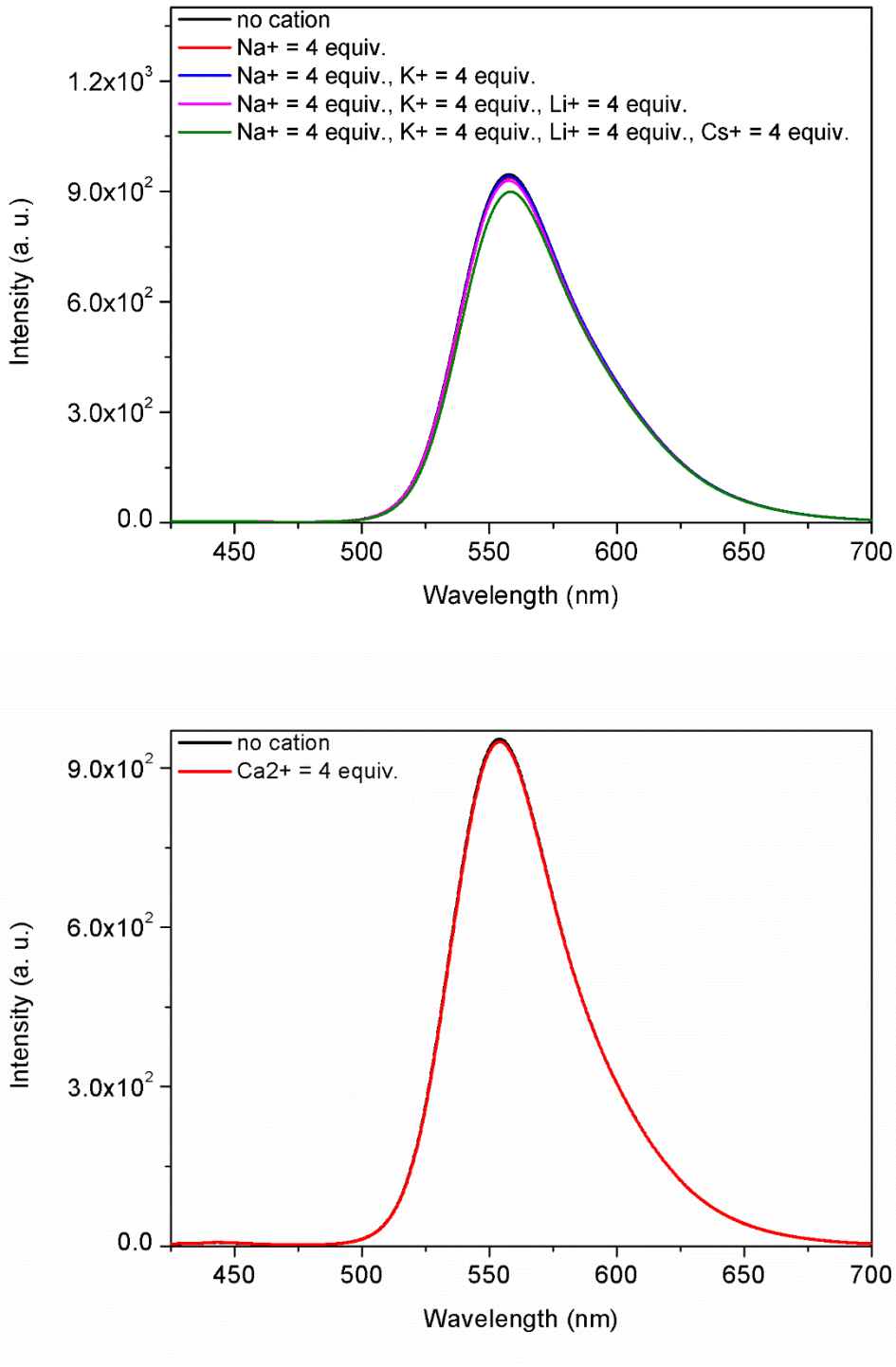

Figure S66. The results of selectivity studies with **3** using emission spectroscopy with Na^+, K^+, Li^+ and Cs^+ cations (top) and Ca^{2+} (bottom) cations in the form of PF_6^- salts.

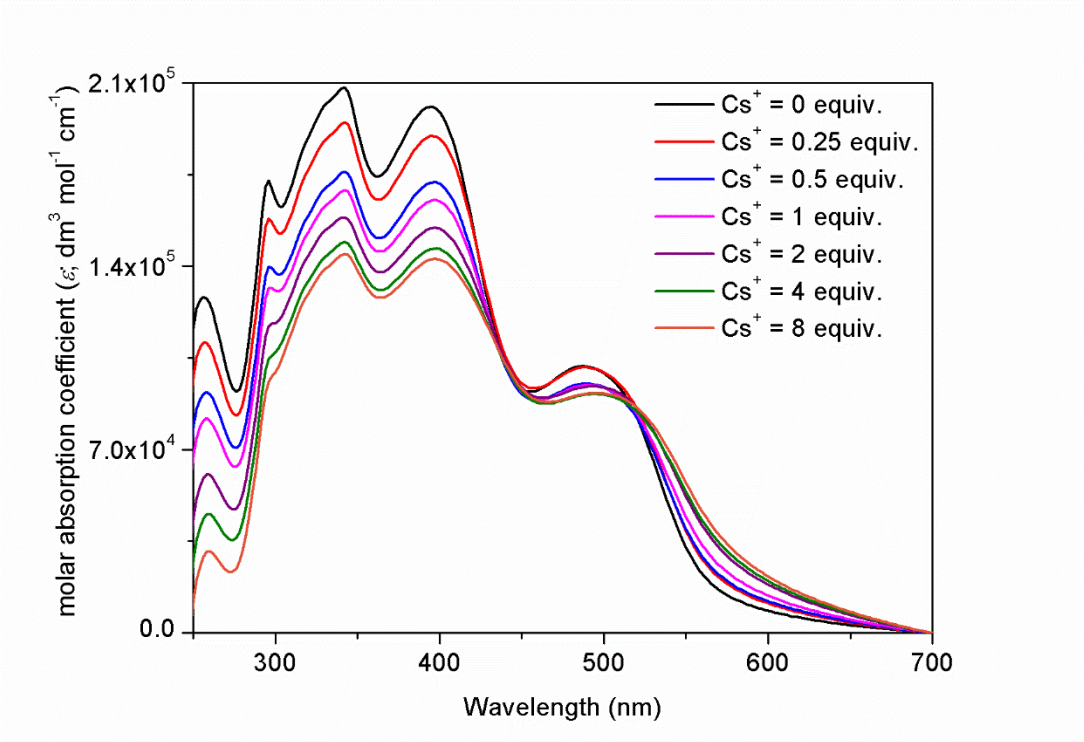

Figure S67. UV-vis spectra of **3** in the presence of various molar equivalents of Cs^+ (THF:water = 1:1 *vol*/*vol*, $C_3 = 2 \cdot 10^{-6}$ M).

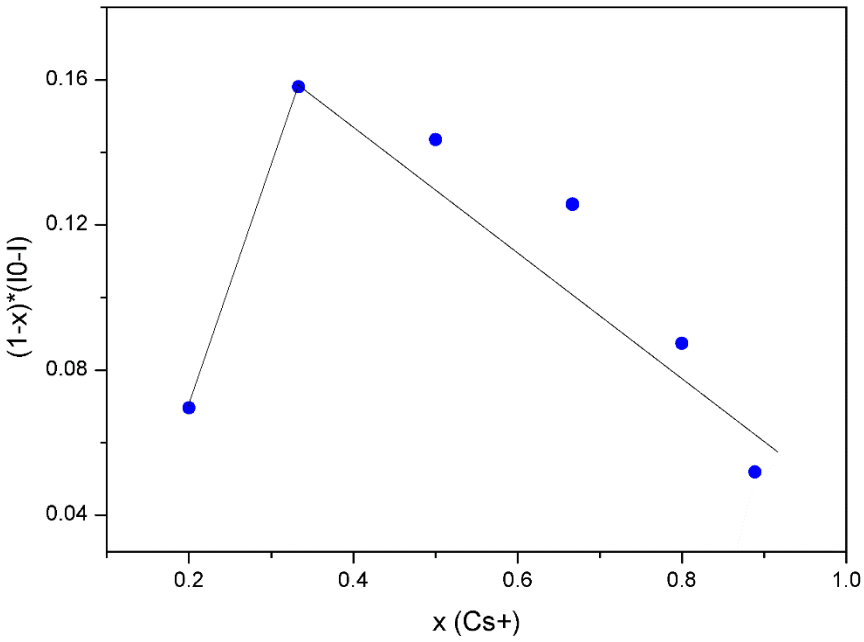

Figure S68. Job's plot regarding the interactions between **3** and Cs^+ using UV-vis spectroscopy (data were collected for, λ_{max} = 395 nm).

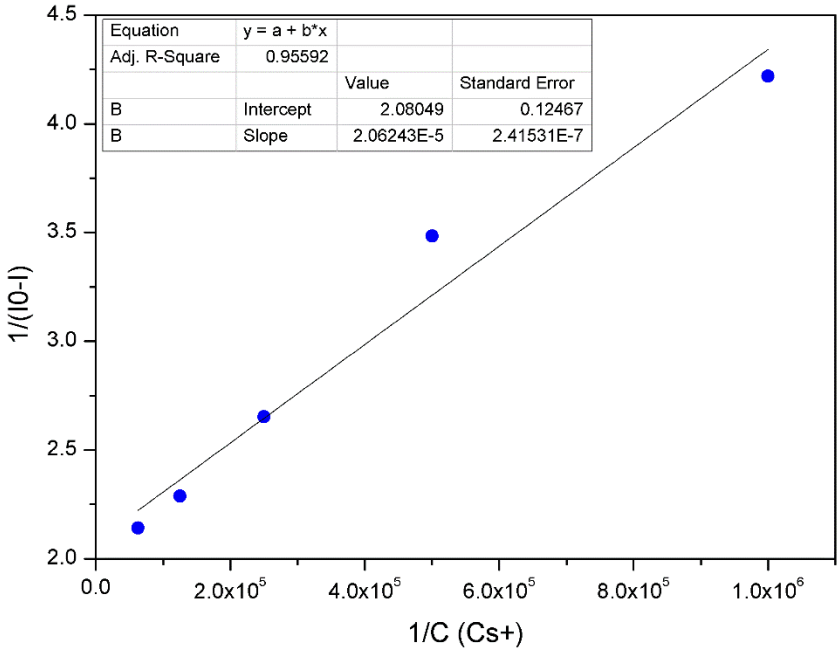

Figure S69. Benesi-Hildebrand plots regarding the interactions between **3** and Cs^+ using UV-vis spectroscopy (data were collected for, λ_{max} = 395 nm). The data for the linear plot are also presented.

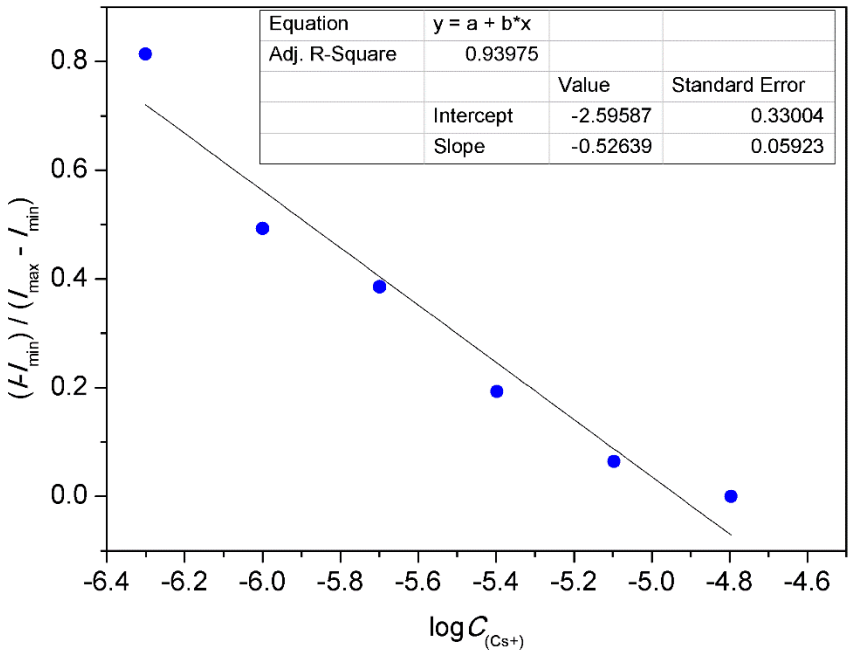

Figure S70. Plot of $(I\text{-}I_{min})/(I_{max}\text{-}I_{min})$ *versus* $\log(C_{Cs+})$ regarding the interactions between **3** and Cs^+ using UV-vis spectroscopy (data were collected for, λ_{max} = 395 nm). The data for the linear plot are also presented.

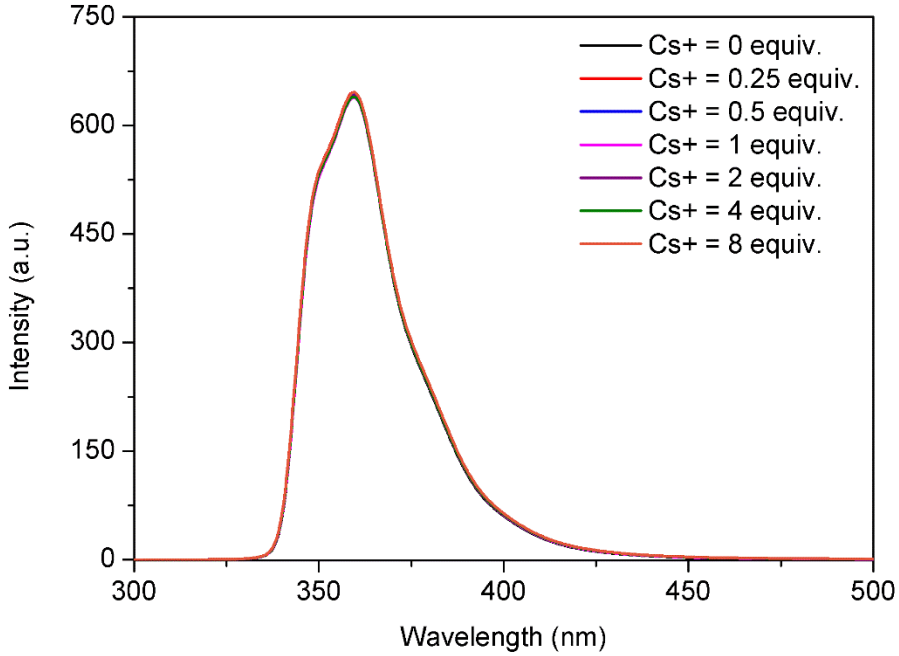

Figure S71. Emission spectra of **11** in the presence of various molar equivalents of Cs^+ (THF:water = 1:1 *vol*/*vol*, λ_{ex} = 325 nm, $C_{\mathbf{11}}$ = $2 \cdot 10^{-5}$ M).

S7. Supporting references

(1) Sakurai, H.; Daiko, T.; Hirao, T. A Synthesis of Sumanene, a Fullerene Fragment. *Science* **2003**, *301* (5641), 1878–1878. https://doi.org/10.1126/science.1088290.

(2) Chen, Q.; Luo, M.; Hammershøj, P.; Zhou, D.; Han, Y.; Laursen, B. W.; Yan, C.-G.; Han, B.-H. Microporous Polycarbazole with High Specific Surface Area for Gas Storage and Separation. *J. Am. Chem. Soc.* **2012**, *134* (14), 6084–6087. https://doi.org/10.1021/ja300438w.

(3) Shrestha, B. B.; Higashibayashi, S.; Sakurai, H. Columnar/Herringbone Dual Crystal Packing of Pyrenylsumanene and Its Photophysical Properties. *Beilstein J. Org. Chem.* **2014**, *10*, 841–847. https://doi.org/10.3762/bjoc.10.80.

(4) Wu, D. H.; Chen, A. D.; Johnson, C. S. An Improved Diffusion-Ordered Spectroscopy Experiment Incorporating Bipolar-Gradient Pulses. *J. Magn. Res. A* **1995**, *115* (2), 260–264. https://doi.org/10.1006/jmra.1995.1176.

(5) Jerschow, A.; Müller, N. Suppression of Convection Artifacts in Stimulated-Echo Diffusion Experiments. Double-Stimulated-Echo Experiments. *J. Magn. Res.* **1997**, *125* (2), 372–375. https://doi.org/10.1006/jmre.1997.1123.

(6) Würth, C.; Grabolle, M.; Pauli, J.; Spieles, M.; Resch-Genger, U. Relative and Absolute Determination of Fluorescence Quantum Yields of Transparent Samples. *Nat. Protoc.* **2013**, *8* (8), 1535–1550. https://doi.org/10.1038/nprot.2013.087.

(7) Brouwer, A. M. Standards for Photoluminescence Quantum Yield Measurements in Solution (IUPAC Technical Report). *Pure Appl. Chem.* **2011**, *83* (12), 2213–2228. https://doi.org/10.1351/PAC-REP-10-09-31.

(8) Urban, M.; Durka, K.; Jankowski, P.; Serwatowski, J.; Luliński, S. Highly Fluorescent Red-Light Emitting Bis(Boranils) Based on Naphthalene Backbone. *J. Org. Chem.* **2017**, *82* (15), 8234–8241. https://doi.org/10.1021/acs.joc.7b01001.

(9) Viel, S.; Ziarelli, F.; Pagès, G.; Carrara, C.; Caldarelli, S. Pulsed Field Gradient Magic Angle Spinning NMR Self-Diffusion Measurements in Liquids. *J. Magn. Res.* **2008**, *190* (1), 113–123. https://doi.org/10.1016/j.jmr.2007.10.010.

(10) Kunde, T.; Nieland, E.; Schröder, H. V.; Schalley, C. A.; Schmidt, B. M. A Porous Fluorinated Organic [4+4] Imine Cage Showing CO_2 and H_2 Adsorption. *Chem. Commun.* **2020**, *56* (35), 4761–4764. https://doi.org/10.1039/D0CC01872D.

(11) Ngamsomprasert, N.; Yakiyama, Y.; Sakurai, H. A Sumanene-Based Aryne, “Sumanyne.” *Chem. Lett.* **2017**, *46* (4), 446–448. https://doi.org/10.1246/cl.161117.

(12) Hanwell, M. D.; Curtis, D. E.; Lonie, D. C.; Vandermeersch, T.; Zurek, E.; Hutchison, G. R. Avogadro: An Advanced Semantic Chemical Editor, Visualization, and Analysis Platform. *J. Cheminform.* **2012**, *4* (1), 17. https://doi.org/10.1186/1758-2946-4-17.

(13) Lee, C.; Yang, W.; Parr, R. G. Development of the Colle-Salvetti Correlation-Energy Formula into a Functional of the Electron Density. *Phys. Rev. B* **1988**, *37* (2), 785–789. https://doi.org/10.1103/PhysRevB.37.785.

(14) Becke, A. D. Density-Functional Thermochemistry. III. The Role of Exact Exchange. *J. Chem. Phys.* **1993**, *98* (7), 5648–5652. https://doi.org/10.1063/1.464913.

(15) Grimme, S.; Antony, J.; Ehrlich, S.; Krieg, H. A Consistent and Accurate *Ab Initio* Parametrization of Density Functional Dispersion Correction (DFT-D) for the 94 Elements H-Pu. *J. Chem. Phys.* **2010**, *132* (15), 154104. https://doi.org/10.1063/1.3382344.

(16) Grimme, S.; Ehrlich, S.; Goerigk, L. Effect of the Damping Function in Dispersion Corrected Density Functional Theory. *J. Comput. Chem.* **2011**, *32* (7), 1456–1465. https://doi.org/10.1002/jcc.21759.

(17) Krishnan, R.; Binkley, J. S.; Seeger, R.; Pople, J. A. Self-Consistent Molecular Orbital Methods. XX. A Basis Set for Correlated Wave Functions. *J. Chem. Phys.* **1980**, *72* (1), 650–654. https://doi.org/10.1063/1.438955.

(18) Cancès, E.; Mennucci, B.; Tomasi, J. A New Integral Equation Formalism for the Polarizable Continuum Model: Theoretical Background and Applications to Isotropic and Anisotropic Dielectrics. *J. Chem. Phys.* **1997**, *107* (8), 3032–3041. https://doi.org/10.1063/1.474659.

(19) Benesi, H. A.; Hildebrand, J. H. A Spectrophotometric Investigation of the Interaction of Iodine with Aromatic Hydrocarbons. *J. Am. Chem. Soc.* **1949**, *71* (8), 2703–2707. https://doi.org/10.1021/ja01176a030.

(20) Goswami, S.; Aich, K.; Das, S.; Das, A. K.; Manna, A.; Halder, S. A Highly Selective and Sensitive Probe for Colorimetric and Fluorogenic Detection of Cd2+ in Aqueous Media. *Analyst* **2013**, *138* (6), 1903. https://doi.org/10.1039/c3an36884j.

(21) Maurya, N.; Bhardwaj, S.; Singh, A. K. Selective Colorimetric and Fluorescence 'Turn-on' Sensor for Ag + and in-Situ Sensing of CN − (off–on-off) via Displacement Approach. *Mat. Sci. Eng. C* **2017**, *74*, 55–61. https://doi.org/10.1016/j.msec.2016.12.131.
(22) Han, J.; Yakiyama, Y.; Takeda, Y.; Sakurai, H. Sumanene-Functionalised Bis(Terpyridine)–Ruthenium(II) Complexes Showing Photoinduced Structural Change and Cation Sensing. *Inorg. Chem. Front.* **2023**, *10* (1), 211–217. https://doi.org/10.1039/D2QI01801B.
(23) Ding, Y.; Xie, Y.; Li, X.; Hill, J. P.; Zhang, W.; Zhu, W. Selective and Sensitive "Turn-on" Fluorescent Zn^{2+} Sensors Based on Di- and Tripyrrins with Readily Modulated Emission Wavelengths. *Chem. Commun.* **2011**, *47* (19), 5431–5433. https://doi.org/10.1039/C1CC11493J.